Doctoral Dissertation

Materials Design of Ultra-High-Molecular-Weight Polyethylene Based on Particle Size Control

Kohei Amada

Supervisor: Prof. Toshiaki Taniike

Graduate School of Advanced Science and Technology

Japan Advanced Institute of Science and Technology

[Materials Science]

March 2026

Referee-in-chief: Professor Toshiaki Taniike
Japan Advanced Institute of Science and Technology

Referees: Professor Masayuki Yamaguchi
Japan Advanced Institute of Science and Technology

Professor Noriyoshi Matsumi
Japan Advanced Institute of Science and Technology

Associate Professor Kosuke Okeyoshi
Japan Advanced Institute of Science and Technology

Associate Professor Ryo Tanaka
Hiroshima University

Abstract

Ultra-high-molecular-weight polyethylene (UHMWPE) exhibits outstanding toughness, impact strength, wear resistance, and self-lubricating properties due to its ultra-high molecular weight above 10^6. However, such an ultra-high molecular weight also results in high melt viscosity and poor melt flowability, limiting its processability in conventional techniques such as injection molding and extrusion molding. As a result, UHMWPE is commonly processed directly from reactor powder using compression molding or ram extrusion. In these methods, particle size has a significant effect on the mechanical properties. Commercial UHMWPE typically consists of macroparticles with average diameters of 80–300 μm, and larger particles tend to result in incomplete particle fusion and interparticle voids during molding, which can deteriorate mechanical properties. Polymer composites with functional fillers can improve properties such as mechanical performance and conductivity. Since melt mixing is not viable for UHMWPE nanocomposites due to the high melt viscosity of the polymer, powder-state mixing is the only practical approach for preparing UHMWPE/filler mixtures. This method relies on simple physical mixing of the polymer particles and fillers, which often results in poor filler dispersion and incomplete coalescence of the polymer particles. These structural deficiencies have hindered the development of multifunctional UHMWPE-based composites. To address the aforementioned limitations, this thesis employs particle size control by introducing microfine UHMWPE synthesized using a nano-sized Ziegler-Natta catalyst. The microfine particles fill interparticle voids and promote particle fusion. The proposed approach establishes a strategy to control filler distribution, which in turn enhances the mechanical properties as well as electrical and thermal conductivities of UHMWPE nanocomposites.

In Chapter 2, UHMWPE composites with graphene nanoplatelets (GNP) were prepared using microfine particles with 1–2 μm and the macroparticles. It was revealed that UHMWPE particle size governed the filler distribution and consequently the mechanical–electrical performance. The macroparticles induced segregated filler networks, achieving conductivity at low filler loadings but with poor mechanical properties, whereas the microfine particles enabled uniform filler dispersion and retained high strength even at higher loadings. A mixed matrix system with the microfine particles and the macroparticles achieved a favorable balance between mechanical performance and electrical conductivity, highlighting the role of UHMWPE particle size as a simple yet powerful design parameter.

In Chapter 3, the influence of sintering and drawing conditions was examined to further improve the mechanical properties of UHMWPE/GNP composites. Increasing sintering temperature effectively enhanced toughness without compromising conductivity, and high-temperature uniaxial drawing achieved an extension ratio of 38.2, demonstrating the superior interfacial fusion of the microfine particles and its potential for high-performance tapes and fibers.

In Chapter 4, the functionality of the microfine particles as a reinforcing and nucleating agent in polypropylene (PP) blends was investigated. The microfine particles enhanced PP crystallinity and stiffness through heterogeneous nucleation, establishing its versatility beyond UHMWPE-based systems.

In conclusion, this thesis establishes a materials-design strategy for UHMWPE and its composites based on particle size control, enabling control over filler distribution. This approach allows the fabrication of composites with well-balanced electrical, thermal, and mechanical properties. The findings provide fundamental insights into structure–property relationships in UHMWPE-based materials and propose a new design strategy for multifunctional polyolefin systems through particle size control.

Keywords: Ziegler-Natta catalyst, Ultra-high-molecular-weight polyethylene, Polymer nanocomposite, Particle size control, Conductivity

Preface

The present thesis is submitted for the Degree of Doctor of Philosophy at Japan Advanced Institute of Science and Technology, Japan. The thesis is consolidation of results of the research work on the topic “Materials Design of Ultra-High-Molecular-Weight Polyethylene Based on Particle Size Control” under the supervision of Prof. Toshiaki Taniike during April 2023– March 2026 at Graduate School of Advanced Science and Technology, Japan Advanced Institute of Science and Technology.

Chapter 1 describes a general introduction and the purpose of this thesis. **Chapter 2** focuses on the control of filler distribution from segregated structure to homogeneous distribution by mixing the macroparticles with the microfine particles and investigates mechanical properties as well as electrical and thermal conductivities of composites. **Chapter 3** elucidates the effects of sintering time and temperature on the mechanical properties of ultra-high-molecular-weight polyethylene nanocomposites and further demonstrates the feasibility of fabricating ultra-high-molecular-weight polyethylene nanocomposites fibers or tapes via solid-state processing using uniaxial elongation. **Chapter 4** examines the role of the microfine particles as a nanofiller within the polypropylene matrix. **Chapter 5** describes the general summary and conclusion of this thesis. To the best of my knowledge, the work is original and no part of this thesis has been plagiarized.

Kohei Amada

Graduate School of Advanced Science and Technology

Japan Advanced Institute of Science and Technology

March 2026

Acknowledgements

First of all, I would like to express my heartfelt gratitude to my supervisor, **Professor Dr. Toshiaki Taniike**, of the Graduate School of Advanced Science and Technology, Japan Advanced Institute of Science and Technology (JAIST), for his invaluable guidance, supervision, encouragement, and support throughout my Ph.D. course. His dedication and insights have been instrumental in the completion of this work.

I am also indebted to **Research Lecturer Dr. Patchanee Chammingkwan** for her valuable guidance, supervision, encouragement, and support during my study in JAIST.

I would like to extend my appreciation to my thesis committee: my second supervisor **Professor Masayuki Yamaguchi, Professor Noriyoshi Matsumi, Associate Professor Kosuke Okeyoshi** at JAIST and **Associate Professor Ryo Tanaka** from Hiroshima University.

I am very grateful to my previous supervisor Professor Tatsuo Kaneko, Professor Kazuaki Matsumura, Dr. Panitha Phulkerd, Dr. Maiko Okajima, Lecturer Kenji Takada, and Dr. Mohammad Asif Ali for their excellent guidance and kind encouragement at professional and personal level. This work could not have been accomplished without their great supporting.

Finally, I would like to give my sincere thanks to my family and all members of Tanike laboratory for their support.

Kohei Amada

Graduate School of Advanced Science and Technology

Japan Advanced Institute of Science and Technology

March 2026

Table of Contents

Chapter 1

General introduction

1.1. Polymers

1.1.1. Polymer science

Polymers refer to macromolecules composed of covalently linked repeating units forming long molecular chains or networks. Unlike small organic molecules, polymers inherently possess a molecular weight distribution (MWD) and exhibit complex molecular structures such as branching, entanglement, and higher-order structures.[1–3] Although natural polymers such as silk and cotton have long been utilized, the advent of synthetic polymers dates back to the discovery of nitrocellulose in 1845. Afterwards, these discoveries led to the development of various synthetic polymers such as celluloid (1861), man-made fiber (1884), urea resin (1896), phenol resin (1907), and melamine resin (1938).[4] Before polymer science was formally established, many of these materials were synthesized through serendipitous discoveries and gradually advanced toward practical applications.

The concept of macromolecules was first proposed by Hermann Staudinger in the 1920s, who demonstrated that so-called macromolecular hypothesis, stating that "unit molecules are linked together in a chain-like structure to form giant molecules," which later became the foundation of modern polymer science.[4] This led to rapid advances in both theoretical understanding and industrial applications throughout the 20th century.

Polymers are regarded as one of the three major categories of materials, alongside metals and ceramics. They possess a unique combination of properties: they are lightweight, easy to process, and their rigidity can be widely tuned from flexible to highly rigid through molecular design.[5,6] They are also relatively inexpensive, corrosion-resistant[7,8] and electrically insulating,[9,10] and can be endowed with various functions.[5,11–14] These characteristics make them promising for applications that reduce environmental impact, such as lightweight components for automobiles or energy-efficient manufacturing enabled by low-temperature

processing. Consequently, the demand for polymer materials is expected to continue expanding in the future.

1.1.2. Classification of polymers according to their origin

Polymers can be classified by their origins such as starting monomer and difference of synthetic route into three categories: synthetic polymers, semi-synthetic polymers, and natural polymers. Representative examples are shown below.

Synthetic polymers: polyolefins (polyethylene, polypropylene), polyamides, polyesters, polyimides, aramids

Semi-synthetic polymers: cellulose acetate, carboxymethyl cellulose, regenerated fibers (viscose rayon)

Natural polymers: natural rubber, proteins, polysaccharides, hemp, silk, cotton, cellulose

Among these, synthetic polymers have been the most actively studied and developed class of polymeric materials, serving as the foundation of modern materials science and industry (Figure 1.1). One of the key features is that, in addition to being lightweight, their mechanical, thermal, electrical properties can be precisely controlled through molecular design compared to semi-synthetic and natural polymers.[10,12,15,16] Even it is same polymer resin, the physical properties can be tune by molecular weight, molecular weight distribution, selection of additives, and processing method, enabling versatile applications in industry. Moreover, it characterizes easy to process, low cost, corrosion resistance, and is adaptable to mass production.

Figure 1.1. Proportion of polyethylene, polypropylene, polyvinyl chloride, and other plastics in global production and applications of plastics. Reproduced from Ref.17.

1.2. Polyolefins

1.2.1. Outline of polyolefins

Polyolefins are the most widely produced and utilized polymeric materials in the world. Representative polyolefins include polyethylene (PE) and polypropylene (PP), as well as polyolefin elastomers and polyolefin rubbers such as ethylene-α-olefin random or block copolymers.[18–21]

Polyethylene is primarily classified based on its branching structure and density, which determine its mechanical and thermal properties. Based on these characteristics, it is divided into low-density polyethylene (LDPE), linear low-density polyethylene (LLDPE), and high-density polyethylene (HDPE).[22] In addition, ultra-high-molecular-weight polyethylene (UHMWPE) is distinguished by its extremely high molecular weight and unique properties.

Polypropylene (PP) is categorized into three types based on stereoregularity: isotactic-polypropylene (i-PP), syndiotactic polypropylene, and atactic polypropylene.[22] The mechanical properties and processability of these polyolefins vary significantly depending on molecular weight and stereoregularity.[23–25] In general, polymers with higher molecular weight enhance mechanical properties but leads to higher melt viscosity, resulting in reduced processability. In particular, UHMWPE possesses an extremely high molecular weight, making it unsuitable for conventional melt-processing techniques such as injection molding, extrusion molding, and blow molding. Therefore, in polyolefin research, the design of polymers that balances mechanical performance and processability has been considered a critical issue.[26]

1.2.2. Olefin polymerization catalysts

Olefin polymerization catalysts[18,21,26] are broadly classified into two categories: heterogeneous (multi-site) catalysts, such as Ziegler-Natta (Figure 1.2a)[27–32] and Phillips systems (Figure 1.2b),[33–36] and homogeneous (single-site) catalysts, such as metallocenes (Figure 1.2c)[37–41] and post-metallocenes.[42–45] In the following sections, the fundamental characteristics of each catalyst and the properties of the obtained polymers are summarized, followed by a discussion of their challenges and recent advances in catalyst developments.

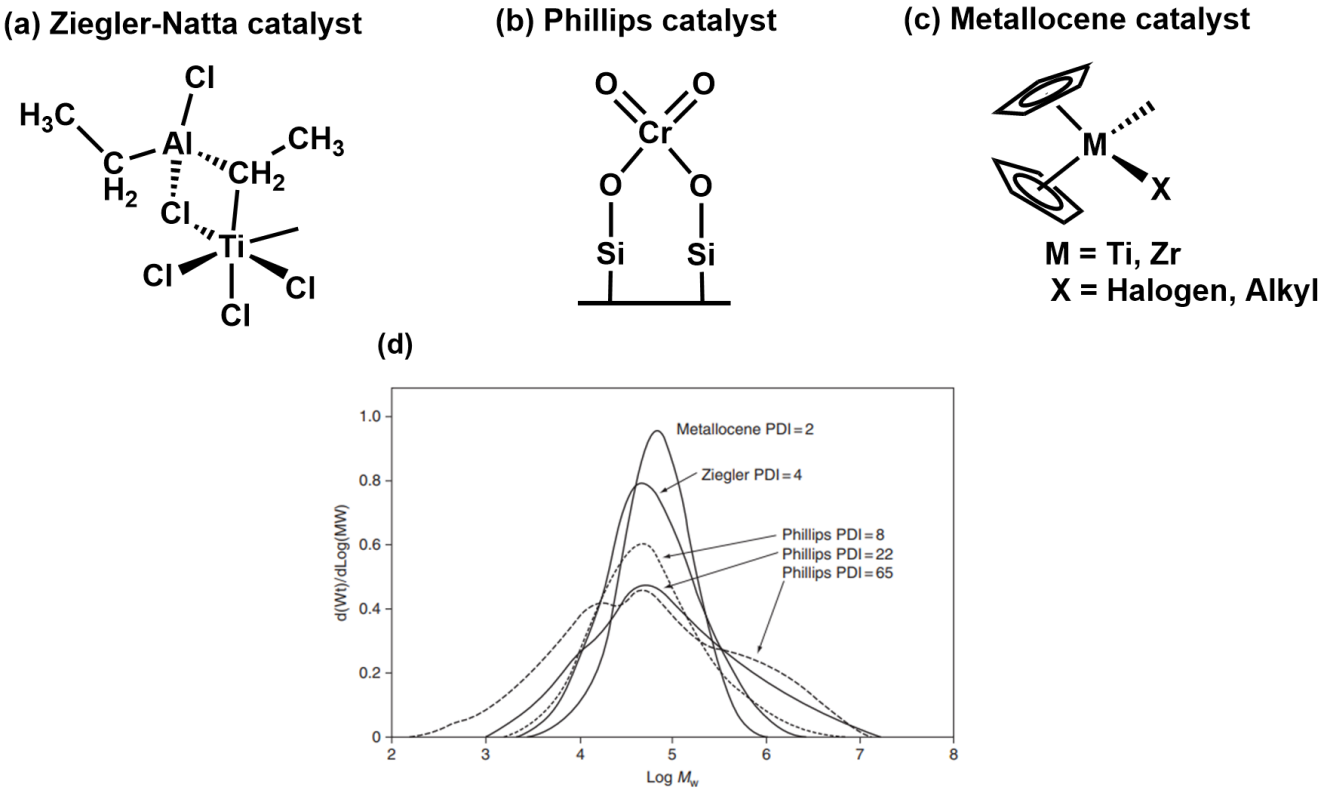

Figure 1.2. Chemical structures of (a) Ziegler-Natta, (b) Phillips catalyst, and (c) metallocene catalyst, and (d) molecular weight distributions synthesized using Ziegler-Natta, Phillips, and metallocene catalysts. (d) is reproduced from Ref.34.

- Ziegler-Natta catalyst: Ziegler-Natta catalysts (ZNC) are polymerization catalysts that play a significant role in polyolefin production and the $MgCl_2$-supported ZNC is the most used catalyst system in polyolefin industry. ZNC is heterogeneous systems in which $TiCl_4$ is supported on $MgCl_2$, and it is activated by alkylaluminum compounds (AlR_3, R= alkyl, aryl, or hydride).[27–32] These catalysts enable the syntheses of LDPE, HDPE, UHMWPE, and i-PP and 99 % of PP is synthesized from ZNC. Its main characteristics include low cost, a moderate MWD (Figure 1.2d), high catalytic activity, high stereospecificity, and low susceptibility to reactor fouling. Owing to these advantages, polymers produced using this catalyst are widely utilized as commodity plastics in products such as plastic bags, bottles, buckets, and wire coatings. The polymerization mechanism using Ziegler-Natta catalysts follows the Cossee-Arlman mechanism (Figure 1.3).[46] In this mechanism, halides on the titanium complex are displaced by alkylaluminum, generating a vacant coordination site at the metal center, allowing the successive insertion of additional monomer units.

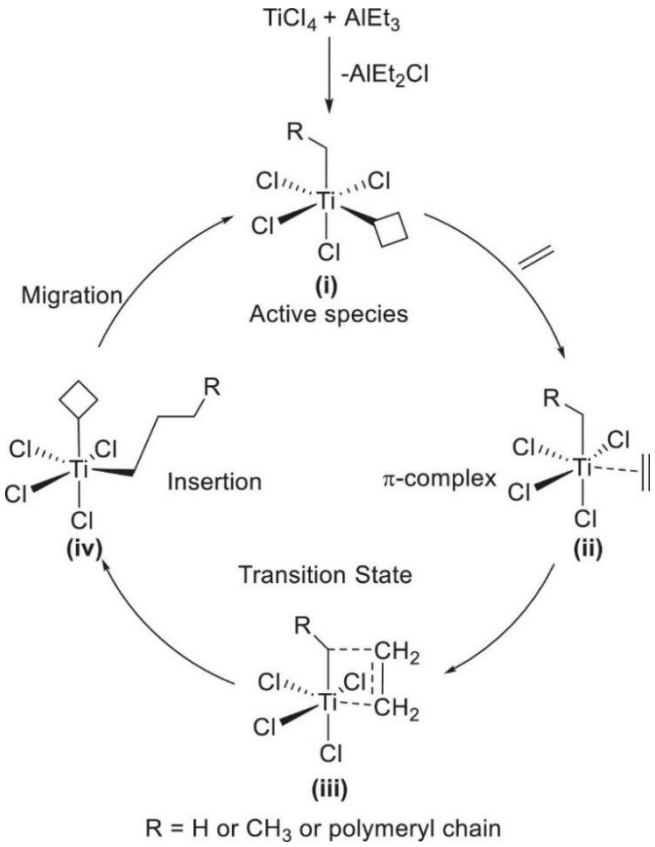

Figure 1.3. Monometallic mechanism for the activation, coordination-insertion, and chain propagation for Ziegler-Natta catalysts. Reproduced from Ref.46.

- Phillips catalyst: The Phillips catalyst is a heterogeneous system in which a chromium compound is supported on SiO_2.[33–36] Polyethylene produced by the Phillips catalysts typically exhibits a broad MWD (～60) (Figure 1.2d) and a predominantly linear structure. These features impart excellent moldability and mechanical durability, making the obtained polyethylene widely used in applications requiring both toughness and processability such as fuel tanks, pipes, and bottles.
- Metallocene catalyst: The metallocene catalyst is a representative homogeneous catalyst used in polyolefin polymerization.[37–41] In general, it is designed as a transition metal complex consisting of a Group 4 metal center (e.g., Zr, Ti, or Hf) coordinated with cyclopentadienyl (Cp) ligands, and it activated by methylaluminoxane. Since all

active sites are uniformly activated, the distribution, composition, and sequence of comonomer incorporation are consistent among polymer chains, producing polymers exhibit a narrow MWD (M_w/M_n<2) (Figure 1.2d). Therefore, metallocene catalysts are particularly effective for the polymerization LLDPE and other copolymers where uniform comonomer distribution is crucial. However, several challenges remain, including high catalyst cost, reactor fouling, and the requirement of large amounts of solvent.

1.3. Ultra-high-molecular-weight polyethylene (UHMWPE)

1.3.1. General Properties

Ultra-high-molecular-weight polyethylene (UHMWPE) is a linear polyethylene with minimal branching and the highest molecular weight among all polyethylene. Owing to its extremely high molecular weight, UHMWPE exhibits outstanding mechanical properties such as exceptional toughness and impact strength,[47–50] along with excellent tribological performance,[50–54] durability, chemical resistance,[13,55] wear resistance,[51–54] and self-lubricating characteristics.[54] Owing to these superior properties, UHMWPE has found applications in mechanical components (e.g., O-ring and gears) as well as in biomedical applications such as artificial joints and catheter components,[56,57] where corrosion resistance and biocompatibility are required. In addition, UHMWPE fibers, commercially known as Dyneema®, are utilized as high-strength fibers in climbing ropes and other demanding applications.

However, as the molecular weight increases, the melt viscosity of UHMWPE becomes exceedingly high, resulting in poor flowability. Consequently, UHMWPE cannot be processed by conventional melt-processing techniques such as injection molding, blow molding, and extrusion molding (Figure 1.4), in which polymer pellets are heated, melted, and shaped into

desired forms. This extremely high melt viscosity is strongly governed by the molecular weight of polymers, and their relationship can be expressed by the Equation (1.1):[58]

$$\eta_0 \propto M_w^{3.4} \qquad (1.1),$$

where η_0 is the zero shear viscosity and M_w is the weight-average molecular weight.

Therefore, UHMWPE is typically processed by compression molding or ram extrusion, where polymer powders are consolidated and sintered in the solid state (Figure 1.5).

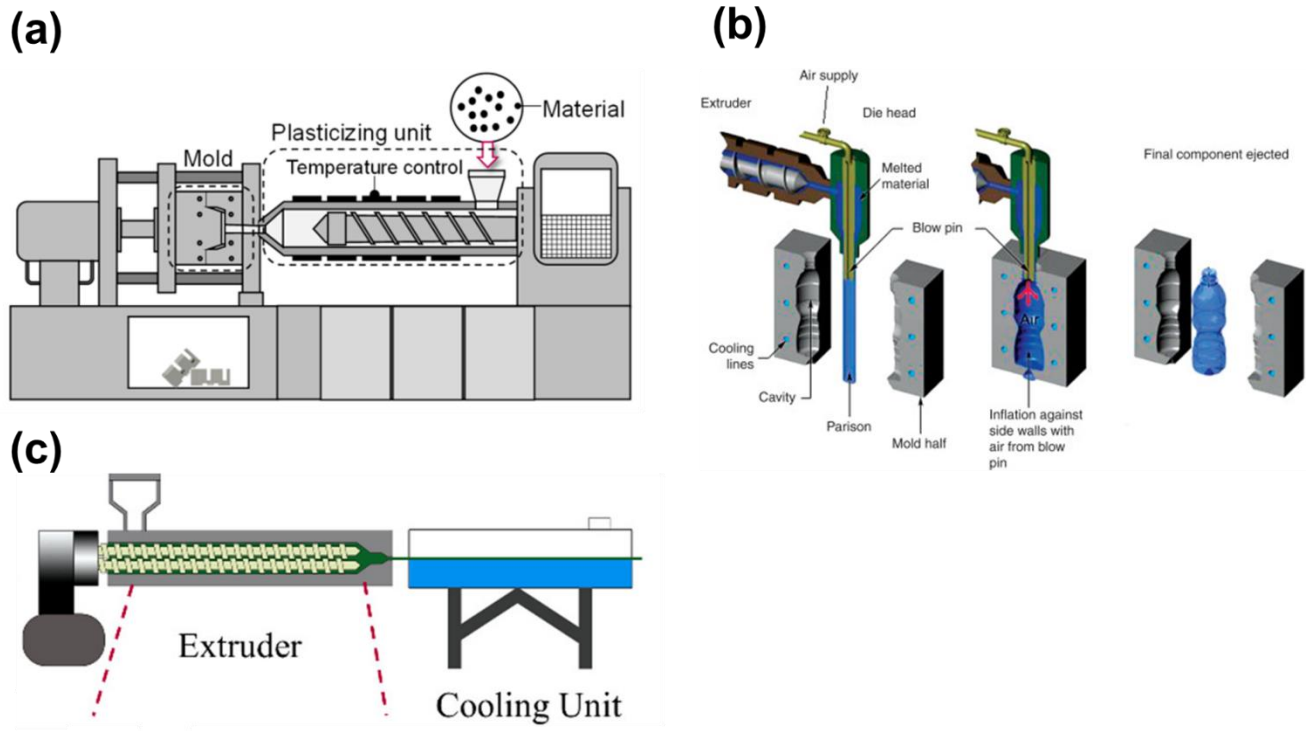

Figure 1.4. Molding techniques for polymer processing: (a) injection molding reproduced from Ref.59, (b) blow molding reproduced from Ref.60, and (c) extrusion molding reproduced from Ref.61.

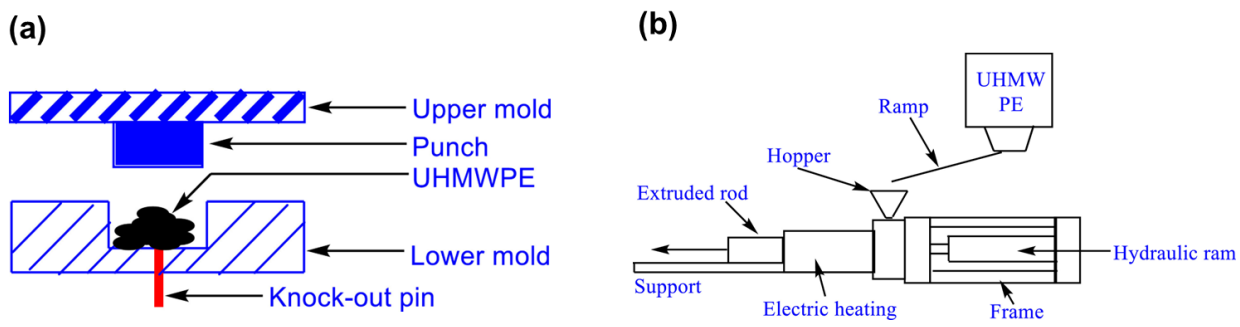

Figure 1.5. Schematic illustration of UHMWPE processing methods: (a) compression molding and (b) ram extrusion. Reproduced from Ref. 46.

1.3.2. Synthesis

Commercial UHMWPE is synthesized using $MgCl_2$-supported Ziegler-Natta catalysts, which are industrially advantageous for slurry and gas-phase processes due to their high scalability, cost-effectiveness, and lower solvent requirements The typical particle size of $MgCl_2$ support ranges from 10 to 100 μm,[62,63] and the active sites are spatially close to each other, leading to the formation of polymer chains in highly confined regions.[29] As polymerization proceeds, the growing chains become entangled even before crystallization, owing to the high local polymer concentration and limited chain mobility. This restricted chain motion substantially increases the melt viscosity.[64] Consequently, conventional melt-processing techniques (e.g., extrusion or injection molding) are difficult to apply to UHMWPE. In contrast, during compression molding and ram extrusion, UHMWPE is sintered in the solid state, and its large particle size leads to insufficient interparticle fusion, resulting in reduced mechanical properties.

For the practical utilization of such highly viscous UHMWPE, the polymers are typically dissolved in decalin (>90 wt%) to obtain ~10 wt% polymer solutions, from which UHMWPE fibers and films are fabricated via gel spinning[65] or solution spinning.[66] However, the use of a large amount of solvent is economically and environmentally undesirable.

Therefore, research on UHMWPE synthesis has primarily focused on improving processability, which can be categorized into three major strategies:

1. Broadening the molecular weight distribution by synthesizing[29,48,67] or blending[68,69] low-molecular-weight polyethylene to improve the flowability of molten state and overall processability.
2. Minimizing chain entanglement during polymerization[27,32,44,70–76] to enable processing at lower temperature or in the solid state. [29,70,77–79]
3. Reducing particle size by designing nano-sized Ziegler-Natta catalysts with controlled active site distribution.[27,32]

Ziegler–Natta catalysts exhibit a replica effect, in which the morphology of the catalyst particles is replicated in the produced polymer.[63,80–83] Therefore, by controlling the morphology and active sites of nano-sized catalysts, smaller and more uniform UHMWPE powder particles can be obtained. This results in improved powder flowability and interfacial fusion, thereby enhancing the moldability during compression molding or sintering.

1.3.3. A replica effect for heterogeneous polyolefin catalysts

In olefin polymerization using heterogeneous catalysts such as Ziegler-Natta catalysts, the morphology of the resulting polymer particles is well known to be strongly influenced by that of the catalyst particles. This phenomenon is referred to as the replica effect.[63,80–83] In this phenomenon, the characteristics of the catalyst particles, such as particle size, structure, and porosity are replicated in the polymer particles through polymer growth within catalyst pores, stress accumulation, and subsequent catalyst fragmentation. Assuming volume conservation between the catalyst and polymer particles, the polymer particle size can be approximately estimated using following Equation (1.2):

$$D_{PE} = \left(\frac{d_{cat}}{d_{PE}} Y\right)^{\frac{1}{3}} D_{cat} \quad (1.2),$$

where d_{cat} and d_{PE} are the densities of catalyst and polymer, $D_{PE}$and D_{cat} are their particle sizes of the polymer and catalyst, and Y is the polymer yield.

Thus, the polymer particle size is proportional to the catalyst particle size and to the one-third power of the polymer yield. Therefore, to reduce the polymer particle size without lowering the yield, it is effective to decrease the catalyst particle size.

The replica effect is a key factor that influencing the final morphology and handling properties of polymer particles, and thus plays a significant role in catalyst design.

1.3.4. Smaller and less-entangled UHMWPE synthesized from nano-dispersed Ziegler-Natta catalysts[27,32]

In conventional Ziegler-Natta catalysts, UHMWPE chains are formed under diffusion-limited conditions within catalyst particles, leading to a highly entangled state that makes melt processing difficult.[64] To address this issue, it is essential to control the distribution of active site of the catalyst particles, which directly influence the polymer morphology. Chammingkwan *et al.* developed a MgO/$MgCl_2$/$TiCl_4$ Ziegler-Natta catalyst using MgO nanoparticles as a core template to induce uniform $MgCl_2$ deposition and obtained nanosized catalyst particle. A surfactant was used to enhance dispersion during the chlorination step (Figure 1.6a). The degree of chlorination of MgO to $MgCl_2$ was controlled by varying the chlorination time, thereby tuning the Ti density and distribution of active sites. Ethylene polymerization was carried out under industrially relevant conditions (70 °C, 0.8 MPa).

The obtained UHMWPE exhibited the viscosity-average molecular weight exceeding 5×10^6 g mol^{-1}, as determined from intrinsic viscosity measurements. The resulting polymer consisted of submicron-sized particles that closely reflected the morphology of the catalyst (Figure 1.6b). Analyses of its thermal behavior, rheological properties (Figure 1.6c), and solid-state drawability indirectly indicated a significantly lower chain entanglement density compared to conventional UHMWPE. In particular, the PE-0.5 sample could be drawn to over 20 times its original length at 125–130 °C, demonstrating a remarkable improvement in processability.

These results demonstrate that nano-dispersed Ziegler-Natta catalysts represent a promising strategy for synthesizing microfine and less-entangled UHMWPE with high molecular weight and excellent drawability.

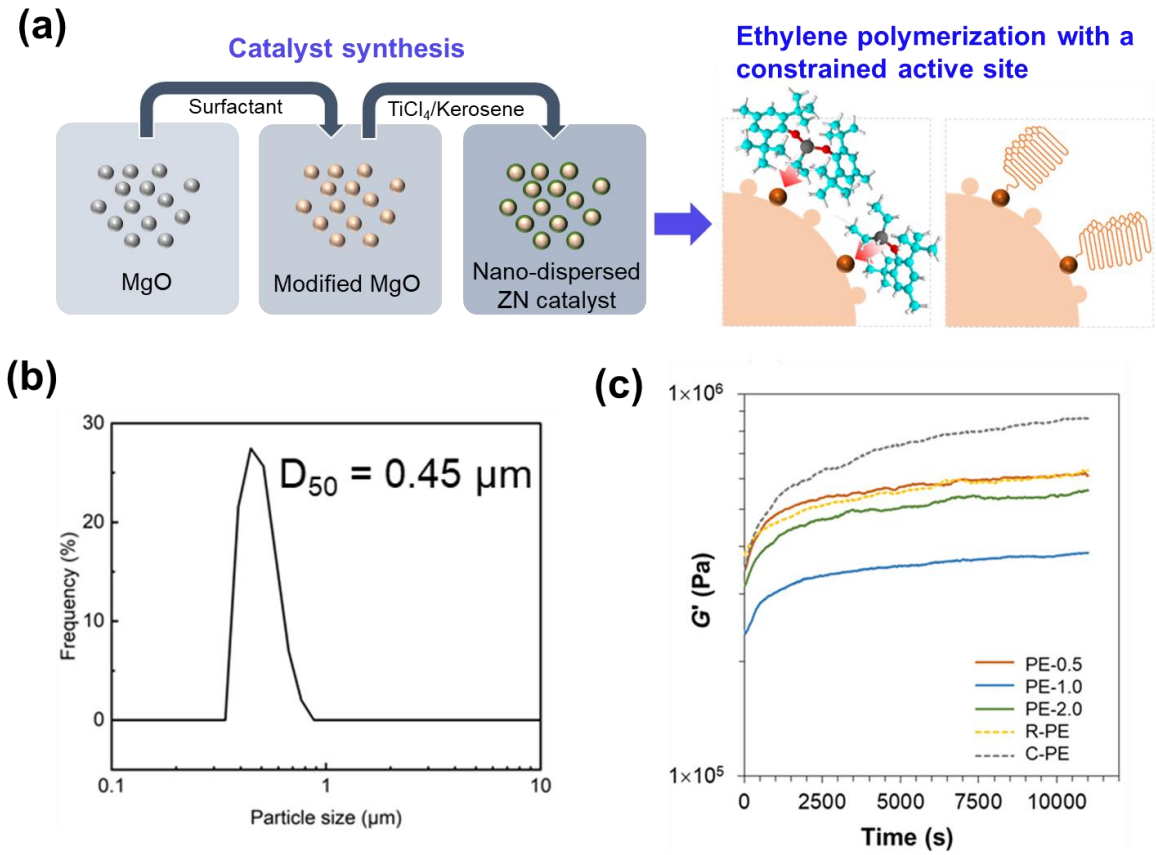

Figure 1.6. (a) Schematic illustration of the synthesis of a nano-dispersed Ziegler-Natta catalyst and UHMWPE. Reproduced from Ref.32. (b) Particle size distribution of obtained

UHMWPE powder. (c) Time-sweep curve of the storage modulus at the fixed strain of 0.5% and frequency of 10 rad s^{-1}. Reproduced from Ref.32.

1.3.5. Structural characteristics of UHMWPE with low chain entanglement

For UHMWPE, its extremely high molecular weight leads to severe chain entanglement and very high melt viscosity, which are the primary factors limiting its processability. Numerous studies have focused on the initial entanglement state,[3,58,64,79,84–87] the degree of crystallinity,[85,88,89] and the hierarchical morphology of crystalline and amorphous regions in UHMWPE.[84,90,91] Conventional melt processing techniques such as extrusion molding, blow molding, and injection molding are largely unsuitable for UHMWPE, so processing has been limited to methods such as solution spinning[66] or gel spinning[65] for high-strength fibers and compression molding[85,86,89,92–94] under constrained conditions.

More recently, research has been devoted to UHMWPE with low chain entanglement,[3,58,64,79,84–87] including the characterization of its distinctive chain dynamics, mechanical behavior, and improved processability.[58,78,79] It has been reported that UHMWPE with less-entanglement exhibits a relatively low modulus in the initial state due to its loosely packed morphology, and that upon heating, it rapidly develops chain entanglements. When heated at rates above 1 °C min^{-1},[95] a phenomenon known as "melt explosion"[64,86,91,95] occurs, characterized by rapid melting and void formation caused by sudden chain relaxation (Figure 1.7).

The chain dynamics of UHMWPE with low chain entanglement cannot be fully explained by conventional polymer relaxation models such as the reptation theory,[96] which assumes an equilibrium entangled network.[98] Instead, they are considered to result from rapid chain diffusion driven by an increase in entropy to relieve the initial non-equilibrium entanglement state. Other studies have reported that reducing voids generated during sintering can improve

the mechanical integrity of UHMWPE.[64,97] Furthermore, the effect of molecular weight[98] and sintering temperature[47,85,87] on interparticle fusion and crystallinity have been explored to achieve enhanced mechanical performance.

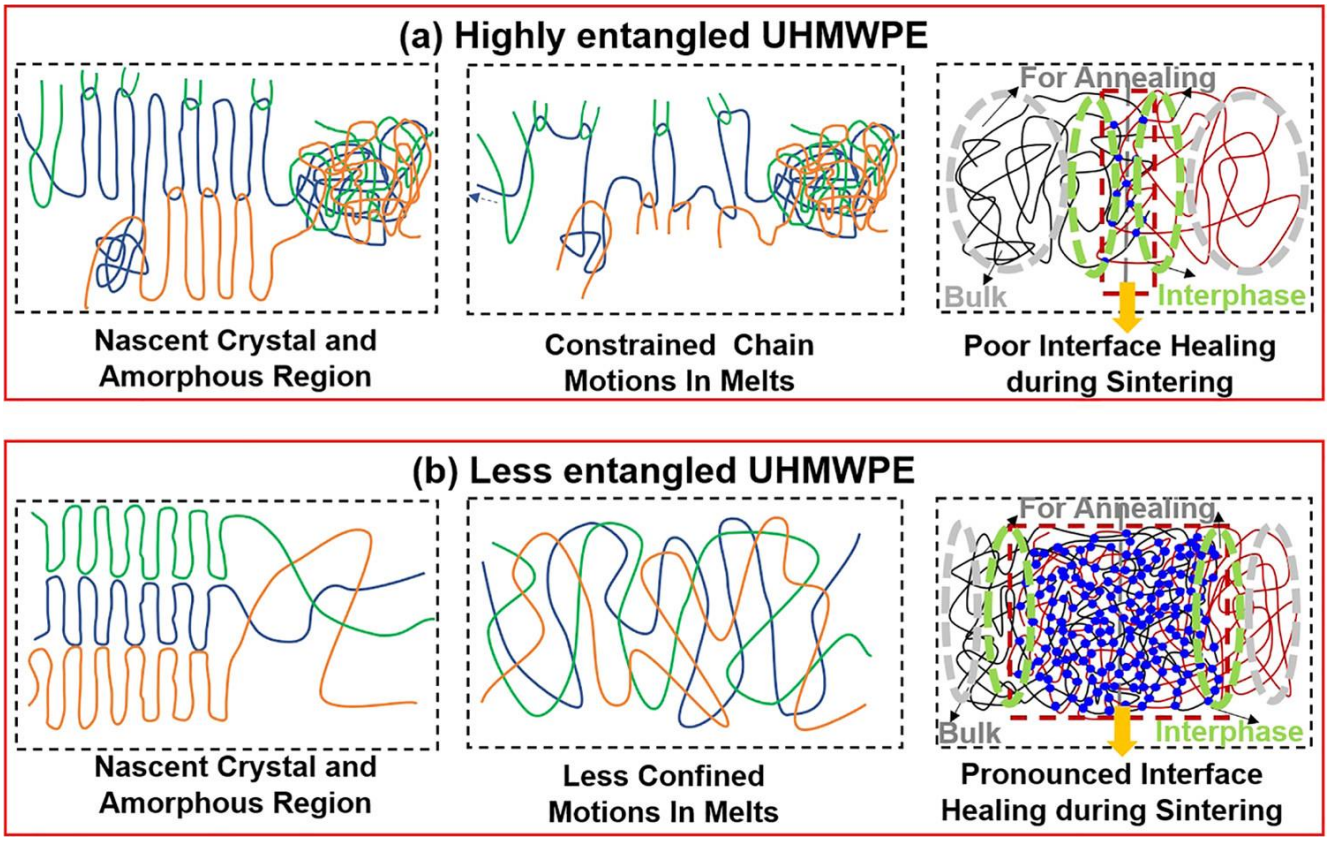

Figure 1.7. Schematic illustration for the influence of the initial entanglement state: (a) highly entangled state and (b) less entangled state. In the highly entangled state, a large number of entanglements in the amorphous regions strongly constrain chain mobility, resulting in poor interfacial fusion. In contrast, in the less entangled state, the less constrained chain mobility promotes rapid chain diffusion driven by an increase in entropy, referred to as a "melt explosion" which enhances interfacial fusion. Reproduced from Ref.64.

1.3.6. Higher-order structure of polyolefins

Crystalline polymers and semi-crystalline polymers form hierarchical structures ranging from the nanometer to the micrometer scale through molecular self-assembly during crystallization (Figure 1.8). In polyethylene, the molecular chains align the c-axis of orthorhombic unit cell, with characteristic reflections from the (200) and (110) lattice planes.[99] The chains repeatedly fold to form fold-chain crystals (FCC), typically 5–30 nm thick, which can stack into larger lamellar assemblies.[99] When the lamellar structures aggregate on the macroscopic scale, they form spherulites,[100,101] typically a few to several tens of micrometers in diameter, consisting of radially oriented crystalline lamellae and interlamellar amorphous regions that grow in multiple directions from a nucleation point, resembling the spokes of a wheel.

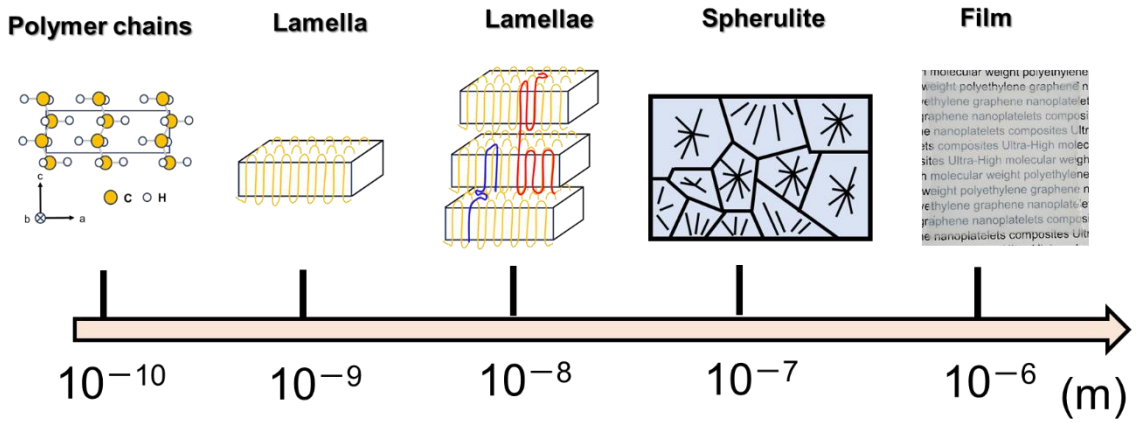

Figure 1.8. Schematic illustration of the hierarchical structure of crystalline polymers and semi-crystalline polymers, showing the structural evolution from molecular chains to lamellae, spherulites, and polymer films.

It is well known that when the crystallization rate is slow, large and well-ordered spherulites are formed,[102,103] leading to reduced light transmittance due to light scattering and decreased toughness because of stress concentration at interspherulitic boundaries.[104,105] Conversely, when the crystallization rate is high, the resulting spherulites are smaller, resulting in less light

scattering and improved toughness due to fewer interspherulitic boundaries. Based on these structural characteristics, polyethylene films with thicknesses exceeding several hundred micrometers are often fabricated, and their macroscopic mechanical properties are evaluated through tensile, bending, and compression tests.

During tensile deformation, the tensile stress (σ_s) and strain (ε) are defined as Equations (1.3) and (1.4):

$$\sigma_s = F/A \quad (1.3),$$

where σ_s is the stress (N m^{-2} or Pa), F is a force (N), and A is the area (m^{-2}).

$$\varepsilon = (L - L_0)/L_0 \quad (1.4),$$

where ε is the strain, L is a stretched length (mm), and L_0 is an initial length (mm).

A representative stress-strain curve is shown below (Figure 1.9). In the elastic region (region I), stress increases linearly with strain according to Hooke's law, mainly due to the stretching of amorphous tie chains and elastic deformation of lamellar stacks.[106,107] From the slope of this linear portion, the elastic modulus, an indicator of material stiffness, can be determined. In this region, the crystalline domains of polymer chains are stretched, and a small strain results in a rapid increase in stress. Beyond region I, the relationship between stress and strain deviates from Hooke's law, entering region II, where linearity is lost. In this region, the stress reaches a maximum and then decreases with increasing strain. This peak point is referred to as the yield stress, marking the onset of plastic deformation.[108] This stress reduction occurs because lamellae begin to shear and fragment, allowing molecular chains to slip between crystalline and amorphous phases.[107] Subsequently, in region III, as strain continues to increase, both amorphous and crystalline regions are stretched, leading to molecular chain alignment and stress transfer through taut-tie molecules, which causes stress to rise again. This phenomenon is generally referred to as strain hardening.[108]

Two main interpretations exist for the mechanism of strain hardening—rubber elasticity and plastic deformation (Figure 1.10). Kimura *et al*.[108] investigated this phenomenon by combining temperature-modulated in situ Raman spectroscopy with tensile testing, discussing strain hardening from both perspectives. They found that below the crystal relaxation temperature, the taut-tie molecules in the amorphous regions between lamellae transmit stress. As strong tensile forces act on these taut-tie molecules, molecular chains are pulled out from the crystalline domains. Consequently, with increasing strain, the fraction of taut-tie chains that bear load increases, resulting in a higher elastic modulus. This mechanism explains the occurrence of strain hardening. Conversely, above the crystal relaxation temperature, crystal relaxation leads to fragmentation of crystalline domains into smaller crystallites, and stretching promotes plastic flow and slippage among these fragments. Thus, strain hardening elasticity shows a negative correlation with stretching temperature above the melting-relaxation transition temperature.

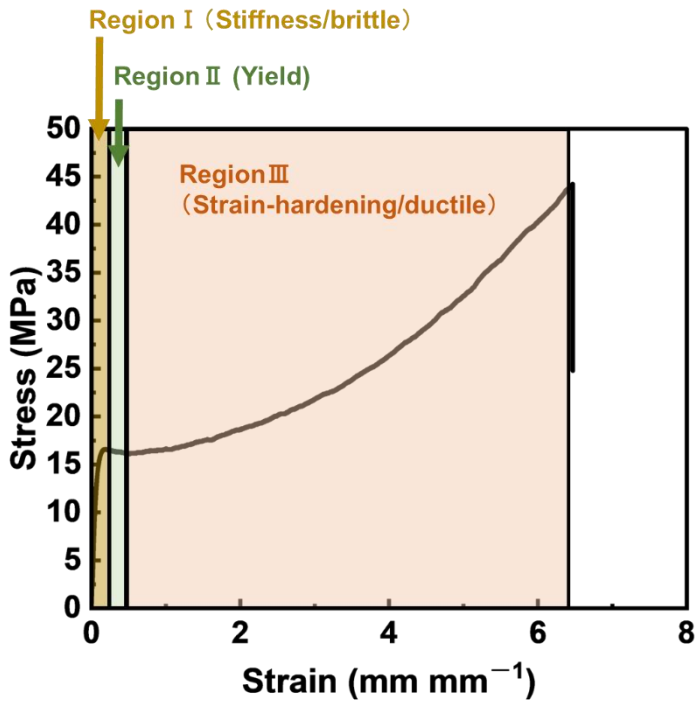

Figure 1.9. Representative stress-strain curve. Regions I, II, and III correspond to the elastic deformation, yielding, and plastic deformation regions, respectively.

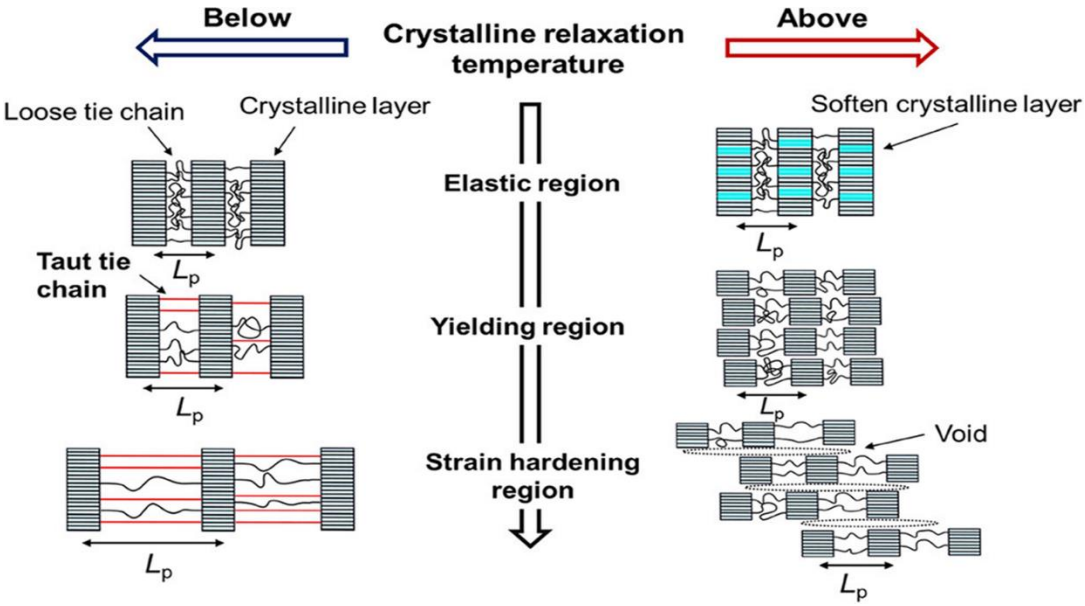

Figure 1.10. Schematic of the deformation mechanism during strain hardening above and below the crystal relaxation temperature. Reproduced from Ref.108.

1.4. Polymer nanocomposites

1.4.1. Definition of polymer nanocomposite (PNC) and key issue for PNC research

PNC[109] is a material consisting of a polymer matrix with nanoscale filler materials such as inorganic[55,110–114] and carbon fillers[10,16,115–121] dispersed throughout and intended to enhance physical properties,[117,120,122] designed to enhance physical properties such as electrical/thermal conductivity[16,110,117,119,122,123] and barrier properties,[124] and to achieve multifunctionality while maintain reasonable cost performance. Representative examples of nanofillers are layered silicates (clay),[125] metal oxide nanoparticles,[110,114] carbon nanotubes,[10,121] graphene[117,118] and graphene nanoplatelets (GNP).[16,119] These fillers have higher specific surface area and aspect ratio than conventional microscale fillers, influencing macroscopic physical properties through interfacial interactions with polymer chains.

The properties of polymer nanocomposites are strongly influenced by the dispersion state of the filler and the interfacial structure. PNC performance depend on filler morphologies (spherical, sheet-like, and fibrous), volume fraction filler, polymer structure, and polymer crystallinity.[114,126,127] When the filler is uniformly dispersed at the nanoscale without aggregation, the efficiency of stress transfer as well as the formation of thermal and electrical conduction pathways are improved, leading to enhanced overall material performance.[114,121,128] In contrast, when the agglomerates are formed, the interfacial area decreases, acting as defect sites that limit mechanical strength and conductivity.[16,120,129] Therefore, controlling the polymer-filler interface, including surface modification of the filler and/or polymer and optimization of filler dispersion, is essential.

1.4.2. Conductive polymer nanocomposites and percolation threshold

In general, well-controlled dispersion of fillers improves the mechanical properties of PNC by enabling homogeneous stress transfer and reducing stress concentration and crack propagation. On the other hand, enhancement of thermal and electrical conductivity in PNC requires the formation of continuous conductive pathways, which can be effectively achieved by structures such as segregated networks.[126,130] Therefore, the morphological control and filler distribution are critical issues in improving PNC performance. Achieving the desired properties at a low filler loadings is a key target of PNC research.[126]

With the increase of filler loading, the properties associated with the nanofiller, such as thermal and electrical conductivity, generally increase. However, higher filler content deteriorates mechanical performance due to disruption of polymer network.[16] As the filler loading increases, fillers approach each other, and there is a certain filler concentration called percolation threshold that they form network, leading to a sharp increase in conductivity and other related properties. (Figure 1.11).[16,126,131–137] Researchers have targeted uniform filler dispersion to maximize the polymer-filler interfacial area at low filler contents, while at higher filler loadings they have sought to reduce the percolation threshold and refine the network structure to enhance conductivity, which is especially important for conductive polymer nanocomposites.

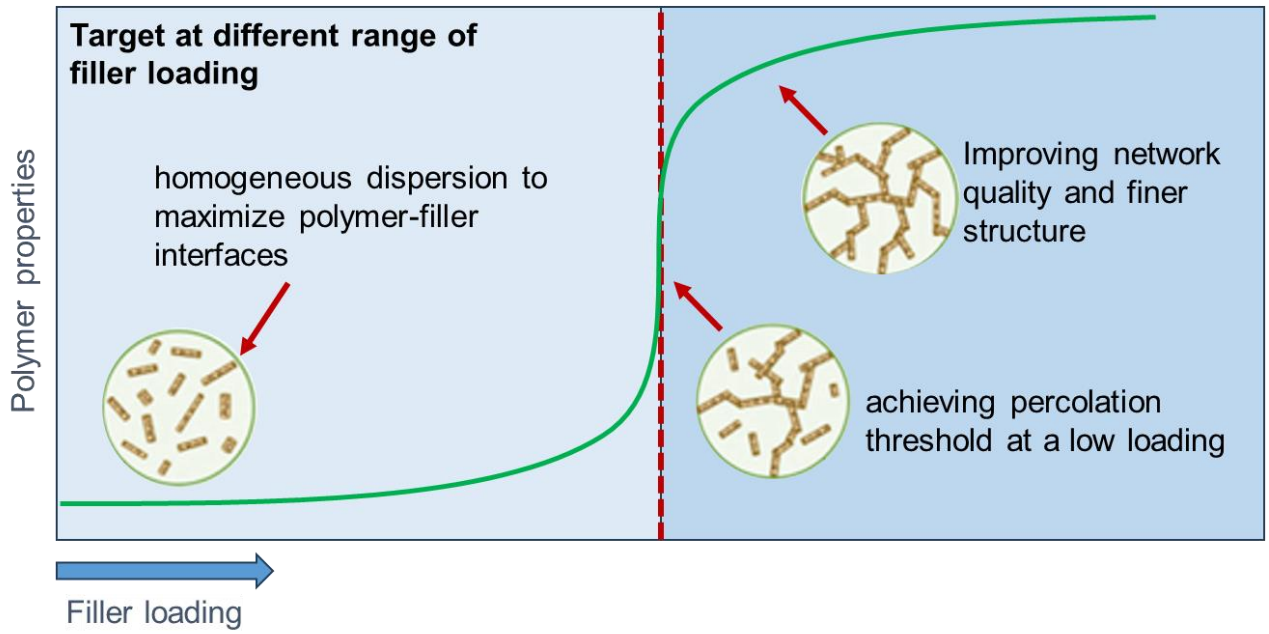

Figure 1.11. Schematic illustration of the effect of filler loading on polymer properties. At low filler content, fillers are well-dispersed, maximizing polymer-filler interactions. As loading approaches the percolation threshold, a connected network forms even at low filler content, A further increase in loading leads to a finer, higher-quality filler network and enhanced polymer properties.

1.4.3. UHMWPE nanocomposites

Due to its extremely high molecular weight and poor melt flowability, UHMWPE is often processed in powder form. When conductive fillers are mixed with UHMWPE through dry-mixing[137] or latex-based blending[131,132,136] methods, the fillers tend to localize at the interfaces between polymer particles, forming a so-called segregated structure. This morphology is advantageous for achieving high electrical and thermal conductivities[138,139] because it allows the formation of effective conductive pathways at low filler contents, thereby significantly reducing the percolation threshold. [16,126,131–137]

However, such segregated structures generally exhibit poor mechanical properties due to insufficient interparticle fusion and limited chain entanglement.[16] Moreover, few reports have investigated the correlation between mechanical properties and electrical/thermal conductivities,[16,130] which is crucial for developing practically applicable UHMWPE-based conductive nanocomposites, as most previous works have mainly focused on enhancing conductivity at high filler loadings and investigating composite morphology.[138,139]

1.5. Purpose of this thesis

UHMWPE is a linear polyethylene with a molecular weight exceeding several million g mol^{-1}. The extremely long molecular chains provide UHMWPE with unique properties such as outstanding mechanical strength, excellent wear resistance, and self-lubricating behavior. Despite these remarkable functional properties, UHMWPE suffers from poor processability due to severe chain entanglement and extremely low melt flow. As a result, conventional processing techniques such as injection molding, blow molding, and extrusion molding are difficult to apply. To address these challenges, this study focuses on the synthesis and application of a novel form of UHMWPE, termed microfine UHMWPE, which consists of submicron-sized particles with reduced chain entanglement. The UHMWPE was synthesized using nanosized Ziegler–Natta catalysts whose active sites were finely tuned to control molecular architecture and reduce interchain entanglement. Using this microfine UHMWPE, conductive polymer nanocomposites were fabricated, and their mechanical properties as well as electrical and thermal conductivities were systematically investigated in Chapters 2 and 3. In Chapter 4, the potential use of microfine UHMWPE as a filler is examined for the first time. In Chapter 2, the dispersion strategy of conductive fillers was studied using three types of polymer matrices: conventional UHMWPE, microfine UHMWPE, and their mixed systems. As discussed in Section 1.3.1 and 1.4.3, UHMWPE exhibits poor flowability, which causes

fillers to segregate at interparticle boundaries. Therefore, the particle size of the matrix (i.e., the size ratio between the matrix and filler) strongly influences the filler distribution. Controlling this distribution enables not only the optimization of mechanical properties but also the tuning of the electrical percolation threshold. Chapter 3 explores the effects of sintering temperature and duration on the morphology of UHMWPE and investigates how these parameters influence the thermal conductivity of UHMWPE-based nanocomposites. By optimizing the sintering conditions, nanocomposites with improved mechanical strength were obtained. Furthermore, the stretchability of these materials was examined below the melting temperature to fabricate fibers from UHMWPE-based films. In Chapter 4, the potential use of microfine UHMWPE as a filler was investigated for the first time. The synthesized microfine UHMWPE has an average particle size of approximately 500 nm, which is comparable to that of conventional nanofillers. Due to its relatively low melting point (~140 °C), smaller UHMWPE is expected to exhibit unique film morphologies and physical properties when used as a filler. Specifically, UHMWPE was melt-blended with PP using a twin-screw extruder, followed by hot pressing to fabricate 200 μm-thick films. The resulting composites were characterized by microscopic observation, differential scanning calorimetry, and tensile testing to analyze the phase morphology, thermal behavior, and mechanical performance of the UHMWPE/PP blend. Finally, Chapter 5 summarizes the structure-property design of UHMWPE and its composites achieved through particle design and structural control, drawing upon the findings discussed in Chapters 2-4.

References

(1) Tardy, B. L.; Mattos, B. D.; Otoni, C. G.; Beaumont, M.; Majoinen, J.; Kämäräinen, T.; Rojas, O. J. Deconstruction and Reassembly of Renewable Polymers and Biocolloids into Next Generation Structured Materials. *Chem. Rev.* **2021**, *121*, 14088–14188. https://doi.org/10.1021/acs.chemrev.0c01333.

(2) Satoh, K.; Kamigaito, M. Stereospecific Living Radical Polymerization: Dual Control of Chain Length and Tacticity for Precision Polymer Synthesis. *Chem. Rev.* **2009**, *109*, 5120–5156. https://doi.org/10.1021/cr900115u.

(3) Wang, Z.; Li, B.; Liu, S.; Zeng, J.; Müller, A. J.; Zhu, C.; Xu, J. Origin of Different Crystal Orientations of Ultrahigh-Molecular-Weight Polyethylene during Uniaxial Stretching: The Effect of Entanglements and Chains Tilt. *Macromolecules* **2025**, *58*, 3841–3848. https://doi.org/10.1021/acs.macromol.5c00224.

(4) 高松秀機. 創造は天才だけのものか　模倣は創造への第一歩; 株式会社化学同人, **1992**.

(5) Gao, Y.; Liu, W.; Zhu, S. Thermoplastic Polyolefin Elastomer Blends for Multiple and Reversible Shape Memory Polymers. *Ind. Eng. Chem. Res.* **2019**, *58*, 19495–19502. https://doi.org/10.1021/acs.iecr.9b03979.

(6) Gao, Y.; Jiang, Z.; Zhang, J.; Tan, H.; Jin, J.; Jiang, W. Models and Theories Regarding the Brittle-Ductile Transition of Rubber-Toughened Thermoplastics and Their Application in the Design of High-Impact Polymer Composites with Balanced Toughness and Rigidity. *Polym. Sci. Technol.* **2025**, *1*, 314–329. https://doi.org/10.1021/polymscitech.5c00023.

(7) Jiang, J.; Zhu, L.; Zhu, L.; Zhang, H.; Zhu, B.; Xu, Y. Antifouling and Antimicrobial Polymer Membranes Based on Bioinspired Polydopamine and Strong Hydrogen-Bonded Poly(*N*-vinyl pyrrolidone). *ACS Appl. Mater. Interfaces* **2013**, *5*, 12895–12904. https://doi.org/10.1021/am403405c.

(8) Roy, M.; Wilsens, C. H. R. M.; Leoné, N.; Rastogi, S. Use of Bis(pyrrolidone)-Based Dicarboxylic Acids in Poly(ester-amide)-Based Thermosets: Synthesis, Characterization, and Potential Route for Their Chemical Recycling. *ACS Sustainable Chem. Eng.* **2019**, *7*, 8842–8852. https://doi.org/10.1021/acssuschemeng.9b00850.

(9) Li, Y.; Han, Y.; Pang, J.; Jin, D.; Sun, Y.; Li, Z. Electric Field Assist on Enhancing the Electrical Breakdown Strength of Cross-Linked Polyethylene for Power Cable Insulation. *Macromolecules* **2024**, *57*, 5497–5506. https://doi.org/10.1021/acs.macromol.4c00358.

(10) Panahi-Sarmad, M.; Noroozi, M.; Abrisham, M.; Eghbalinia, S.; Teimoury, F.; Bahramian, A. R.; Dehghan, P.; Sadri, M.; Goodarzi, V. A Comprehensive Review on Carbon-Based Polymer Nanocomposite Foams as Electromagnetic Interference Shields and Piezoresistive Sensors. *ACS Appl. Electron. Mater.* **2020**, *2*, 2318–2350. https://doi.org/10.1021/acsaelm.0c00490.

(11) Ohsedo, Y.; Oono, M.; Saruhashi, K.; Watanabe, H.; Miyamoto, N. New composite thixotropic hydrogel composed of a polymer hydrogelator and a nanosheet. *R. Soc. open sci.* **2017**, *4*, 171117. https://doi.org/10.1098/rsos.171117.

(12) Yu, Y.; Peng, S.; Blanloeuil, P.; Wu, S.; Wang, C. H. Wearable Temperature Sensors with Enhanced Sensitivity by Engineering Microcrack Morphology in PEDOT:PSS-PDMS Sensors. *ACS Appl. Mater. Interfaces* **2020**, *12*, 36578–36588. https://doi.org/10.1021/acsami.0c07649.

(13) Sun, B.; Li, J.; Guo, Y.; Li, H.; Mi, H. Y.; Dong, B.; Liu, C.; Shen, C. Superhydrophobic UHMWPE Foams with High Mechanical Robustness and Durability Fabricated by Supercritical CO_2Foaming. *ACS Sustainable Chem. Eng.* **2021**, *9*, 12663–12673. https://doi.org/10.1021/acssuschemeng.1c04573.

(14) Shibasaki, Y.; Mori, T.; Fujimori, A.; Jikei, M.; Sawada, H.; Oishi, Y. Poly(amide-ether) Thermoplastic Elastomers Based on Monodisperse Aromatic Amide Hard Segments as Shape-Memory and Moisture-Responsive Materials. *Macromolecules* **2018**, *51*, 9430–9441. https://doi.org/10.1021/acs.macromol.8b01817.

(15) Amada, K.; Mai, L. T. T.; Chammingkwan, P.; Taniike, T. Conductive and Stretchable Ultra-High Molecular Weight Polyethylene Nanocomposites through Controlled Filler Distribution from Homogeneous to Semi-Segregated Networks. *ACS Appl. Eng. Mater.***2025**, 3, 547–559. https://doi.org/10.1021/acsaenm.4c00817.

(16) Alam, F.; Choosri, M.; Gupta, T. K.; Varadarajan, K. M.; Choi, D.; Kumar, S. Electrical, mechanical and thermal properties of graphene nanoplatelets reinforced UHMWPE nanocomposites. *Mater. Sci. Eng., B* **2019**, *241*, 82–91. https://doi.org/10.1016/j.mseb.2019.02.011.

(17) Siracusa, V.; Blanco, I. Bio-Polyethylene (Bio-PE), Bio-Polypropylene (Bio-PP) and Bio-Poly(ethylene terephthalate) (Bio-PET): Recent Developments in Bio-Based Polymers Analogous to Petroleum-Derived Ones for Packaging and Engineering Applications. *Polymers* **2020**, *12*, 1641. https://doi.org/10.3390/polym12081641.

(18) Klapper, M.; Joe, D.; Nietzel, S.; Krumpfer, J. W.; Müllen, K. Olefin Polymerization with Supported Catalysts as an Exercise in Nanotechnology. *Chem. Mater*. **2014**, *26*, 802–819. https://doi.org/10.1021/cm402309z.

(19) Wang, X.; Hu, S.; Guo, Y.; Li, G.; Xu, R. Toughened High-Flow Polypropylene with Polyolefin-Based Elastomers. *Polymers* **2019**, *11*, 1976. https://doi.org/10.3390/polym11121976.

(20) Langlais, M.; Baulu, N.; Dronet, S.; Dire, C.; Jean-Baptiste-dit-Dominique, F.; Albertini, D.; D'Agosto, F.; Montarnal, D.; Boisson, C. Multiblock Copolymers Based on Highly Crystalline Polyethylene and Soft Poly(ethylene-*co*-butadiene) Segments: Towards Polyolefin Thermoplastic Elastomers. *Angew. Chem., Int. Ed.* **2023**, *62*, e202310437. https://doi.org/10.1002/anie.202310437.

(21) Delferro, M.; Marks, T. J. Multinuclear Olefin Polymerization Catalysts. *Chem. Rev*. **2011**, *111*, 2450–2485. https://doi.org/10.1021/cr1003634.

(22) George Wypych. *Handout of Polymers, 3rd Edition*, 3rd ed.; ChemTec Publishing, **2022**.

(23) Long, C.; Dong, Z.; Liu, X.; Yu, F.; Shang, Y.; Wang, K.; Feng, S.; Hou, X.; He, C.; Chen, Z.-R. Simultaneous enhancement in processability and mechanical properties of polyethylenes via tuning the molecular weight distribution from unimodal to bimodal shape. *Polymer* **2022**, *258*, 125287. https://doi.org/10.1016/j.polymer.2022.125287.

(24) Zou, C.; Dai, S.; Chen, C. Ethylene Polymerization and Copolymerization Using Nickel 2-Iminopyridine-*N*-oxide Catalysts: Modulation of Polymer Molecular Weights and Molecular-Weight Distributions. *Macromolecules* **2018**, *51*, 49–56. https://doi.org/10.1021/acs.macromol.7b02156.

(25) Natta, G. Properties of isotactic, atactic, and stereoblock homopolymers, random and block copolymers of α-olefins. *J. Polym. Sci.* **1959**, *34*, 531–549. https://doi.org/10.1002/pol.1959.1203412738.

(26) Stürzel, M.; Mihan, S.; Mülhaupt, R. From Multisite Polymerization Catalysis to Sustainable Materials and All-Polyolefin Composites. *Chem. Rev*. **2016**, *116*, 1398–1433. https://doi.org/10.1021/acs.chemrev.5b00310.

(27) Chammingkwan, P.; Bando, Y.; Terano, M.; Taniike, T. Nano-Dispersed Ziegler-Natta Catalysts for 1 μm-Sized Ultra-High Molecular Weight Polyethylene Particles. *Front. Chem.* **2018**, *6*, 524. https://doi.org/10.3389/fchem.2018.00524.

(28) Chammingkwan, P.; Kogawa, T.; Miyamoto, Y.; Jinnai, T.; Mai, L. T. T.; Wada, T.; Taniike, T. Key Role of Catalyst Pore Structure in Rubber Retention and Distribution of High-Impact Polypropylene Copolymer. *Ind. Eng. Chem. Res.* **2023**, *62*, 15469–15478. https://doi.org/10.1021/acs.iecr.3c02678.

(29) Gote, R. P.; Zhao, J.; Romano, D.; Rastogi, S. Solid-State Processing of In Situ Blended Prepolymer with Z-N Synthesized UHMWPE: Role of the Prepolymer. *Macromolecules* **2025**, *58*, 3604–3621. https://doi.org/10.1021/acs.macromol.4c03097.

(30) Antinucci, G.; Cannavacciuolo, F. D.; Ehm, C.; Budzelaar, P. H. M.; Cipullo, R.; Busico, V. $MgCl_2$-Supported Ziegler-Natta Catalysts for Propene Polymerization: Before Activation. *Macromolecules* **2024**, *57*, 5712–5719. https://doi.org/10.1021/acs.macromol.4c00932.

(31) Chammingkwan, P.; Thang, V. Q.; Terano, M.; Taniike, T. $MgO/MgCl_2/TiCl_4$ Core-Shell Catalyst for Establishing Structure-Performance Relationship in Ziegler-Natta Olefin Polymerization. *Top. Catal.* **2014**, *57*, 911–917. https://doi.org/10.1007/s11244-014-0251-2

(32) Chammingkwan, P.; Bando, Y.; Mai, L. T. T.; Wada, T.; Thakur, A.; Terano, M.; Sinthusai, L.; Taniike, T. Less Entangled Ultrahigh-Molecular-Weight Polyethylene Produced by Nano-Dispersed Ziegler-Natta Catalyst. *Ind. Eng. Chem. Res.* **2021**, *60*, 2818–2827. https://doi.org/10.1021/acs.iecr.0c05432.

(33) McDaniel, M. P. Influence of Catalyst Porosity on Ethylene Polymerization. *ACS Catal.* **2011**, *1*, 1394–1407. https://doi.org/10.1021/cs2003033.

(34) McDaniel, M. P. A Review of the Phillips Supported Chromium Catalyst and Its Commercial Use for Ethylene Polymerization. *Adv. Catal.* **2010**, *53*, 123–606. https://doi.org/10.1016/S0360-0564(10)53003-7.

(35) 外崎 究;谷池 俊明;寺野 稔. Phillips 触媒を用いたエチレン重合における分子量分布および分岐構造の制御因子; 高分子論文集 **2011**, *68*, 326–331. https://doi.org/10.1295/koron.68.326.

(36) Jongkind, M. K.; van Kessel, T.; Velthoen, M. E. Z.; Friederichs, N.; Weckhuysen, B. M. Tuning the Redox Chemistry of a Cr/SiO_2 Phillips Catalyst for Controlling Activity, Induction Period and Polymer Properties. *ChemPhysChem* **2020**, *21*, 1665–1674. https://doi.org/10.1002/cphc.202000488.

(37) Zheng, X.; Smit, M.; Chadwick, J. C.; Loos, J. Fragmentation Behavior of Silica-Supported Metallocene/MAO Catalyst in the Early Stages of Olefin Polymerization. *Macromolecules* **2005**, *38*, 4673–4678. https://doi.org/10.1021/ma0502912.

(38) Kaminsky, W. Discovery of Methylaluminoxane as Cocatalyst for Olefin Polymerization. *Macromolecules* **2012**, *45*, 3289–3297. https://doi.org/10.1021/ma202453u.

(39) Tisse, V. F.; Boisson, C.; Prades, F.; McKenna, T. F. L. A systematic study of the kinetics of polymerisation of ethylene using supported metallocene catalysts. *Chem. Eng. J.* **2010**, *157*, 194–203. https://doi.org/10.1016/j.cej.2009.12.006.

(40) Coates, G. W. Precise Control of Polyolefin Stereochemistry Using Single-Site Metal Catalysts. *Chem. Rev.* **2000**, *100*, 1223–1252. https://doi.org/10.1021/cr990286u.

(41) Kaminsky, W. The discovery of metallocene catalysts and their present state of the art. *J. Polym. Sci., Part A: Polym. Chem.* **2004**, *42*, 3911–3921. https://doi.org/10.1002/pola.20292.

(42) Antonov, A. A.; Bryliakov, K. P. Post-metallocene catalysts for the synthesis of ultrahigh molecular weight polyethylene: recent advances. *Eur. Polym. J.* **2021**, *142*, 110162. https://doi.org/10.1016/j.eurpolymj.2020.110162.

(43) Yang, H.; Lolage, S.; van der Eem, J.; Rastogi, S.; Romano, D. Silica-supported catalyst for the synthesis of low entangled UHMWPE suitable for solid-state processing. *Mol. Catal.* **2024**, *552*, 113668. https://doi.org/10.1016/j.mcat.2023.113668.

(44) Li, W.; Chen, T.; Guan, C.; Gong, D.; Mu, J.; Chen, Z. R.; Zhou, Q. Influence of Polyhedral Oligomeric Silsesquioxane Structure on the Disentangled State of Ultrahigh Molecular Weight Polyethylene Nanocomposites during Ethylene in Situ Polymerization. *Ind. Eng. Chem. Res.* **2015**, *54*, 1478–1486. https://doi.org/10.1021/ie504273r.

(45) Klosin, J.; Fontaine, P. P.; Figueroa, R. Development of Group IV Molecular Catalysts for High Temperature Ethylene-α-Olefin Copolymerization Reactions. *Acc. Chem. Res.* **2015**, *48*, 2004–2016. https://doi.org/10.1021/acs.accounts.5b00065.

(46) Patel, K.; Chikkali, S. H.; Sivaram, S. Ultrahigh molecular weight polyethylene: Catalysis, structure, properties, processing and applications. *Prog. Polym. Sci.*. **2020**, *109*, 101290. https://doi.org/10.1016/j.progpolymsci.2020.101290.

(47) Sui, Y.; Li, J.; Qiu, Z.; Cui, Y.; Cong, C.; Meng, X.; Ye, H.; Zhou, Q. Effects of the sintering temperature on the superior cryogenic toughness of ultra-high molecular weight polyethylene (UHMWPE). *Chem. Eng. J.* **2022**, *444*, 136366. https://doi.org/10.1016/j.cej.2022.136366.

(48) Chen, Y.; Li, W.; Zhang, L.; Ye, C.; Tao, G.; Ren, C.; Jiang, B.; Wang, J.; Yang, Y. In Situ Synthesized Self-Reinforced HDPE/UHMWPE Composites with High Content of Less Entangled UHMWPE and High Gradient-Distributed Oriented Structures. *ACS Appl. Polym. Mater.* **2023**, 5, 88–98. https://doi.org/10.1021/acsapm.2c01213.

(49) Diop, M. F.; Burghardt, W. R.; Torkelson, J. M. Well-mixed blends of HDPE and ultrahigh molecular weight polyethylene with major improvements in impact strength achieved via solid-state shear pulverization. *Polymer* **2014**, *55*, 4948–4958. https://doi.org/10.1016/j.polymer.2014.07.050.

(50) Lee, K. H.; Sinha, T. K.; Choi, K. W.; Oh, J. S. Ultra-high-molecular-weight polyethylene reinforced polypropylene and polyamide composites toward developing low-noise automobile interior. *J. Appl. Polym. Sci.* **2020**, *137*, 48720. https://doi.org/10.1002/app.48720.

(51) Chen, X.; Wang, X.; Cao, C.; Yuan, Z.; Yu, D.; Li, F.; Chen, X. Elongational Flow Field Processed Ultrahigh Molecular Weight Polyethylene/Polypropylene Blends with Distinct Interlayer Phase for Enhanced Tribological Properties. *Polymers* **2021**, *13*, 1933. https://doi.org/10.3390/polym13121933.

(52) Bracco, P.; Bellare, A.; Bistolfi, A.; Affatato, S. Ultra-High Molecular Weight Polyethylene: Influence of the Chemical, Physical and Mechanical Properties on the Wear Behavior. A Review. *Materials* **2017**, *10*, 791. https://doi.org/10.3390/ma10070791.

(53) Cheng, H.; Cao, C.; Zhang, Q.; Wang, Y.; Liu, Y.; Huang, B.; Sun, X.-L.; Guo, Y.; Xiao, L.; Chen, Q.; Qian, Q. Enhancement of Electromagnetic Interference Shielding Performance and Wear Resistance of the UHMWPE/PP Blend by Constructing a Segregated Hybrid Conductive Carbon Black-Polymer Network. *ACS Omega* **2021**, *6*, 15078–15088. https://doi.org/10.1021/acsomega.1c01240.

(54) Li, B.; Fan, C.; Wang, H.; Ren, M.; Wu, P.; Wang, X.; Liu, X. A composite with excellent tribological performance derived from oxy-fluorinated UHMWPE particle/polyurethane. *RSC Adv.* **2014**, *4*, 9321–9325. https://doi.org/10.1039/c3ra47715k.

(55) Ren, X.; Li, H.; Mi, H. Y.; Guo, Y.; Jing, X.; Dong, B.; Liu, C.; Shen, C. Superhydrophobic ultra-high molecular weight polyethylene nanocomposite foams fabricated by supercritical CO_2 foaming for selective oil absorption. *Appl. Surf. Sci.* **2022**, *602*, 154344. https://doi.org/10.1016/j.apsusc.2022.154344.

(56) Lekkala, S.; Inverardi, N.; Grindy, S. C.; Hugard, S.; Muratoglu, O. K.; Oral, E. Irradiation Behavior of Analgesic and Nonsteroidal Anti-Inflammatory Drug-Loaded UHMWPE for Joint Replacement. *Biomacromolecules* **2024**, *25*, 2312–2322. https://doi.org/10.1021/acs.biomac.3c01179.

(57) Sharma, V.; Bose, S.; Kundu, B.; Bodhak, S.; Mitun, D.; Balla, V. K.; Basu, B. Probing the Influence of ?-Sterilization on the Oxidation, Crystallization, Sliding Wear

Resistance, and Cytocompatibility of Chemically Modified Graphene-Oxide-Reinforced HDPE/UHMWPE Nanocomposites and Wear Debris. *ACS Biomater. Sci. Eng.* **2020**, *6*, 1462–1475. https://doi.org/10.1021/acsbiomaterials.9b01327.

(58) Rastogi, S.; Yao, Y.; Ronca, S.; Bos, J.; van der Eem, J. Unprecedented High-Modulus High-Strength Tapes and Films of Ultrahigh Molecular Weight Polyethylene via Solvent-Free Route. *Macromolecules* **2011**, *4*, 5558–5568. https://doi.org/10.1021/ma200667m.

(59) Knoll, J.; Heim, H.-P. Analysis of the Machine-Specific Behavior of Injection Molding Machines. *Polymers* **2024**, *16,* 54. https://doi.org/10.3390/polym16010054.

(60) Cherrington, R.; Goodship, V. 1-Introduction to Multifunctionality and Manufacture. *Design and Manufacture of Plastic Components for Multifunctionality*; Elsevier **2016**, 1–18. https://doi.org/10.1016/B978-0-323-34061-8.00001-6.

(61) Quan, Y.; Shen, R.; Ma, R.; Zhang, Z.; Wang, Q. Sustainable and Efficient Manufacturing of Metal-Organic Framework-Based Polymer Nanocomposites by Reactive Extrusion. *ACS Sustainable Chem. Eng.* **2022**, *10*, 7216–7222. https://doi.org/10.1021/acssuschemeng.2c01720.

(62) Taniike, T.; Funako, T.; Terano, M. Multilateral characterization for industrial Ziegler-Natta catalysts toward elucidation of structure-performance relationship. *J. Catal.* **2014**, *311*, 33–40. https://doi.org/10.1016/j.jcat.2013.10.023.

(63) Klaue, A.; Kruck, M.; Friederichs, N.; Bertola, F.; Wu, H.; Morbidelli, M. Insight into the Synthesis Process of an Industrial Ziegler-Natta Catalyst. *Ind. Eng. Chem. Res.* **2019**, *58*, 886–896. https://doi.org/10.1021/acs.iecr.8b05296.

(64) Wang, H.; Yan, X.; Tang, X.; Ma, Y.; Fan, X.; Li, W.; Yu, W.; Wang, J.; Yang, Y. Contribution of the Initially Entangled State and Particle Size to the Sintering Kinetics of UHMWPE. *Macromolecules* **2022**, *55*, 1310–1320. https://doi.org/10.1021/acs.macromol.1c02058.

(65) Litvinov, V. M.; Xu, J.; Melian, C.; Demco, D. E.; Möller, M.; Simmelink, J. Morphology, Chain Dynamics, and Domain Sizes in Highly Drawn Gel-Spun Ultrahigh Molecular Weight Polyethylene Fibers at the Final Stages of Drawing by SAXS, WAXS, and ^{1}H Solid-State NMR. *Macromolecules* **2011**, *44*, 9254–9266. https://doi.org/10.1021/ma201888f.

(66) Smith, P.; Lemstra, P. J. Ultra-high strength polyethylene filaments by solution spinning/drawing. 3. Influence of drawing temperature. *Polymer* **1980**, *21*, 1341–1343. https://doi.org/10.1016/0032-3861(80)90205-0.

(67) Ma, Z.; Wang, W.; Pang, W.; Liao, D.; Zou, C. Preparation of Toughened Bimodal Ultrahigh-Molecular-Weight Polyethylene by a Coanchoring Strategy. *ACS Appl. Polym. Mater.* **2024**, *6*, 13210–13216. https://doi.org/10.1021/acsapm.4c02479.

(68) Hees, T.; Schirmeister, C. G.; Pfohl, P.; Hofmann, D.; Muelhaupt, R. Self-Reinforcement via 1D Nanostructure Formation during Melt Blending of Thermoplastics and Thermoplastic Elastomers with Nanophase-Separated UHMWPE/HDPE Wax Reactor

Blends. *ACS Appl. Polym. Mater.* **2021**, *3*, 3455–3464. https://doi.org/10.1021/acsapm.1c00384.

(69) Hofmann, D.; Kurek, A.; Thomann, R.; Schwabe, J.; Mark, S.; Enders, M.; Hees, T.; Mülhaupt, R. Tailored Nanostructured HDPE Wax/UHMWPE Reactor Blends as Additives for Melt-Processable All-Polyethylene Composites and in Situ UHMWPE Fiber Reinforcement. *Macromolecules* **2017**, *50*, 8129–8139. https://doi.org/10.1021/acs.macromol.7b01891.

(70) Wu, S. L.; Qiao, J.; Guan, J.; Chen, H. M.; Wang, T.; Wang, C.; Wang, Y. Nascent disentangled UHMWPE: Origin, synthesis, processing, performances and applications. *Eur. Polym. J.* **2023**, *184*, 111799. https://doi.org/10.1016/j.eurpolymj.2022.111799.

(71) Romano, D.; Ronca, S.; Rastogi, S. A Hemi-Metallocene Chromium Catalyst with Trimethylaluminum-Free Methylaluminoxane for the Synthesis of Disentangled Ultra-High Molecular Weight Polyethylene. *Macromol. Rapid Commun.* **2015**, *36*, 327–331. https://doi.org/10.1002/marc.201400514.

(72) Chen, P.; Yang, H.; Chen, T.; Li, W. Weakly Entangled Ultrahigh Molecular Weight Polyethylene Prepared via Ethylene Extrusion Polymerization. *Ind. Eng. Chem. Res.* **2015**, *54*, 11024–11032. https://doi.org/10.1021/acs.iecr.5b03059.

(73) Gote, R. P.; Mandal, D.; Patel, K.; Chaudhuri, K.; Vinod, C. P.; Lele, A. K.; Chikkali, S. H. Judicious Reduction of Supported Ti Catalyst Enables Access to Disentangled Ultrahigh Molecular Weight Polyethylene. *Macromolecules* **2018**, *51*, 4541–4552. https://doi.org/10.1021/acs.macromol.8b00590.

(74) Bando, Y.; Chammingkwan, P.; Terano, M.; Taniike, T. Synthesis of Ultrahigh Molecular Weight Polyethylene Using MgO/$MgCl_2$/$TiCl_4$ Core–Shell Catalysts. *Macromol. Chem. Phys.* **2018**, *219*, 1800011. https://doi.org/10.1002/macp.201800011.

(75) Yue, Z.; Wang, N.; Cao, Y.; Li, W.; Dong, C. D. Reduced Entanglement Density of Ultrahigh-Molecular-Weight Polyethylene Favored by the Isolated Immobilization on the $MgCl_2$ (110) Plane. *Ind. Eng. Chem. Res.* **2020**, *59*, 3351–3358. https://doi.org/10.1021/acs.iecr.9b06780.

(76) Pandey, A.; Champouret, Y.; Rastogi, S. Heterogeneity in the Distribution of Entanglement Density during Polymerization in Disentangled Ultrahigh Molecular Weight Polyethylene. *Macromolecules* **2011**, *44*, 4952–4960. https://doi.org/10.1021/ma2003689.

(77) Gote, R. P.; Romano, D.; van der Eem, J.; Zhao, J.; Zhou, F.; Rastogi, S. Unprecedented Mechanical Properties in Linear UHMWPE Using a Heterogeneous Catalytic System. *Macromolecules* **2023**, *56*, 361–378. https://doi.org/10.1021/acs.macromol.2c02215.

(78) Gote, R. P.; van der Eem, J.; Zhao, J.; Lolage, S.; Traidia, A.; Zhang, Y.; Romano, D.; Rastogi, S. Influence of Molecular Weight and Entanglement Density on the Creep Response of the Uniaxially Drawn Tapes of Dis-UHMWPE. *Macromolecules* **2023**, *56*, 6903–6919. https://doi.org/10.1021/acs.macromol.3c01180.

(79) Zhou, F.; Zhao, J.; Rastogi, S. Paradox in Sintering of Nascent Ultrahigh Molecular Weight Polymers in the Solid State. *Macromolecules* **2025**, *58*, 4602–4614. https://doi.org/10.1021/acs.macromol.5c00731.

(80) Philippaerts, A.; Ensinck, R.; Baulu, N.; Cordier, A.; Woike, K.; Berthoud, R.; De Cremer, G.; Severn, J. R. Influence of the particle size of the $MgCl_2$ support on the performance of Ziegler Catalysts in the polymerization of ethylene to ultra-high molecular weight polyethylene and the resulting polymer properties. *J. Polym. Sci., Part A: Polym. Chem.* **2017**, *55*, 2679–2690. https://doi.org/10.1002/pola.28674.

(81) Abboud, M.; Denifl, P.; Reichert, K.-H. Study of the morphology and kinetics of novel Ziegler-Natta catalysts for propylene polymerization. *J. Appl. Polym. Sci.* **2005**, *98*, 2191–2200. https://doi.org/10.1002/app.22412.

(82) Vestberg, T.; Denifl, P.; Wilén, C.-E. Porous versus novel compact Ziegler-Natta catalyst particles and their fragmentation during the early stages of bulk propylene polymerization. *J. Appl. Polym. Sci.* **2008**, *110*, 2021–2029. https://doi.org/10.1002/app.28411.

(83) Mckenna, T. F.; Soares, J. B. P. Single particle modelling for olefin polymerization on supported catalysts: A review and proposals for future developments; *Chem. Eng. Sci.* **2001**, *56*, 3931–3949. https://doi.org/10.1016/S0009-2509(01)00069-0.

(84) Liu, K.; De Boer, E. L.; Yao, Y.; Romano, D.; Ronca, S.; Rastogi, S. Heterogeneous Distribution of Entanglements in a Nonequilibrium Polymer Melt of UHMWPE: Influence on Crystallization without and with Graphene Oxide. *Macromolecules* **2016**, *49*, 7497–7509. https://doi.org/10.1021/acs.macromol.6b01173.

(85) Dong, P.; Zhang, Q.; Wang, K.; Zhu, B.-H.; Su, W.; Li, J. F.; Fu, Q. Pursuit of the correlation between yield strength and crystallinity in sintering-molded UHMWPE. *Polymer* **2021**, *215*,123352. https://doi.org/10.1016/j.polymer.2020.123352.

(86) Wang, Z.; Li, B.; Christakopoulos, F.; Xie, K.; Zhu, C.; Xu, J.; Müller, A. J. Structure Formation and Unexpected Ultrafast Re-Entanglement Dynamics of Disentangled Ultrahigh Molecular Weight Polyethylene. *Macromolecules* **2024**, *57*, 10240–10252. https://doi.org/10.1021/acs.macromol.4c01733.

(87) Deplancke, T.; Lame, O.; Rousset, F.; Aguili, I.; Seguela, R.; Vigier, G. Diffusion versus Cocrystallization of Very Long Polymer Chains at Interfaces: Experimental Study of Sintering of UHMWPE Nascent Powder. *Macromolecules* **2014**, *47*, 197–207. https://doi.org/10.1021/ma402012f.

(88) Deng, B.; Chen, L.; Zhong, Y.; Li, X.; Wang, Z. The effect of temperature on the structural evolution of ultra-high molecular weight polyethylene films with pre-reserved shish crystals during the stretching process. *Polymer* **2023**, *267*, 125690. https://doi.org/10.1016/j.polymer.2023.125690.

(89) Drakopoulos, S. X.; Forte, G.; Ronca, S. Relaxation Dynamics in Disentangled Ultrahigh Molecular Weight Polyethylene via Torsional Rheology. *Ind. Eng. Chem. Res.* **2020**, *59*, 4515–4523. https://doi.org/10.1021/acs.iecr.9b06401.

(90) Zhao, J.; Miyoshi, T.; Rastogi, S. Influence of Topological Constraints on the Segmental Motion in the Crystalline Region of Semicrystalline Ultra-High-Molecular-Weight Polyethylene. *Macromolecules* **2025**, *58*, 9300–9314. https://doi.org/10.1021/acs.macromol.5c01330.

(91) Litvinov, V.; Christakopoulos, F.; Lemstra, P. J. Disentangled Melt of Ultrahigh-Molecular-Weight Polyethylene: Fictitious or Real? *Macromolecules* **2024**, *57*, 3719–3730. https://doi.org/10.1021/acs.macromol.4c00271.

(92) Barron, D.; Birkinshaw, C. Ultra-high molecular weight polyethylene - Evidence for a three-phase morphology. *Polymer* **2008**, *49*, 3111–3115. https://doi.org/10.1016/j.polymer.2008.05.004.

(93) Zhang, H.; Zhao, S.; Yu, X.; Xin, Z.; Ye, C.; Li, Z.; Xia, J. Nascent Particle Sizes and Degrees of Entanglement Are Responsible for the Significant Differences in Impact Strength of Ultrahigh Molecular Weight Polyethylene. *J. Polym. Sci., Part B: Polym. Phys.* **2019**, *57*, 632–641. https://doi.org/10.1002/polb.24819.

(94) Yilmaz, G.; Uslu, E. A new approach for high-quality production of UHMWPE by applying powder vibration densification before sintering. *Powder Technol.* **2023**, *427*, 118741. https://doi.org/10.1016/j.powtec.2023.118741.

(95) Wang, W.; Wang, H.; Chen, J. Research on Chain Diffusion and Entanglement via Controlling the Sintering Process of Nascent UHMWPE. *Macromolecules* **2024**, *57*, 2205–2217. https://doi.org/10.1021/acs.macromol.3c02361.

(96) Rastogi, S.; Lippits, D. R.; Peters, G. W. M.; Graf, R.; Yao, Y.; Spiess, H. W. Heterogeneity in polymer melts from melting of polymer crystals. *Nat. Mater.* **2005**, *4*, 635–641. https://doi.org/10.1038/nmat1437.

(97) Yan, X.; Zhang, Y.; Tang, X.; Ren, C.; Li, W.; Wang, J.; Yang, Y. Interplay of Particle Size and Temperature on Low-Entanglement Ultrahigh-Molecular-Weight Polyethylene Sintering in Blended Compositions: Analysis of Entanglement and Crystal Structure. *Ind. Eng. Chem. Res.* **2023**, *62*, 7950–7961. https://doi.org/10.1021/acs.iecr.3c00845.

(98) Deplancke, T.; Lame, O.; Rousset, F.; Seguela, R.; Vigier, G. Mechanisms of Chain Reentanglement during the Sintering of UHMWPE Nascent Powder: Effect of Molecular Weight. *Macromolecules* **2015**, *48*, 5328–5338. https://doi.org/10.1021/acs.macromol.5b00618.

(99) Kanomi, S.; Marubayashi, H.; Miyata, T.; Jinnai, H. Reassessing chain tilt in the lamellar crystals of polyethylene. *Nat. Commun.* **2023**, *14*, 5531. https://doi.org/10.1038/s41467-023-41138-4.

(100) Liu, J.; Li, Y. Annealing-induced high impact toughness of isotactic polypropylene realized by introducing ultra-high molecular weight polyethylene. *Polym. Bull.* **2025**, *82*, 2229–2249. https://doi.org/10.1007/s00289-024-05621-2.

(101) Wang, J.; Niu, H.; Dong, J.; Du, J.; Han, C. C. Morphology and mechanical properties of polypropylene/poly (propylene-1-octene) in-reactor alloys prepared by Metallocene/Ziegler-Natta hybrid catalyst. *Polymer* **2012**, *53*, 1507–1516. https://doi.org/10.1016/j.polymer.2012.02.017.

(102) Speranza, V.; Salomone, R.; Pantani, R. Effects of Pressure and Cooling Rates on Crystallization Behavior and Morphology of Isotactic Polypropylene. *Crystals* **2023**, *13*, 922. https://doi.org/10.3390/cryst13060922.

(103) Pakula, T.; Kryszewski, M. Determination of the temperature dependence of spherulite growth rate in low-density polyethylene using the small-angle light scattering technique. *Eur. Polym. J.* **1976**, *12*, 47–51. https://doi.org/10.1016/0014-3057(76)90122-1.

(104) Ohlberg, S. M.; Roth, J.; Raff, R. A. V. Relationship between impact strength and spherulite growth in linear polyethylene. *J. Appl. Polym. Sci.* **1959**, *1*, 114–120. https://doi.org/10.1002/app.1959.070010118.

(105) Molnár, J.; Sepsi, Ö.; Erdei, G.; Lenk, S.; Ujhelyi, F.; Menyhárd, A. Modeling of light scattering and haze in semicrystalline polymers. *J. Polym. Sci.* **2020**, *58*, 1787–1795. https://doi.org/10.1002/pol.20200027.

(106) Kawai, T. Mechanism of Deformation of Crystalline Polymers. *J. Mater. Sci. Soc. Jpn*. **1966**, *15*, 335–339. https://doi.org/10.2472/jsms.15.335.

(107) Higuchi, Y.; Kubo, M. Deformation and Fracture Processes of a Lamellar Structure in Polyethylene at the Molecular Level by a Coarse-Grained Molecular Dynamics Simulation. *Macromolecules* **2017**, *50*, 3690–3702. https://doi.org/10.1021/acs.macromol.6b02613.

(108) Kimura, S.; Kida, T.; Takeshita, H.; Tokumitsu, K. Temperature Dependence of Strain-Hardening Behavior of Polyethylene Solids Evaluated by SAXS, WAXD, and Raman Spectroscopy. *Macromolecules* **2025**, *58*, 3151–3159. https://doi.org/10.1021/acs.macromol.5c00095.

(109) Kumar, S. K.; Benicewicz, B. C.; Vaia, R. A.; Winey, K. I. 50th Anniversary Perspective: Are Polymer Nanocomposites Practical for Applications? *Macromolecules* **2017**, *50*, 714–731. https://doi.org/10.1021/acs.macromol.6b02330.

(110) Zhang, X.; Maira, B.; Hashimoto, Y.; Wada, T.; Chammingkwan, P.; Thakur, A.; Taniike, T. Selective localization of aluminum oxide at interface and its effect on thermal conductivity in polypropylene/polyolefin elastomer blends. *Compos. B Eng.* **2019**, *162*, 662–670. https://doi.org/10.1016/j.compositesb.2019.01.043.

(111) Kiseleva, T.; Grigoreva, T.; Kovaliova, S.; Il'in, M.; Yakuta, E.; Devyatkina, E.; Malyshkina, I.; Ivanenko, I.; Vosmerikov, S.; Lyakhov, N. Dielectric Performance of UHMWPE-MgFe2O4 Composites Depending on Polymer Crystallinity, and the Concentration and Size of Mechanochemically Synthesized Ferrite Particles. *Powders* **2023**, *2*, 578–587. https://doi.org/10.3390/powders2030036.

(112) Drakopoulos, S. X.; Manika, G. C.; Nogales, A.; Kim, T.; Robbins, A. B.; Claudio, G.; Minnich, A. J.; Ezquerra, T. A.; Psarras, G. C.; Martin-Fabiani, I.; Ronca, S. Gold/ultra-high molecular weight polyethylene nanocomposites for electrical energy storage: Enhanced recovery efficiency upon uniaxial deformation. *J. Appl. Polym. Sci.* **2021**, *138*, 51232. https://doi.org/10.1002/app.51232.

(113) Celebi Efe, G.; Altinsoy, I.; Yener, S. Ç.; Yener, T.; Ipek, M.; Bindal, C.; Ucisik, A. H. Fabrication and Characterization of UHMWPE–Ni Composites for Enhanced Electromagnetic Interference Shielding. *Arab. J. Sci. Eng.* **2021**, *46*, 5455–5465. https://doi.org/10.1007/s13369-020-04952-2.

(114) Toyonaga, M.; Chammingkwan, P.; Terano, M.; Taniike, T. Well-Defined Polypropylene/Polypropylene-Grafted Silica Nanocomposites: Roles of Number and

Molecularweight of Grafted Chains on Mechanistic Reinforcement. *Polymers* **2016**, *8*, 300. https://doi.org/10.3390/polym8080300.

(115) Fu, C.; Zhang, R.; Tian, J.; Yang, Q.; Xue, P.; Chen, X. Polymer chain conformations in hybrid composites of UHMWPE incorporated by GNP/MWCNT. *J. Polym. Res.* **2023**, *30*, 245. https://doi.org/10.1007/s10965-023-03629-2.

(116) Gupta, T. K.; Choosri, M.; Varadarajan, K. M.; Kumar, S. Self-sensing and mechanical performance of CNT/GNP/UHMWPE biocompatible nanocomposites. *J. Mater. Sci.* **2018**, *53*, 7939–7952. https://doi.org/10.1007/s10853-018-2072-3.

(117) Alaferdov, A. V.; Lebedev, O. V.; Roggero, U. F. S.; Hernandez-Figueroa, H. E.; Nista, S. V. G.; Trindade, G. M.; Danilov, Y. A.; Ozerin, A. N.; Moshkalev, S. A. Highly conductive nanographite/ultra-high-molecular-weight polyethylene composite. *Results Mater.* **2022**, *15*, 100298. https://doi.org/10.1016/j.rinma.2022.100298.

(118) Pan, X.; Shen, L.; Schenning, A. P. H. J.; Bastiaansen, C. W. M. Transparent, High-Thermal-Conductivity Ultradrawn Polyethylene/Graphene Nanocomposite Films. *Adv. Mater.* **2019**, *31*, 1904348. https://doi.org/10.1002/adma.201904348.

(119) Sun, X.; Wang, G.; Xu, Z.; Wang, Z.; Zhao, G. Advanced fabrication of ultra-high molecular weight polyethylene/ graphite nanoplates foam for enhanced oil–water separation and thermal insulation via a novel omnidirectional gas escape barrier mechanism. *Chem. Eng. J.* **2025**, *503*, 158360. https://doi.org/10.1016/j.cej.2024.158360.

(120) Dalai, N.; Sreekanth, P. S. R. UHMWPE / nanodiamond nanocomposites for orthopaedic applications: A novel sandwich configuration based approach. *J. Mech. Behav. Biomed. Mater.* **2021**, *116*, 104327. https://doi.org/10.1016/j.jmbbm.2021.104327.

(121) Bin, Y.; Kitanaka, M.; Zhu, D.; Matsuo, M. Development of Highly Oriented Polyethylene Filled with Aligned Carbon Nanotubes by Gelation/Crystallization from Solutions. *Macromolecules* **2003**, *36*, 6213–6219. https://doi.org/10.1021/ma0301956.

(122) Shi, A.; Li, Y.; Liu, W.; Xu, J. Z.; Yan, D. X.; Lei, J.; Li, Z. M. Highly thermally conductive and mechanically robust composite of linear ultrahigh molecular weight polyethylene and boron nitride via constructing nacre-like structure. *Compos. Sci. Technol.* **2019**, *184*, 107858. https://doi.org/10.1016/j.compscitech.2019.107858.

(123) Sun, X.; Pan, X.; Wu, Y.; Wang, G.; Xu, R.; Li, J.; Yan, L.; Heng, Z.; Liang, M.; Zou, H.; Zhou, S. Fabrication of Thermally Conductive and Wear-Resistant UHMWPE-Based Composites for Nuclear Shielding Applications. *Ind. Eng. Chem. Res.* **2024**, 63, 11030–11043. https://doi.org/10.1021/acs.iecr.4c01240.

(124) Kapuscinsky, N.; Ignatusha, P.; Islam, A.; Ezzine, M.; Du, N.; Meek, K. M. Polymeric Coatings for Preventing Hydrogen Embrittlement in Industrial Storage and Transmission Systems. *ACS Appl. Eng. Mater.* **2024**, *2*, 2488–2503. https://doi.org/10.1021/acsaenm.4c00367.

(125) Pal, A.; Kaur, P.; Dwivedi, N.; Rookes, J.; Bohidar, H. B.; Yang, W.; Cahill, D. M.; Manna, P. K. Clay-Nanocomposite Based Smart Delivery Systems: A Promising Tool for Sustainable Farming. *ACS Agric. Sci. Technol.* **2023**, *3*, 3–16. https://doi.org/10.1021/acsagscitech.2c00140.

(126) Pang, H.; Xu, L.; Yan, D.-X.; Li, Z.-M. Conductive polymer composites with segregated structures. *Prog. Polym.Sci.* **2014**, *39*, 1908–1933. https://doi.org/10.1016/j.progpolymsci.2014.07.007.

(127) Su, X.; Wang, R.; Li, X.; Araby, S.; Kuan, H. C.; Naeem, M.; Ma, J. A comparative study of polymer nanocomposites containing multi-walled carbon nanotubes and graphene nanoplatelets. *Nano Mater. Sci.* **2022**, *4*, 185–204. https://doi.org/10.1016/j.nanoms.2021.08.003.

(128) Liu, J.; Moreno, A.; Chang, J.; Morsali, M.; Yuan, J.; Sipponen, M. H. Fully Biobased Photothermal Films and Coatings for Indoor Ultraviolet Radiation and Heat Management. *ACS Appl. Mater. Interfaces* **2022**, *14*, 12693–12702. https://doi.org/10.1021/acsami.2c00718.

(129) Siraj, S.; Al-Marzouqi, A. H.; Iqbal, M. Z.; Ahmed, W. Impact of Micro Silica Filler Particle Size on Mechanical Properties of Polymeric Based Composite Material. *Polymers* **2022**, *14*, 4830. https://doi.org/10.3390/polym14224830.

(130) Cheng, H.; Bai, L.; Lin, G.; Zhang, X.; Wu, C.; Ma, S.; Liu, X.; Huang, B.; Chen, Q.; Qian, Q.; Cao, C. Hugely improved electromagnetic interference shielding and mechanical properties for UHMWPE composites via constructing an oriented conductive carbon nanostructures (CNS) networks. *J. Mater. Res. Technol.* **2023**, *26*, 6520–6531. https://doi.org/10.1016/j.jmrt.2023.08.256.

(131) Jia, L.-C.; Yan, D.-X.; Cui, C.-H.; Jiang, X.; Ji, X.; Li, Z.-M. Electrically conductive and electromagnetic interference shielding of polyethylene composites with devisable carbon nanotube networks. *J. Mater. Chem. C* **2015**, *3*, 9369–9378. https://doi.org/10.1039/c5tc01822f.

(132) Liu, Z.; Bai, G.; Huang, Y.; Ma, Y.; Du, F.; Li, F.; Guo, T.; Chen, Y. Reflection and absorption contributions to the electromagnetic interference shielding of single-walled carbon nanotube/polyurethane composites. *Carbon* **2007**, *45*, 821–827. https://doi.org/10.1016/j.carbon.2006.11.020.

(133) Huang, J.; Mao, C.; Zhu, Y.; Jiang, W.; Yang, X. Control of carbon nanotubes at the interface of a co-continuous immiscible polymer blend to fabricate conductive composites with ultralow percolation thresholds. *Carbon* **2014**, *73*, 267–274. https://doi.org/10.1016/j.carbon.2014.02.063.

(134) Jia, L.-C.; Yan, D.-X.; Cui, C.-H.; Ji, X.; Li, Z.-M. A Unique Double Percolated Polymer Composite for Highly Efficient Electromagnetic Interference Shielding. *Macromol. Mater. Eng.* **2016**, *301*, 1232–1241. https://doi.org/10.1002/mame.201600145.

(135) Wu, H.-Y.; Zhang, Y.-P.; Jia, L.-C.; Yan, D.-X.; Gao, J.-F.; Li, Z.-M. Injection Molded Segregated Carbon Nanotube/Polypropylene Composite for Efficient Electromagnetic Interference Shielding. *Ind. Eng. Chem. Res.* **2018**, *57*, 12378–12385. https://doi.org/10.1021/acs.iecr.8b02293.

(136) Yan, D.-X.; Pang, H.; Li, B.; Vajtai, R.; Xu, L.; Ren, P.-G.; Wang, J.-H.; Li, Z.-M. Structured Reduced Graphene Oxide/Polymer Composites for Ultra-Efficient

Electromagnetic Interference Shielding. *Adv. Funct. Mater.* **2015**, *25*, 559–566. https://doi.org/10.1002/adfm.201403809.

(137) Jiang, X.; Yan, D. X.; Bao, Y.; Pang, H.; Ji, X.; Li, Z. M. Facile, green and affordable strategy for structuring natural graphite/polymer composite with efficient electromagnetic interference shielding. *RSC Adv.* **2015**, *5*, 22587–22592. https://doi.org/10.1039/c4ra11332b.

(138) Gu, J.; Li, N.; Tian, L.; Lv, Z.; Zhang, Q. High thermal conductivity graphite nanoplatelet/UHMWPE nanocomposites. *RSC Adv.* **2015**, *5*, 36334–36339. https://doi.org/10.1039/C5RA03284A.

(139) Guo, Y.; Cao, C.; Luo, F.; Huang, B.; Xiao, L.; Qian, Q.; Chen, Q. Largely enhanced thermal conductivity and thermal stability of ultra high molecular weight polyethylene composites *via* BN/CNT synergy. *RSC Adv.* **2019**, *9*, 40800–40809. https://doi.org/10.1039/c9ra08416a.

Chapter 2

Controlling filler distribution from homogeneous to semi-segregated networks in UHMWPE/graphene nanoplatelet (GNP) nanocomposites

ABSTRACT:

Efforts to enhance the multifunctionality of ultra-high-molecular-weight polyethylene (UHMWPE) involve integrating nanomaterials to impart properties such as electrical and thermal conductivity. However, the inherent high viscosity and processing limitations pose challenges for controlling distribution of nanofillers in nanocomposites. In this Chapter, I introduce a strategy to control the distribution of nanofillers in the solvent-free solid-state fabrication of UHMWPE/graphene nanoplatelet (GNP) nanocomposites. By utilizing extremely fine UHMWPE particles, synthesized from a nano-dispersed Ziegler-Natta catalyst, either as the matrix or mixed with commercial UHMWPE powder, the control of the GNP distribution, ranging from homogeneous to semi-segregated structures, was achieved. Mechanical properties, especially elongation at break and toughness, were found to be significantly influenced by the filler distribution pattern. The electrical and thermal conductive properties of these nanocomposites were also investigated, revealing that precise control over filler distribution overcomes the conventional trade-off between mechanical and conductive properties. In this Chapter, I demonstrate the feasibility of designing and optimizing conductive yet stretchable UHMWPE nanocomposites, providing versatility toward various types of nanofillers.

KEYWORDS: Ultra-high-molecular-weight polyethylene / Nanocomposite / Graphene nanoplatelet / Conductivity / Stretchability

2.1. Introduction

Ultra-high-molecular-weight polyethylene (UHMWPE) is linear polyethylene with a molecular weight exceeding 1 million g mol^{-1}.[1–6] Its semi-crystalline structure comprises ordered crystalline lamellae and disordered amorphous regions, interconnected by tie molecules and entangled chains that act as physical crosslinks between the lamellae.[7–10] This molecular architecture imparts UHMWPE with outstanding mechanical and tribological properties, including exceptional toughness, durability, chemical and abrasion resistance, and self-lubricating properties among all thermoplastics currently available.[11–14] With a low density of 0.93–0.95 g cm^{-3}, UHMWPE films are highly promising in terms of their strength-to-weight ratio, often compared to Kevlar.[15] However, due to its ultra-high-molecular-weight and strong intramolecular interactions, which result in a viscosity approximately 2,500 times higher than that of high-density polyethylene (HDPE),[16,17] typical bulk products are fabricated using solid-state consolidation methods, such as compression molding of reactor powder. In this process, grain boundary defects caused by incomplete compaction and inter-diffusion of polymer chains often become a processing issue that leads to mechanical failure.[18]

Owing to the excellent intrinsic properties of UHMWPE, efforts have been made to introduce new functionalities, such as electrical conductivity,[19–22] thermal conductivity,[21,23] and electromagnetic shield properties[22,24,25] through the incorporation of nanomaterials. As the polymer melt lacks the viscous flow state, the introduction of nanofillers is predominantly done by pre-mixing UHMWPE powder with nanofillers followed by compression molding to form nanocomposite sheets or films.[20,21,25] In this fabrication process, fillers concentrate at the boundaries between UHMWPE particles due to the incompatibility between the two phases, as well as the high viscosity and low mobility of UHMWPE chains. This results in a segregated structure where the fillers form a continuous or semi-continuous network along polymer particle interfaces. Such a segregated structure is particularly promising for conductive

properties, as the continuous network shortens the filler-filler distance and enables achieving the percolation threshold at a low loading.[21,24,26,27] On the other hand, the presence of agglomerated fillers at the interfaces impedes compaction and polymer chain diffusion, leading to deterioration in mechanical properties or potentially brittle films. While UHMWPE tape and fibers can achieve ultimate tensile strength through stretching for effective chain alignment,[6,28,29] the weak boundaries caused by the segregated network of fillers significantly limit this capability. Attempts have been made to control the distribution of fillers in the polymer matrix to mitigate the mechanical deterioration. One method involves forming homogeneous filler distribution, which can be accomplished through solution processing, where fillers are added to a polymer solution followed by solvent evaporation, gelation-crystallization or gel-spinning.[30–33] Nonetheless, UHMWPE has limited solubility, necessitating a large quantity of solvents. Alternative ways to avoid the use of a large amount of solvents includes the mechanochemical synthesis,[34] swelling treatment,[35] and in-situ polymerization.[36–39] Although these methods assist in the homogeneous distribution of fillers, resulting in enhanced mechanical properties of nanocomposites, a trade-off with conductive properties often arises. This highlights the need for a method to control the filler distribution, ranging from homogeneous to segregated networks, to resolve this trade-off and to suit the desired properties, all within a simple preparation protocol.

From the replicating phenomenon where polymer chains grow and encapsulate a single catalyst particle to form a single polymer particle,[2,4,29,40] the size of final polymer particles directly correlates with the catalyst particle size. Chammingkwan *et al.* developed a nano-sized Ziegler-Natta catalyst using MgO nanoparticles as a support.[3,4,40] Chlorination of MgO with $TiCl_4$ formed a thin $MgCl_2$ layer, onto which $TiCl_4$ adsorbed, creating a core-shell $MgO/MgCl_2/TiCl_4$ structure. Through surface modification to enable the dispersion of MgO in a hydrocarbon solvent, a nanocatalyst with nano-level dispersion was successfully synthesized,

facilitating the synthesis of less entangled and extremely fine UHMWPE particles with sizes ranging from 1 to 2 μm.[4,40] In this Chapter, I synthesized and exploited these UHMWPE particles as a polymer matrix to fabricate UHMWPE/GNP nanocomposites. Leveraging an extremely small polymer particle size, nanocomposites with homogeneous GNP distribution were achieved in a solvent-free and straightforward solid-state processing approach for the first time. Furthermore, controlling filler distribution into a semi-segregated structure could also be achieved by mixing fine UHMWPE with commercially available UHMWPE powder. I found that by precisely controlling filler distribution, I can achieve both conductive and stretchable UHMWPE nanocomposites, despite these properties requiring opposite extremes in filler distribution patterns.

2.2. Methods

2.2.1. Materials

MgO nanoparticles with the mean particle size of 50 nm (Wako Pure Chemical Industries Ltd.) were used after dehydration at 160 °C under vacuum for 2 h. Polyoxyethylene alkylamine (PA) was purchased from NOF Corp. Titanium tetrachloride ($TiCl_4$, Kanto Chemical Industry Co., Ltd.) and kerosene of research grade (Wako Pure Chemical Industries, Ltd.) were used as received. *n*-Heptane was dried under molecular 3 Å, followed by N_2 bubbling for 2 h prior to use. Triethylaluminium (TEA) was donated by Tosoh Finechem Corp. Commercial ultra-high-molecular-weight polyethylene (UHMWPE) powder (M_w = 3,000,000–6,000,000 g mol^{-1}, denoted as Large) was purchased from Sigma-Aldrich Co., LCC. MIPELON PM-200 (the viscosity average molecular weight= 1.8×10^6 g mol^{-1}, D_{50}=10 μm, denoted as Middle) was provided from Mitsui Chemical, Inc. Graphene nanoplatelets (GNP, 6–8 nm thick and 5 μm width) were purchased from Tokyo Chemical Industry Co., Ltd. Irganox 1010 was purchased

from Toyotsu Chemiplas Corp. Ethanol (purity > 99.5%, Kanto chemical Industry Co., Ltd.) was used as received.

2.2.2. Nano-dispersed Ziegler-Natta catalyst preparation and characterization

A nano-dispersed MgO-based Ziegler-Natta type catalyst was prepared according to the previously reported procedure.[4,40] First, MgO nanoparticles were organically modified using PA as a surface modifier. In the modification procedure, 2.0 g of dehydrated MgO nanoparticles suspended in 8.0 mL of PA and 25 mL of kerosene was sonicated for 1 h to assist nanoparticle dispersion, followed by heat treatment at 160 °C for 1 h. The organically modified MgO was repetitively washed with heptane for eight times. After the last washing, the supernatant was removed and the solid product was redispersed in 100 mL of heptane. Thereafter, 30 mL of $TiCl_4$ was added to the suspension and the chlorination was performed at the heptane reflux temperature for 1 h. The obtained catalyst was repetitively washed with heptane and kept as a slurry in heptane.

The Ti content of a catalyst was analyzed using a colorimetric method with ultraviolet-visible spectrometry (UV-vis, Jasco V670). A catalyst (50 mg) was dissolved in a hot aqueous solution of H_2SO_4 and HCl. After dissolution, 200 μL of H_2O_2 (35% aqueous solution) was added, forming a yellowish titanium peroxo complex. The Ti content was calculated based on an adsorption intensity at 410 nm using an external calibration curve acquired from Ti standard solutions. The catalyst particle size was analyzed using light scattering (LA-950V2, HORIBA Ltd.) in heptane suspension under N_2 atmosphere. The mean particle size (D_{50}) was defined as the particle diameter at 50% in the cumulative number-based particle size distribution.

2.2.3. Synthesis of ultra-high-molecular-weight polyethylene

Ethylene polymerization was carried out in a 1 L stainless steel reactor equipped with a mechanical stirrer rotating at 500 rpm. After replacing the atmosphere through repetitive evacuation and N_2 purging, 500 mL of heptane as a polymerization medium and 1.0 mmol of TEA as an activator were introduced. The solvent was saturated with 0.8 MPa of ethylene at 70 °C for 30 min. A predetermined amount of a catalyst was then injected to initiate the polymerization at 70 °C and 0.8 MPa of ethylene pressure. After 30 min of polymerization, the resulting polymer was filtered, redispersed in ethanol using an ultrasonic homogenizer (UH-50, SMT Co. Ltd.), and finally dried under vacuum at 60 °C for 6 h. The sample is labeled as Small.

2.2.4. Preparation of nanocomposites

A 500 μm-thick nanocomposite film was prepared through compression molding. Small powder, along with Irganox1010 as a stabilizer (0.7 wt%), and GNPs at a desired loading amount were physically blended in a dry powder form until GNPs were homogeneously distributed in the powder matrix. The blended powder was then filled into a 5 cm × 5 cm hollow aluminum sheet, sandwiched between polyimide films and iron plates, and placed in a hot press machine (AH-2003, AS ONE Corp.). The blended powder was compressed at a contact pressure at room temperature for 5 min before raising the temperature to 160 °C. Subsequently, the powder was hot-pressed at 20 MPa at 160 °C for 5 min, and then quenched to room temperature. The nanocomposite films are denoted as Small/GNP*x*, where *x* represents the GNP loading in weight percent. Reference films with the identical GNP content were also prepared using the same procedure, except commercially available UHMWPE powder (Large) was used as a matrix. These samples are denoted as Large/GNP*x*.

2.2.5. Characterization

The particle size of UHMWPE was analyzed by light scattering in ethanol suspension. The morphology of UHMWPE particles and the film cross-section was observed by scanning electron microscope (SEM, S-4100, Hitachi High-Tech Science Corp.) operated at an acceleration voltage of 15 kV. A sample was coated by Pt or Au prior to the measurement. The GNP distribution was observed from the film cross-section using optical microscopes (BX51, Olympus Corp. with a digital camera (DP28 camera, Olympus Corp.) and BH-2, Olympus Corp.). Mechanical properties of nanocomposites were measured using a tensile tester (Abe Dat-100, Abecks Inc.) at room temperature and a cross-head speed of 1.5 mm min^{-1}. Dumbbell shape specimens were die-cut from the film sample and the measured properties were reported as an average value from repetitive tests. Electrical conductivity of nanocomposite films was measured by a four-point probe method on an Ossila four-point probe (T2001A3, Ossila BV). Electrical conductivity of the samples with very low conductivity (< 10^{-7} S cm^{-1}) was measured by a super insulation resistance tester (SM7110, HIOKI E. E. Corp.) with a plate sample electrode (SME-8310, HIOKI E. E. Corp.). Thermal diffusivity was measured using a laser flash method on an ai-Phase mobile 1u/2 instrument (Hitachi High-Tech Science Corp.). Thermal conductivity was calculated from the thermal diffusivity using Equation (2.1)

$$K = \alpha \rho C_p \quad (2.1),$$

where K and α are the thermal conductivity and thermal diffusivity of the nanocomposite. ρ and C_p are the density and heat capacity of the nanocomposite.

2.3. Results and discussion

2.3.1. Synthesis of a nanosized Ziegler-Natta catalyst and microfine UHMWPE

A nano-dispersed catalyst was synthesized according to the previously reported procedure.[4,40] It was used in ethylene polymerization to prepare polymers with a small particle size. Figure 2.1a depicts the number-based particle size distribution of organically modified MgO and the resulting catalyst. The particle size and the nano-dispersed nature of the catalyst were maintained from the organically modified MgO support, with the mean particle size (D_{50}) of 68 nm. The Ti content of the catalyst was analyzed as 0.81 wt% and the catalyst exhibited a moderate activity in ethylene polymerization of 2,200 g-Polymer g-Cat^{-1} in 30 min of polymerization. The appearance of the reactor powder after polymerization is shown in Figure 2.1b. Due to the nanosize of the catalyst particles, small polyethylene particles were produced. These particles encountered electrostatic attraction during polymerization, leading to the agglomeration of as-obtained reactor powder. However, physically agglomerated particles can be redispersed in ethanol with the aid of sonication. The redispersion process resulted in polymer powder with an extremely small particle size of 448 nm and relative span factor (RSF) of 0.486 (Figure 2.1c). The viscosity average molecular weight (M_v) was measured as 4.42 million g mol^{-1}, indicating that the polyethylene produced is ultra-high-molecular-weight polyethylene (UHMWPE), denoted as Small.

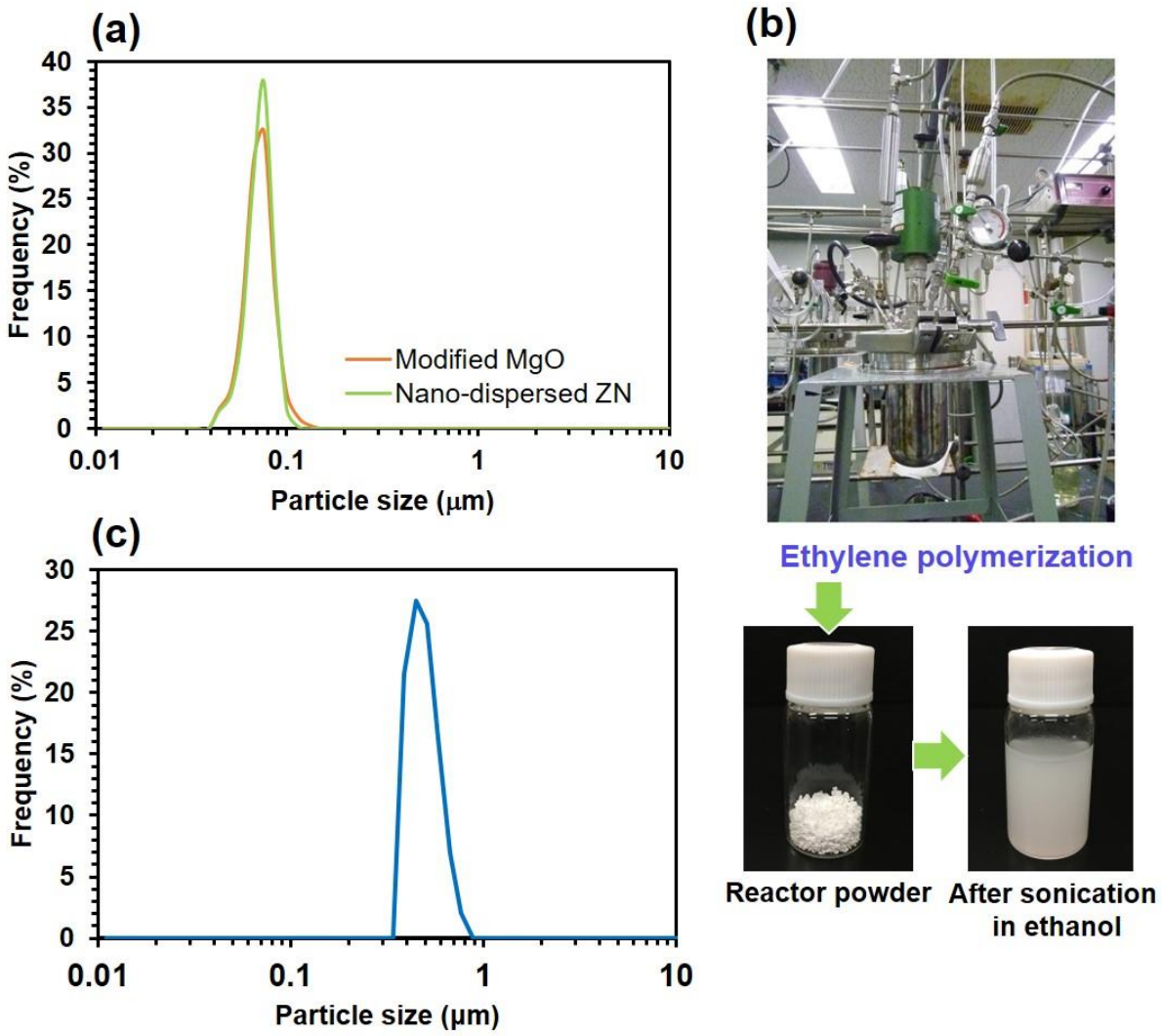

Figure 2.1. A nano-dispersed catalyst and obtained polymers: a) Number-based particle size distribution of organically modified MgO and the resultant catalyst, b) appearance of as-obtained reactor powder and after redispersion by sonication in ethanol, and c) number-based particle size distribution of polymer powder after redispersion.

2.3.2. UHMWPE/GNP nanocomposites with a single matrix

Nanocomposite films were prepared by direct physical mixing of Small powder and GNP in the presence of a stabilizer, followed by compression molding. The samples are denoted as Small/GNP*x*, where *x* represents the GNP loading at 0.5, 1.0, 3.0, and 5.0 wt%. The reference

nanocomposites were also prepared using commercial UHMWPE powder (measured M_v = 5.28 million g mol^{-1}, D_{50} = 69.5 μm, RSF = 1.09) as the matrix at identical GNP loadings, denoted as Large/GNP*x*. Figure 2.2 illustrates the film preparation process and the appearance of the samples. SEM images of the polymer particles as well as their particle size distribution analyzed by light scattering for both Small and Large samples are provided in Figure 2.3. From the photographs in Figure 2.2, while both of the Small/GNP and Large/GNP mixed powder appeared homogeneous in color, Small/GNP exhibited a lighter grey hue compared to Large/GNP due to the lower bulk density of Small and its small particles covering the GNPs. After compression molding, the films exhibited the black color from GNPs even at low loading levels. The Small/GNP films exhibited a uniform appearance across all weight loadings in contrast to the Large/GNP films that showed non-uniformity above 3.0 wt%, which was believed to result from GNP agglomerations.

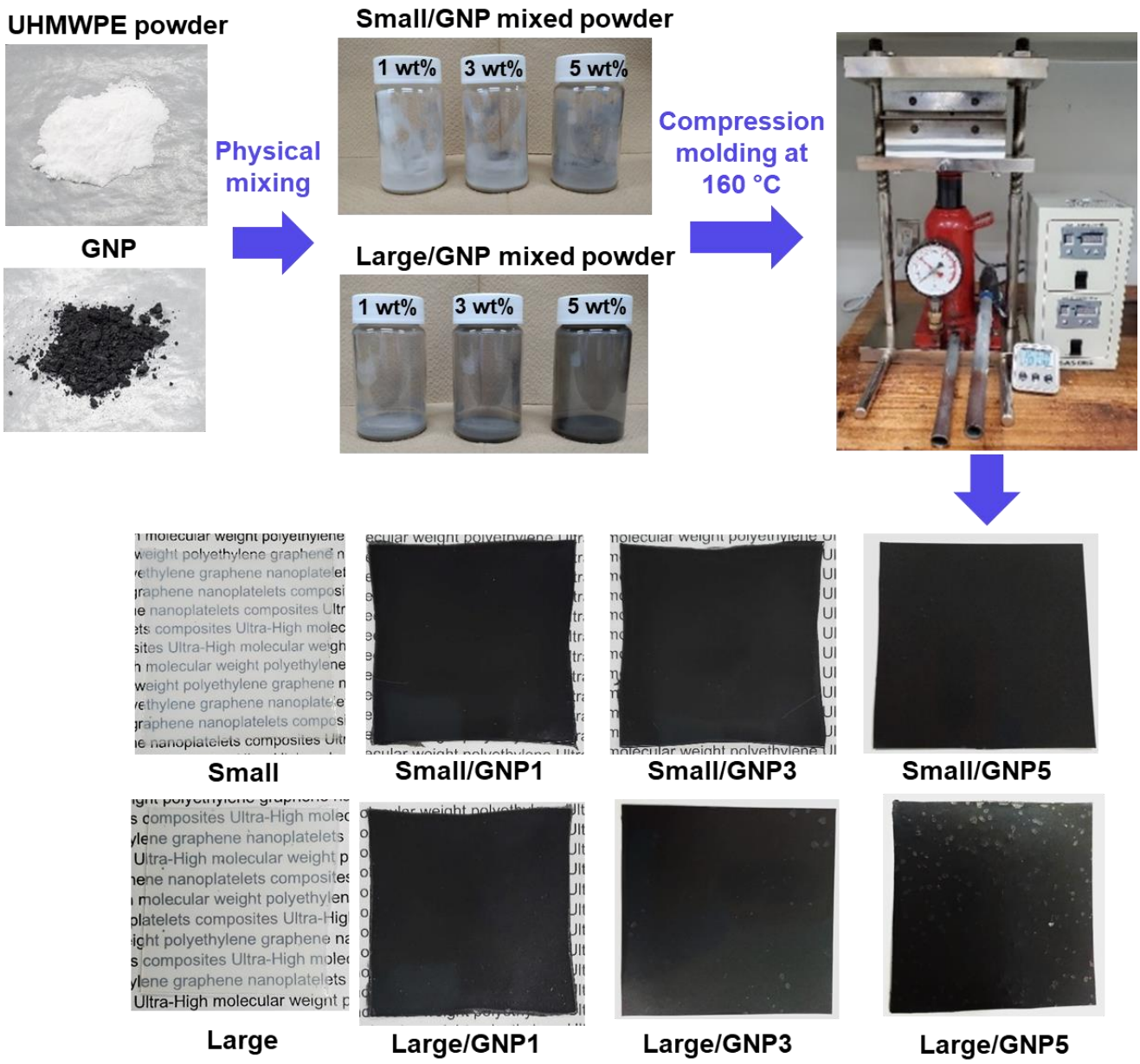

Figure 2.2. Film preparation process and appearance of samples before and after compression molding.

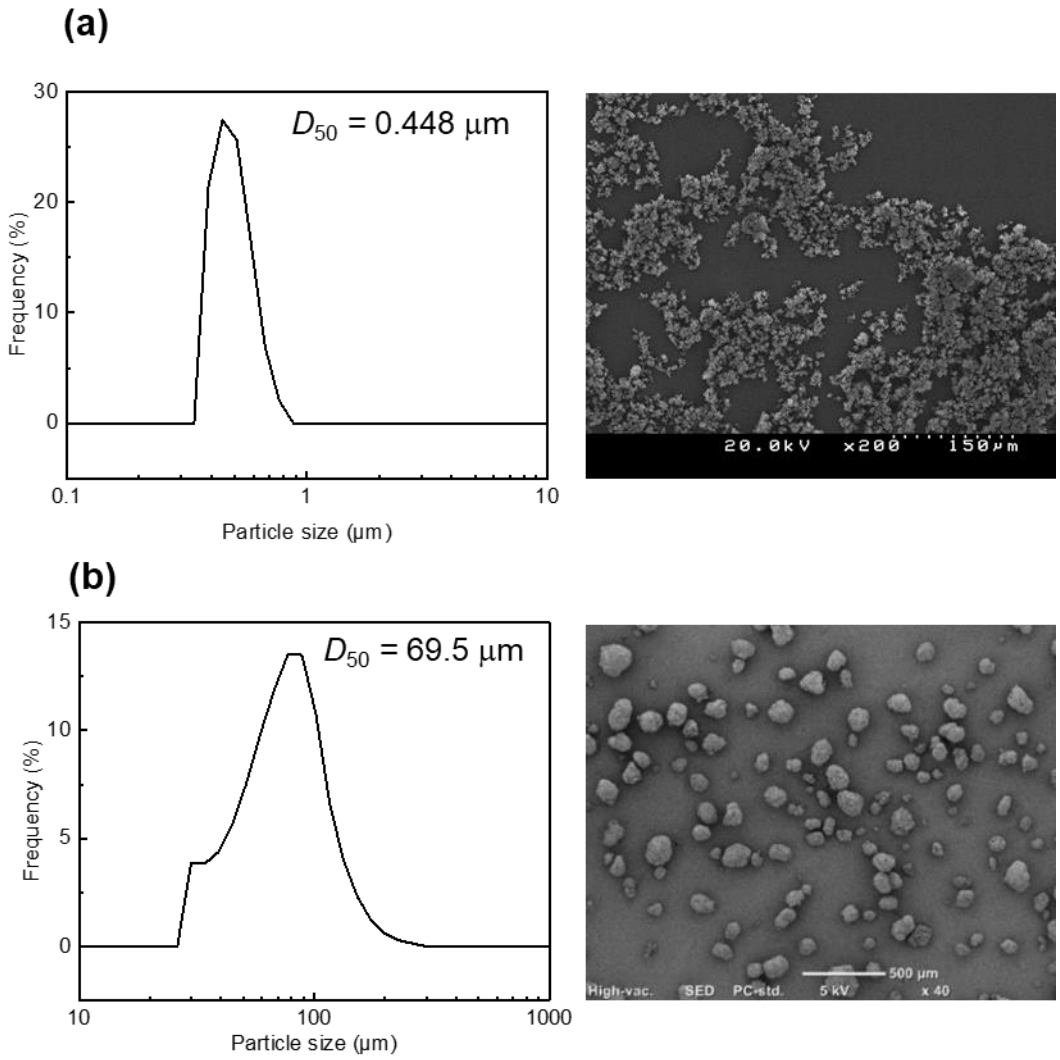

Figure 2.3. Particle size distribution acquired by light scattering and SEM images of UHMWPE powder: a) Small and b) Large.

The morphology of the film cross-section was observed by SEM. In Figure 2.4a, Small/GNP5 exhibited a smooth cross-sectional surface, indicating complete fusion of polymer particles across the film thickness. There were only trace presences of dark spots from large GNP particles and voids. The distribution of GNPs in the polymer matrix was observed by the optical microscope. Figure 2.4b shows that GNPs were homogeneously distributed throughout the matrix. Optical microscope observation in the transmission mode using a thin cross-

sectional specimen further confirmed the homogeneous distribution of the fillers (Figure 2.4c). In the case of Large/GNP, the SEM image evidenced the presence of large voids along the interfaces of original Large particles (Figure 2.4d). Optical microscope images revealed that these are indeed interconnected networks of GNPs (Figure 2.4e,f), referred to as a segregated structure.[26,27,41] Such a structure prevented the polymer particles from complete fusion. It is worth noting that the segregated structure is typically observed in the solid-state processing of polymer nanocomposites, where fillers deposited on the polymer particles remain localized at the original interface due to the high viscosity of the polymer matrix. This is a particularly relevant process in UHMWPE nanocomposites, where melt processing is not viable.[42,43] On the other hand, achieving a homogeneous distribution of fillers typically requires either the dissolution of UHMWPE followed by solution blending with nanofillers[25,26,44] or in-situ blending during polymerization using nanofillers as catalyst supports.[36,45,46] The former necessitates a large amount of a solvent for dissolution, while the latter is limited by the low production yield. I demonstrate for the first time that the homogeneous distribution of fillers can be achieved via solvent-free solid-state processing of UHMWPE nanocomposites, by leveraging the extremely fine polymer particles.

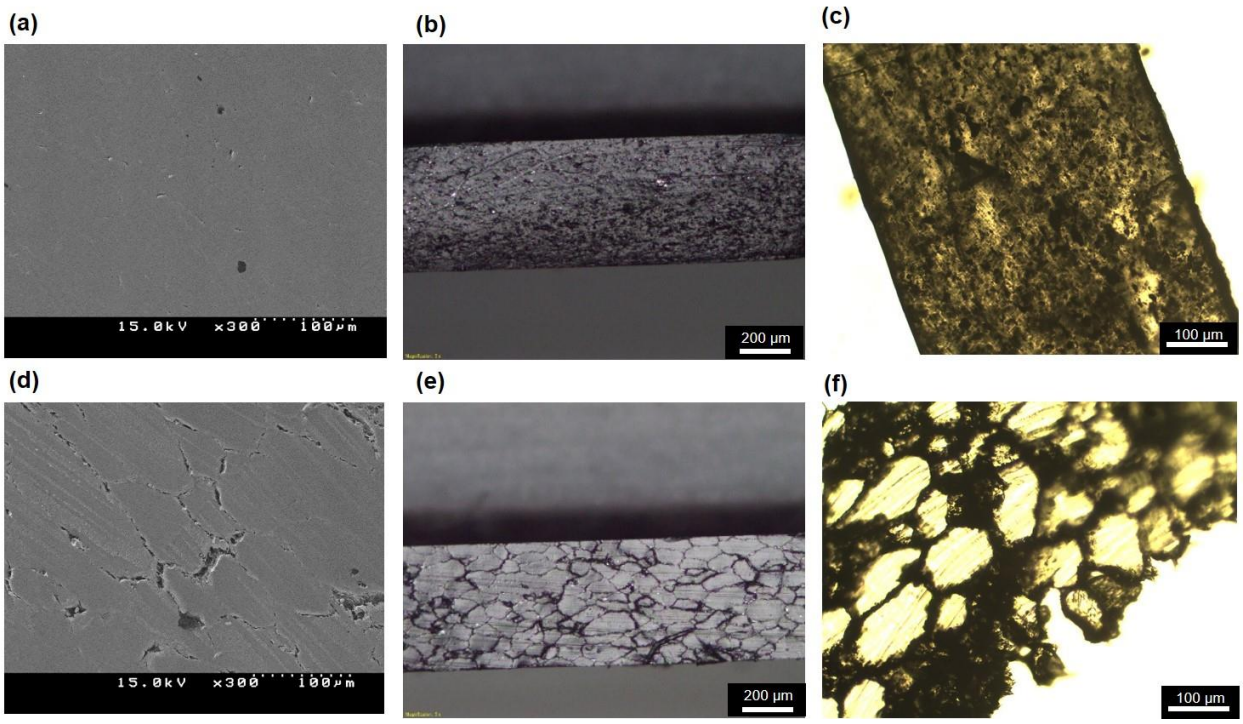

Figure 2.4. SEM and optical microscope images of cross-sectioned films: a-c) Small/GNP, and d-f) Large/GNP nanocomposites. All images were taken from 5.0 wt% GNP loading, except c and f that were taken from 3.0 wt% GNP loading.

The tensile properties of the nanocomposites were evaluated at room temperature using a tensile tester. The representative stress-strain curves are plotted in Figure 2.5 with inset photographs illustrating the specimen appearance after break for the samples containing 5.0 wt% GNPs. The mechanical properties acquired from the stress-strain curve are summarized in Table 2.1. As seen in Figure 2.5, both of the pristine Small and Large samples exhibited the strain hardening behavior, which is attributed to the polymer chain entanglement and chain orientation.[8,9] The increase in the tensile strength after the yield point was similar for both of the samples, suggesting similarity in the entanglement network. On the other hand, the elongation at break was higher by 28 % for Small, resulting in higher ultimate tensile strength at the break point, and consequently, greater toughness. It is commonly known that

consolidated UHMWPE is prone to fusion defects due to incomplete compaction (voids) and insufficient inter-particle diffusion.[47] During the sintering process especially with short sintering times, chain diffusion through a mechanism known as chain explosion—where the radius of gyration increases abnormally—plays a significant role.[48] The much smaller particle size of Small not only increases the contact interfaces to promote the intertwining of chains across adjacent particles at the interfaces, but also creates smaller interparticle voids in compaction. This enhances the likelihood of polymer chains from nearby particles reaching each other within the interparticle voids, thereby improving the quality of fusion and enhancing ductility. The introduction of GNPs resulted in deterioration in the mechanical properties, particularly the decrease in elongation at break and toughness with increasing GNP loadings. Such deterioration was much more pronounced in the Large matrix. For instance, Large/GNP5 exhibited a 96 % reduction in elongation at break from the pristine polymer, whereas Small/GNP5 experienced only an 18 % reduction. Accordingly, Small/GNP5 still retained exceptional stretchability, exceeding 500 %, which surpasses many types of pristine polymer.[49] The reduction in ductility upon the incorporation of fillers has been extensively reported in UHMWPE nanocomposites[21,45,46] as fillers residing at the polymer particle interfaces prevent the contact and complete fusion of adjacent polymer particles. Additionally, the surface mismatch between polymers and GNP particles, i.e., the much lower external surface area of Large compared to GNPs, further promotes GNP agglomeration and fusion defects that weaken the interfaces. On the contrary, the homogeneous distribution of GNPs in the Small matrix allowed the majority of polymer particles to remain in contact and fuse. This resulted in remarkably higher mechanical properties, 115 % higher ultimate tensile strength and 4400 % higher toughness, for Small/GNP compared to Large/GNP at the same 5.0 wt% loading.

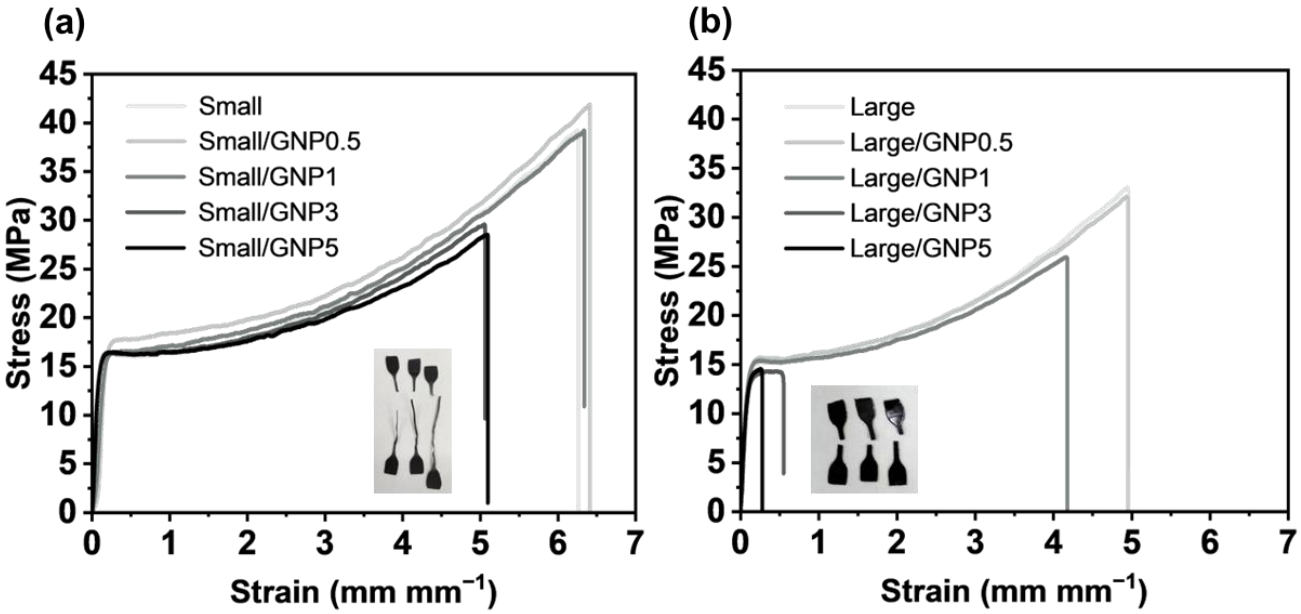

Figure 2.5. Representative stress-strain curves of a) Small/GNP, and b) Large/GNP nanocomposites. Inset photographs show the appearance of specimens at break for 5.0 wt% GNP loading.

Table 2.1. Mechanical properties of UHMWPE/GNP nanocomposites.

Sample	U.T.S. (MPa)	Strain at break (mm mm^{-1})	Young's modulus (MPa)	Toughness (MJ m^{-3})	Stress at yield (MPa)
Small	41±1.5	6.3±0.25	250±7.1	150±10	17±0.1
Small/GNP0.5	43±0.9	6.6±0.19	200±7.1	170±7.1	18±0.1
Small/GNP1	39±1.6	6.2±0.13	150±3.5	150±6.0	17±0.2
Small/GNP3	32±1.2	5.2±0.18	250±4.4	110±5.7	17±0.1
Small/GNP5	30±1.3	5.2±0.22	280±13	110±6.4	17±0.1
Large	33±0.2	4.9±0.15	220±9.7	100±3.4	15±0.1

Large/GNP0.5	33±1.2	5.0±0.18	190±14	100±5.9	16±0.1
Large/GNP1	27±0.5	4.2±0.06	190±8.4	80±1.6	15±0.1
Large/GNP3	15±0.2	0.58±0.05	180±3.9	7.6±0.8	15±0.2
Large/GNP5	14±0.6	0.21±0.06	230±9.1	2.3±0.9	n.a.

The electrical conductivity of the nanocomposites was measured and plotted against the GNP loading. Note that additional samples with high GNP loadings were also prepared to observe the percolation threshold. For Large/GNP films at 10 and 17.5 wt%, they were too brittle to undergo die-cutting for mechanical testing (see Figure 2.6 for the film appearance). Therefore, only the mechanical properties of Small films were measured and the results are provided in Table 2.2. As depicted in Figure 2.7a, the electrical conductivity for both Small/GNP and Large/GNP films increased with the increase in the GNP loading. However, Large/GNP with a segregated structure exhibited superior conductivity compared to Small/GNP with a homogeneous GNP distribution. An abrupt change in the electrical conductivity was evident for Large/GNP at a very low loading of around 2 wt% (corresponding to 0.8 vol%), while for Small/GNP, it occurred in the range of 5−10 wt%. The former is consistent with literature where the electrical percolation threshold was reported at 2−3 wt% for UHMWPE/GNP nanocomposites with the segregated structure.[21,22] No available literature was found for the electrical percolation threshold of UHMWPE/GNP nanocomposites with a homogeneous GNP distribution; however, a threshold of around 10 wt% was reported for melt-blended high-density polyethylene (HDPE)/GNP[50] and HDPE/expanded graphite nanocomposites.[51] This result clearly showed that controlling the distribution of fillers to

preferentially form a segregated network benefits the formation of an efficient conductive path, facilitating better electron transportation.

It has been well-accepted that the macroscopic conductance of polymer composites follows a power scaling law dependence on the filler volume fraction. Above the percolation threshold, the conductivity follows the Equation (2.2)

$$\sigma = \sigma_f \left(\phi - \phi_c\right)^{t_P} \quad (2.2),$$

where σ and σ_F are the electrical conductivity of the composite and filler. ϕ, ϕ_c and t_P are the volume fraction of fillers, the critical volume fraction of fillers at which a significant increase in conductivity occurs (percolation threshold), and the universal critical exponent that describes the nature of the percolation, in which $t_P \approx 2$ represents the percolation in three dimensions.[52–54]

Figure 2.7b presents a plot of log σ versus log ($\phi - \phi_c$). The t_P values acquired from the slope are 4.2 and 2.9 for Small/GNP and Large/GNP, respectively. The t_P value higher than 2 might indicate the higher-dimensionality of the system or specific types of percolation. The larger value for Small/GNP indicated that after reaching the percolation threshold, the conductive network of Small/GNP became more efficient, which is believed to result from the formation of finer network structures in the Small matrix. Additionally, the agglomeration of fillers in Large/GNP might create vacancy defects that act as scattering centers for charge carriers, leading to a small increase in the electrical conductivity with loadings above the percolation threshold. It is important to emphasize that in this high loading range, Small/GNP retained flexibility which was not the case for Large/GNP, thereby gaining benefits over Large/GNP in terms of conductivity and stretchability.

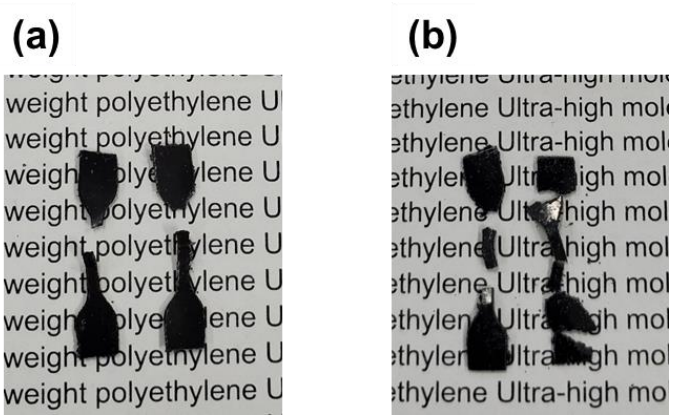

Figure 2.6. Film appearance of Large/GNP with high loadings after die-cutting: a) Large/GNP10, and b) Large/GNP17.5.

Table 2.2. Mechanical properties of Small/GNP nanocomposites with high loadings.

Sample	U.T.S. (MPa)	Strain at break (mm mm^{-1})	Young's modulus (MPa)	Toughness (MJ m^{-3})	Stress at yield (MPa)
Small/GNP10	26±0.8	4.4±0.16	310±16	85±3.7	17±0.2
Small/GNP17.5	18±0.3	0.70±0.12	180±6.3	11±2.2	18±0.3

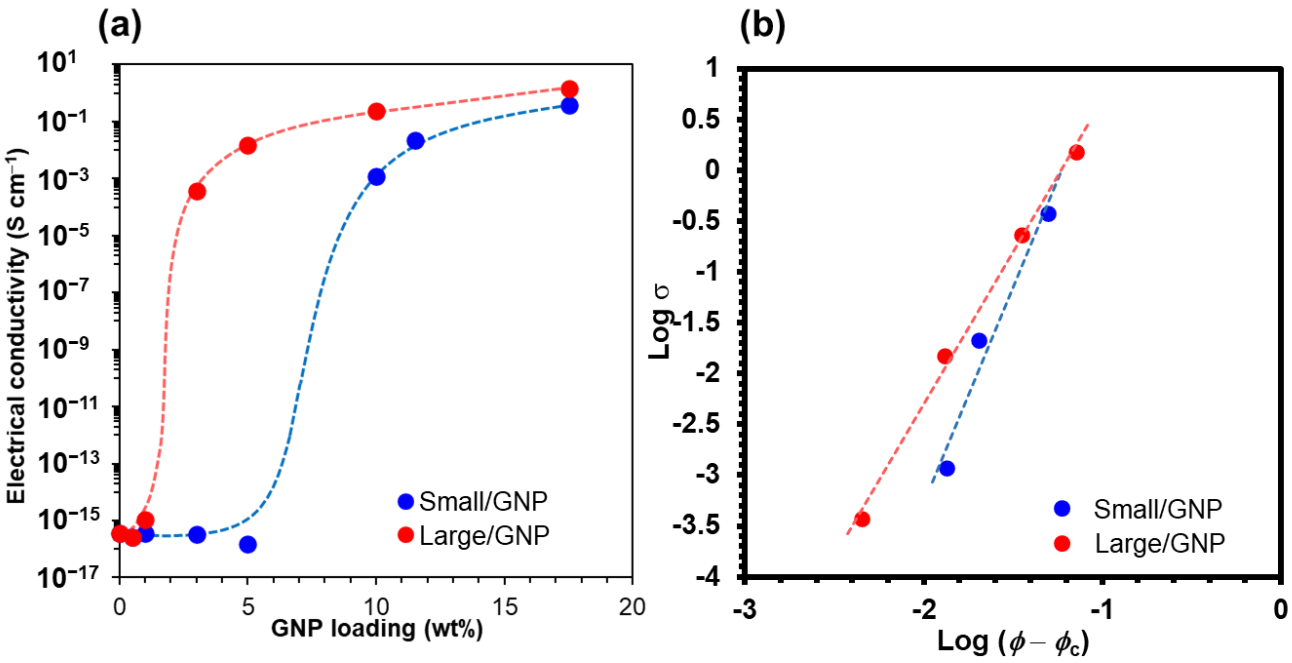

Figure 2.7. Electrical conductivity of nanocomposites: a) Relationship between electrical conductivity and GNP loadings, and b) plots of log σ versus log ($\phi - \phi_c$) above the percolation threshold.

Figure 2.8a showed the thermal conductivity of nanocomposites. Similar to the electrical conductivity, the thermal conductivity increased with the loading. On the other hand, the increment is rather linear in the studied range. The gradual increase in thermal conductivity with filler loading is commonly observed in polymer nanocomposites.[55] This is explained by the ability of polymers to transport thermal energy via phonons due to its semi-crystalline nature, in contrast to an electron transport that required a connected or percolation network of fillers.[55–58] Furthermore, the difference in the thermal conductivity between the Large and Small matrices was negligible at low loadings but became more pronounced as the loading increased. This contrasts with electrical conductivity, which approached similar values at a high loading. Such a different response suggests that the thermal conductive pathway differs from electrical conductivity, relying on both the matrix and filler distribution. Particularly, the

distribution of GNPs may impact the polymer's crystalline structure and subsequent heat transfer properties.

Several models have been established to explain the thermal conductivity of polymer nanocomposites. Figure 2.8b presents fittings of the experimental data with common models, including Maxwell-Eucken, Cheng-Vachon, Agari, and Lewis-Nielsen. While the former two models consider only the volume fraction of fillers and the intrinsic thermal conductivity of the matrix and fillers,[59] Agari model incorporates the thermal conductivity network for spherical particles,[60] and Lewis-Nielsen model accounts for filler aspect ratio and how they are oriented with respect to the thermal flow.[61] The thermal conductivity of GNPs was set at 380 W m^{-1} K^{-1} for fittings.[56,57] It was found that Lewis-Neilsen model provided the best fitting for the experimental data. This model is expressed in Equation (2.3)[61]

$$\frac{\boldsymbol{K}}{\boldsymbol{K_1}} = \frac{(\mathbf{1}+\boldsymbol{AB\phi})}{(\mathbf{1}-\boldsymbol{B\psi\phi})} \qquad (2.3),$$

where A is the generalized Einstein coefficient k_E, expressed as $A = k_E - 1$, and it depends on the shape of the fillers and orientation. B is related to the relative thermal conductivity of the two phases, given by the Equation $B = (K_2/K_1 - 1)/(K_2/K_1 + A)$ where K_1 and K_2 are the thermal conductivity of the matrix and fillers, respectively. ϕ is the volume fraction of the filler and the parameter ψ is related to the maximum packing fraction (ϕ_m) of fillers, expressed as $\psi = 1 + (1 - \phi_m)/\phi_m^2$. The values for parameters A and ϕ_m for different particle shapes and packings are given in literature.[61] However, GNPs have an irregular shape and the maximum packing volume is not known. Therefore, A and ϕ_m were used as adjustable parameters. The results of the fitting give relatively large A values of 23 and 34 for the Small and Large systems, respectively. The obtained ϕ_m values are 0.176 for Small and 0.181 for Large, reasonably close to each other since the same fillers were used. As A is related to the shape and aspect ratio of

the fillers, a lager *A* value for Large indicates the formation of a longer thermally conductive path compared to Small.

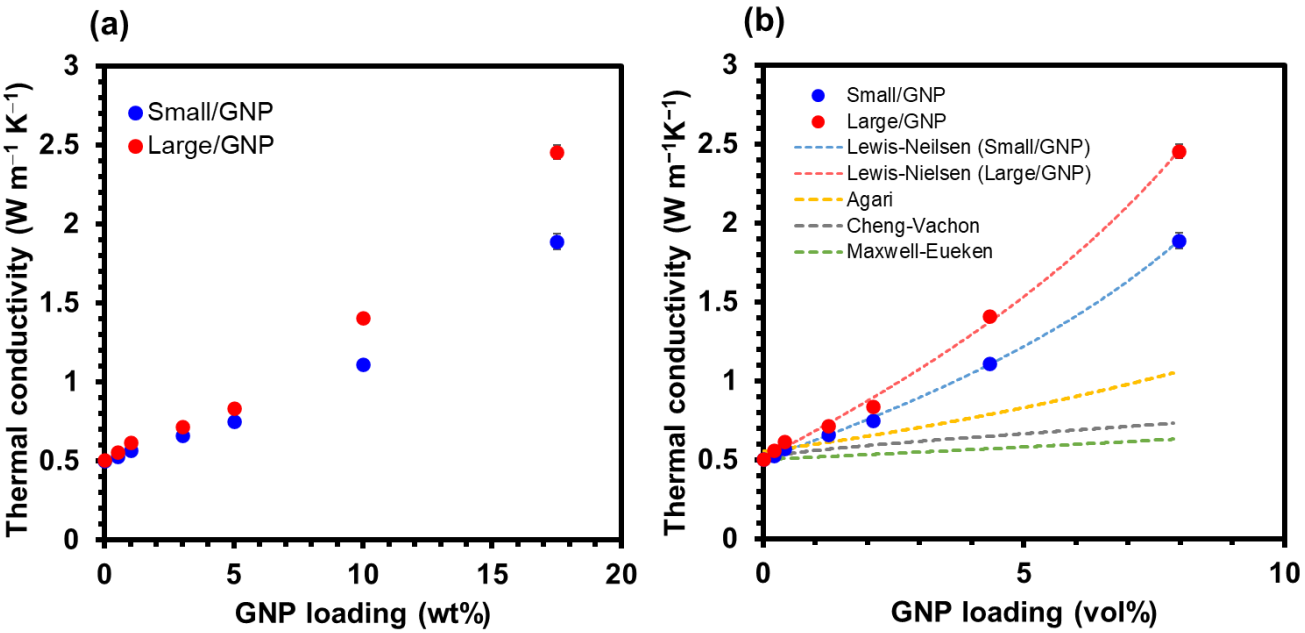

Figure 2.8. Thermal conductivity of nanocomposites: a) Relationship between thermal conductivity and GNP loadings, and b) fittings of thermal conductivity with different models.

2.3.3. UHMWPE/GNP nanocomposites with a semi-segregated structure

The results in 2.3.2. indicated that UHMWPE/GNP nanocomposites with a homogeneous GNP distribution have superior mechanical properties and stretchability, whereas those with a segregated structure exhibit better conductive properties at equivalent loadings. In this section, I aimed to improve the conductive properties while maintaining the mechanical properties of the composite film by forming a semi-segregated network using a mixed matrix. Specifically, Small powder and GNPs were physically blended prior to blending with Large. The mixture was finally subjected to compression molding. The weight ratio between Small and Large was set at 25:75, 50:50, and 75:25. The film samples are designated as Mix*m*/GNP*x*, where *m*

represents the weight percentage of Small in the mixed matrix, and *x* corresponds to the GNP loading. It must be noted that this approach was analogous to a ternary blend, where immiscible polymers such as HDPE[62,63] and polypropylene[41] were exploited as a continuous phase within the UHMWPE matrix to facilitate the distribution of fillers within this phase. However, complete polymer fusion requires chain entanglements and cocrystallization at the boundary, which is unlikely between different polymer chain microstructures. In addition, significant differences in melt viscosity between the host matrix and the continuous phase can lead to severe phase separation, and the inferior mechanical properties of the continuous phase may limit its overall performance. These issues are circumvented in this Chapter as the same type of polymer was exploited. Optical microscope images of the cross-sectioned films prepared from the mixed matrix at 5.0 wt% GNP loading are shown in Figure 2.9a,b. In contrast to Large/GNP5, in which GNPs appeared as thick continuous lines (Figure 2.9c), the Mix25/GNP5 film did not show such rigid thick lines, but consisted of Small domains with dispersed GNPs between Large particles. Compared with Small/GNP5 having the same loading (Figure 2.9d), the particle density of GNPs in these domains was much greater. Assuming all GNPs preferentially situate in the Small domain, the local density would be equivalent to a loading of 17.4 wt%, and indeed these domains showed a similar particle density to that of the Small/GNP17.5 sample (Figure 2.9e,f). Likewise, the use of a mixed matrix results in the successful formation of a semi-segregated structure, where GNPs are preferentially distributed within the Small phase.

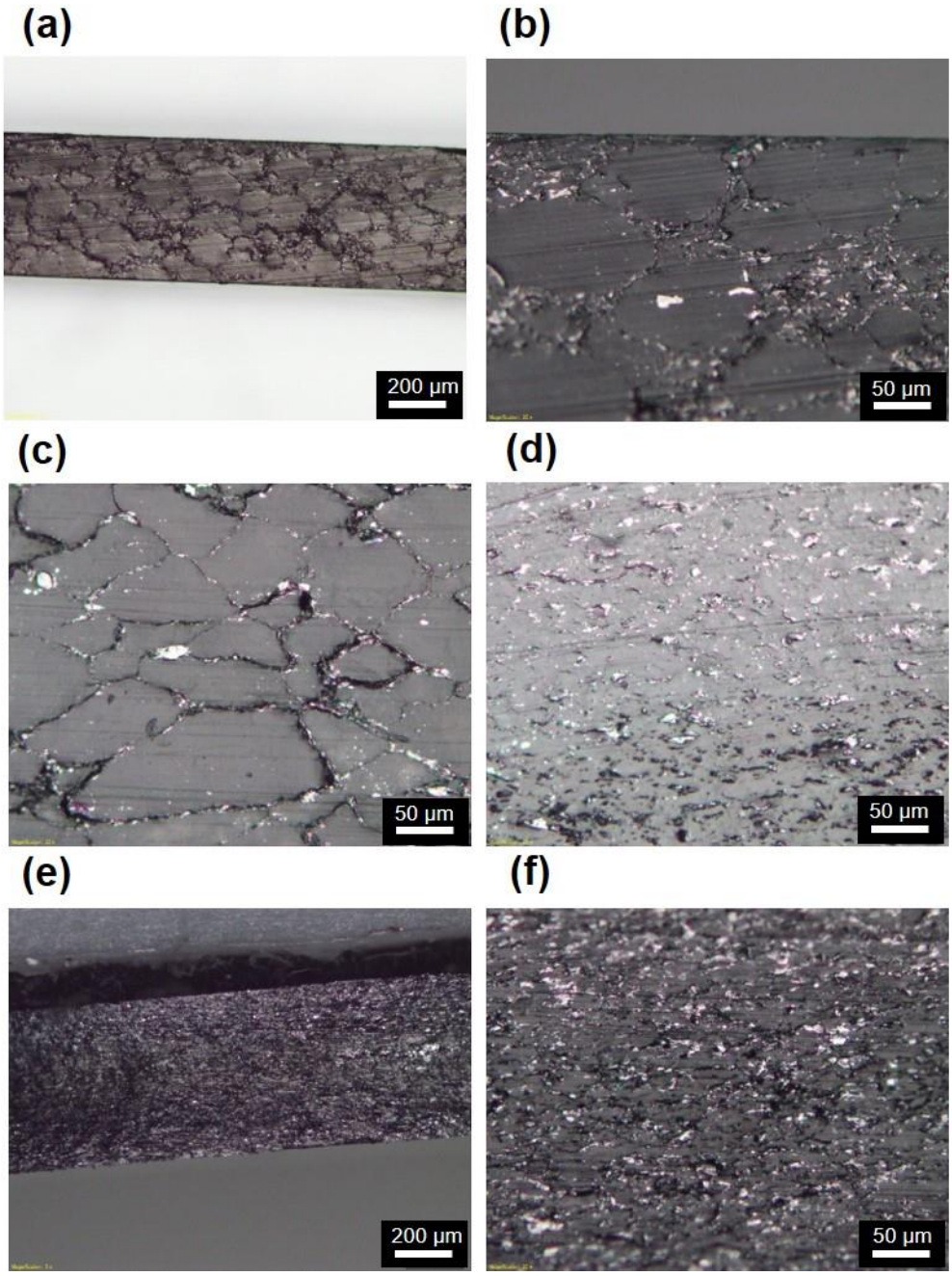

Figure 2.9. Optical microscope images of cross-sectioned UHMWPE/GNP films: a,b) Mix25/GNP5 at different magnifications, c) Large/GNP5, d) Small/GNP5, and e,f) Small/GNP17.5 at different magnifications.

Figure 2.10 shows the stress-strain curves of the films, with mechanical properties obtained from the curves presented in Table 2.3. For pristine polymer samples (Figure 2.10a,e), the

elongation at break of the mixed matrix laid between Small and Large, with elongation at break approaching that of Small as the Small fraction increased. When the ratio of Small to Large was 25:75, the properties of Mix25 were only slightly better than that of Large, indicating that the fusion of Large dominated the mechanical properties of the film. This is reasonable considering the ideal close packing volume of 74 %, where Small primarily fills the interparticle voids, but the interfaces of Large remain in contact. Stretchability is then governed by the weakest boundary, which is the interface between Large particles.

The stress-strain curves of the nanocomposites prepared using the mixed matrix are presented in Figure 2.10b,c. It can be seen that the formation of the semi-segregated structure significantly improved the mechanical properties of the nanocomposites compared to UHMWPE/GNP having the segregated structure. The degree of improvement increased with the Small fraction (Table 2.3). For clarity, the toughness and elongation at break were plotted in bar charts against loadings in Figure 2.10d,e. It is important to note that while the mechanical properties of the pristine films approximately follow the rule of mixtures of two types of polymers, the mechanical properties of the nanocomposites are dominated by the dispersion of GNPs in the Small domain. This is evidenced by much better mechanical properties for Mix25 compared to Large matrices in the presence of GNPs. Additionally, the elongation at break of Mix25/GNP3 was found to be close to that of Small/GNP10 (see Table 2.2), both of which contain a similar GNP particle density in the Small matrix.

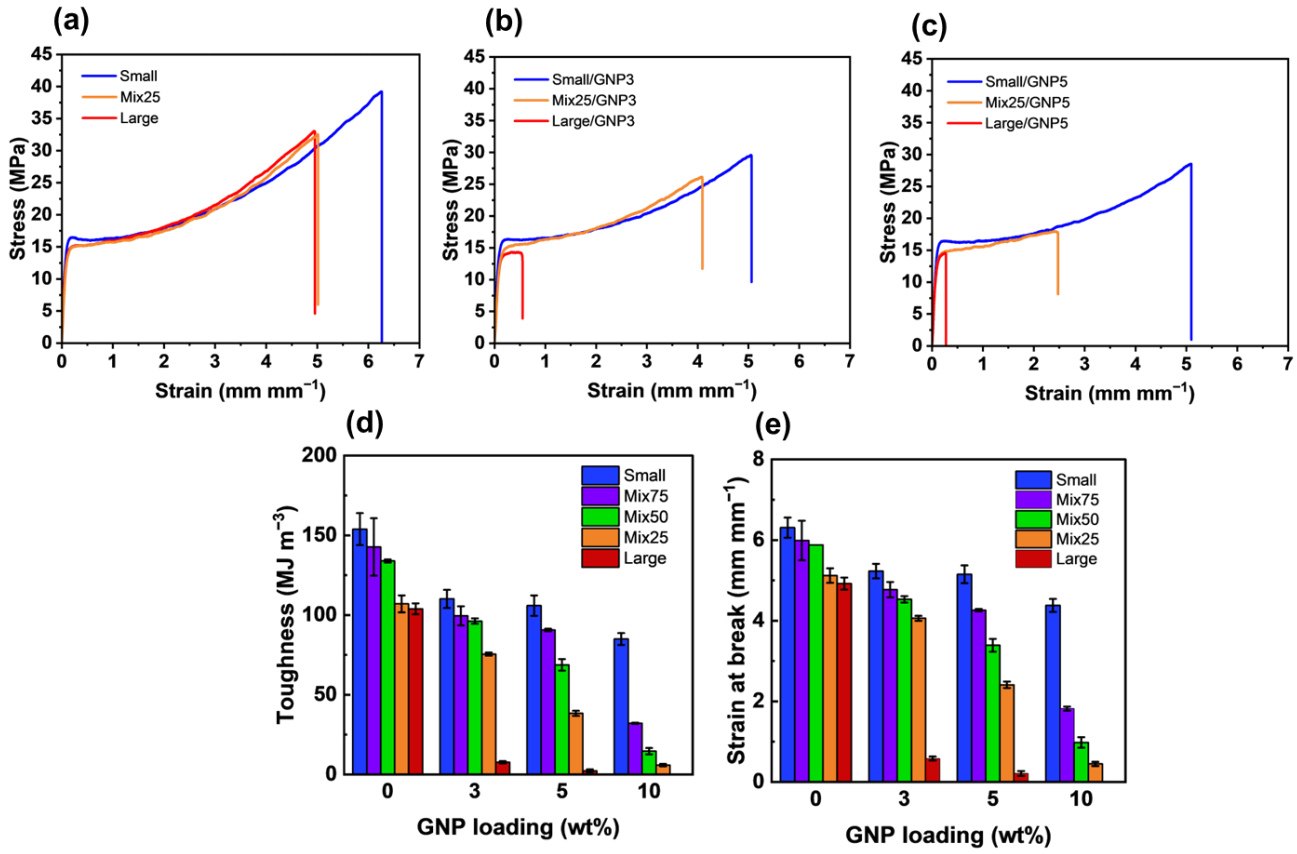

Figure 2.10. Mechanical properties UHMWPE/GNP nanocomposites with semi-segregated networks: Stress-strain curves of a) pristine UHMWPE films, b) UHMWPE/GNP3 films, c) UHMWPE/GNP5 films, d) toughness of nanocomposites, and e) strain at break acquired from the stress-strain curves.

Table 2.3. Mechanical properties of UHMWPE/GNP nanocomposites prepared using the mixed matrix at different Small and Large ratios.

Sample	U.T.S. (MPa)	Strain at break (mm mm^{-1})	Young's modulus (MPa)	Toughness (MJ m^{-3})	Stress at yield (MPa)
Mix25	34±1.2	5.1±0.18	200±1.8	110±5.3	15±0.1
Mix25/GNP3	26±0.4	4.1±0.06	210±4.5	76±1.0	15±0.1
Mix25/GNP5	18±0.3	2.4±0.08	220±6.8	38±1.6	15±0.1
Mix25/GNP10	17±0.3	0.45±0.05	150±11	5.8±0.79	n.a.
Mix50	38±0.2	5.9±0.0	130±4.7	130±1.0	16±0.2
Mix50/GNP3	30±0.6	4.5±0.08	170±29	96±1.7	18±0.6
Mix50/GNP5	25±0.5	3.4±0.16	170±2.9	69±3.6	18±0.1
Mix50/GNP10	17±0.3	0.98±0.13	170±24	15±2.0	17±0.3
Mix75	39±3.4	6.0±0.49	160±10	140±18	17±0.2
Mix75/GNP3.0	30±1.3	4.8±0.19	160±18	100±6.0	17±0.2
Mix75/GNP5.0	29±0.3	4.3±0.03	210±6.6	91±0.8	18±0.1
Mix75/GNP10.0	19±0.2	1.8±0.05	190±23	32±0.4	18±0.3

The conductive properties of nanocomposites prepared using the mixed matrix with the Small to Large ratio of 25:75 were evaluated. As shown in Figure 2.11a, the threshold for electrical conductivity of the nanocomposites was found at around 3.0 wt% loading,

significantly lower than that of nanocomposites with the homogeneous GNP distribution. At this loading, the local density of GNPs in the Small phase is calculated as 12.4 wt%, exceeding the percolation threshold for the Small/GNP system. Therefore, the observed shift of the percolation threshold to a lower loading is attributed to domain-specific densification, allowing the threshold to be achieved specially within that domain. Figure 2.11b depicts the thermal conductivity of the nanocomposites. By forming the semi-segregated structure, the thermal conductivity improved similarly to the electrical conductivity. The values obtained with the semi-segregated structure were also very close to those of the segregated structure, signifying that the network formed by the densification of fillers in the Small domain effectively promotes thermal conduction.

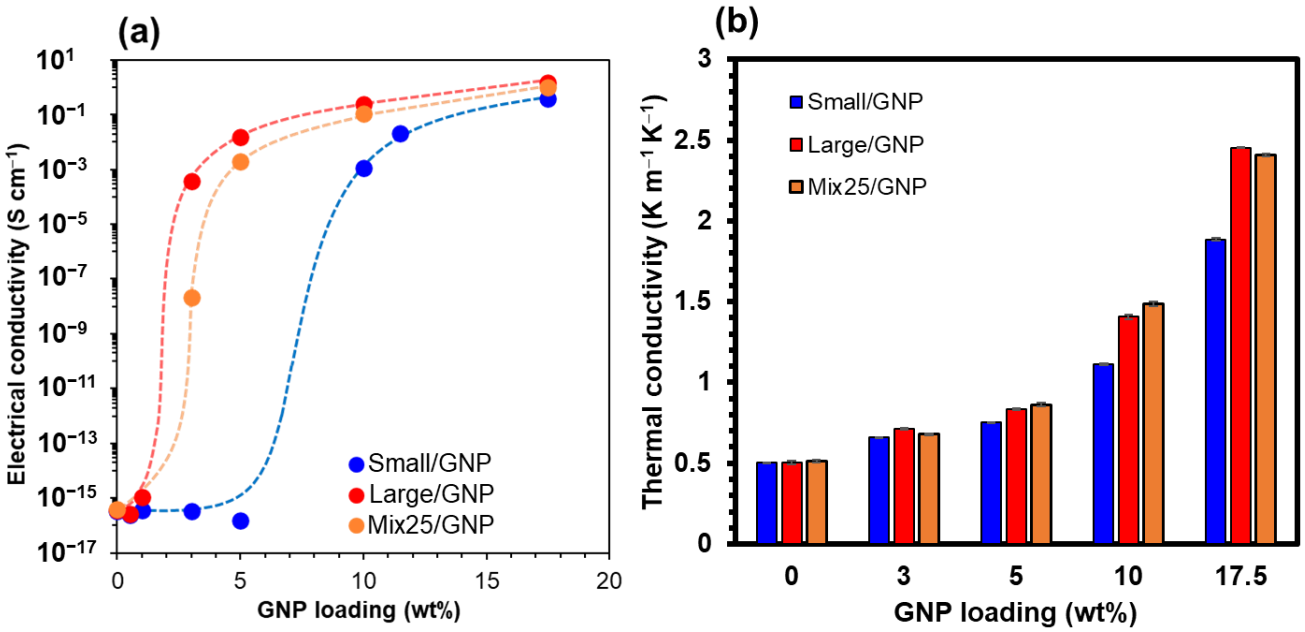

Figure 2.11. Properties Mix25/GNP nanocomposites with a semi-segregated structure: a) Electrical conductivity, and b) thermal conductivity. Properties for Small/GNP and Large/GNP were also plotted for comparison.

The mechanical and electrical properties of the nanocomposites consisting of middle-sized UHMWPE (average particle size: 10 μm) and 5 wt% GNP, referred to as Middle/GNP5, were evaluated and compared with those of previously reported systems such as Mix25/GNP. The GNP was uniformly dispersed within the matrix in Middle/GNP5 (Figure 2.12), a trend consistent with that observed in Small/GNP. Middle/GNP5 exhibited a toughness of 100 MJ m^{-3} and an electrical conductivity of 1.2×10^{-16} S cm^{-1} (Figure 2.13). This result indicated that selecting an intermediate particle size (Middle) cannot replicate the synergistic effects of the Mix/GNP systems. Consequently, the formation of a semi-segregated structure is essential to achieve a balance between electrical conductivity and toughness.

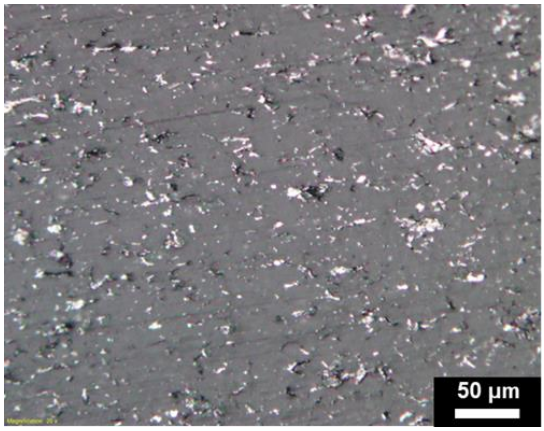

Figure 2.12. Optical microscope images of cross-sectioned Middle/GNP5 film.

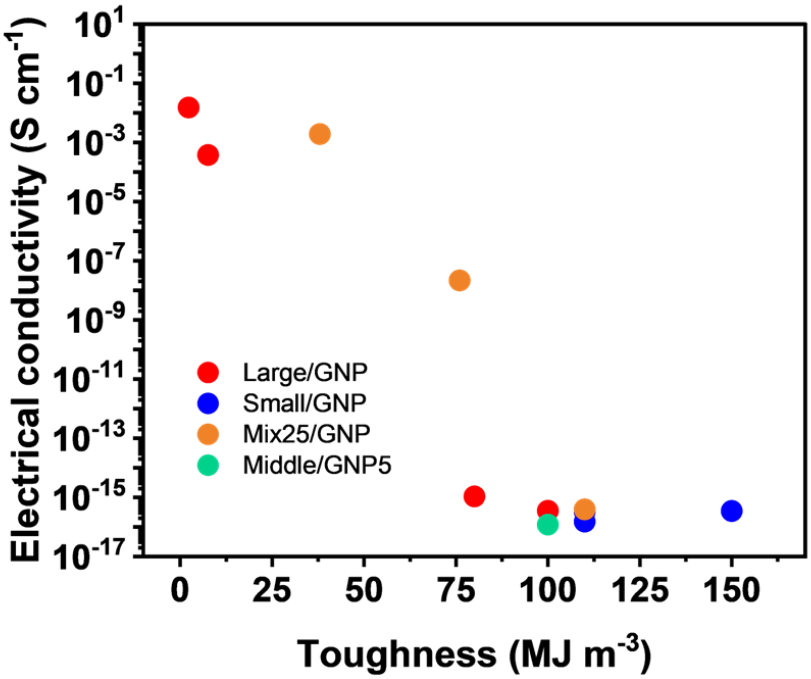

Figure 2.13. Effects of UHMWPE particle size and particle size control on the correlation between electrical conductivity and toughness.

Lastly, from an application perspective, the conductivity of 10^{-6} S cm^{-1} is required to meet the antistatic criterion of thin films.[52] This level of conductivity is satisfied at approximately 3.0 wt% for the segregated structure, 5.0 wt% for the semi-segregated structure, and 10.0 wt% for the homogeneous distribution. At loadings satisfying the criterion, the nanocomposite film with the homogeneous GNP distribution exhibited the highest elongation at break and toughness, followed by the semi-segregated structure and the segregated structure. Similarly, thermal conductivity followed the same trend, as illustrated in the three-dimensional plot in Figure 2.14. Unlike the commonly observed trade-off between mechanical properties and conductive properties, precise control of filler distribution resulted in simultaneous improvements in both attributes. Specifically, improvements in conductive properties can be achieved with increased loadings. At the same time, the deterioration in elongation at break

and toughness with increased loadings can be overcome by controlling the GNP distribution pattern from the segregated structure to semi-segregated structure or homogeneous distribution. This finding provides a straightforward and effective approach to design and optimize conductive and stretchable UHMWPE nanocomposite films, which can be applied to any types of nanofillers.

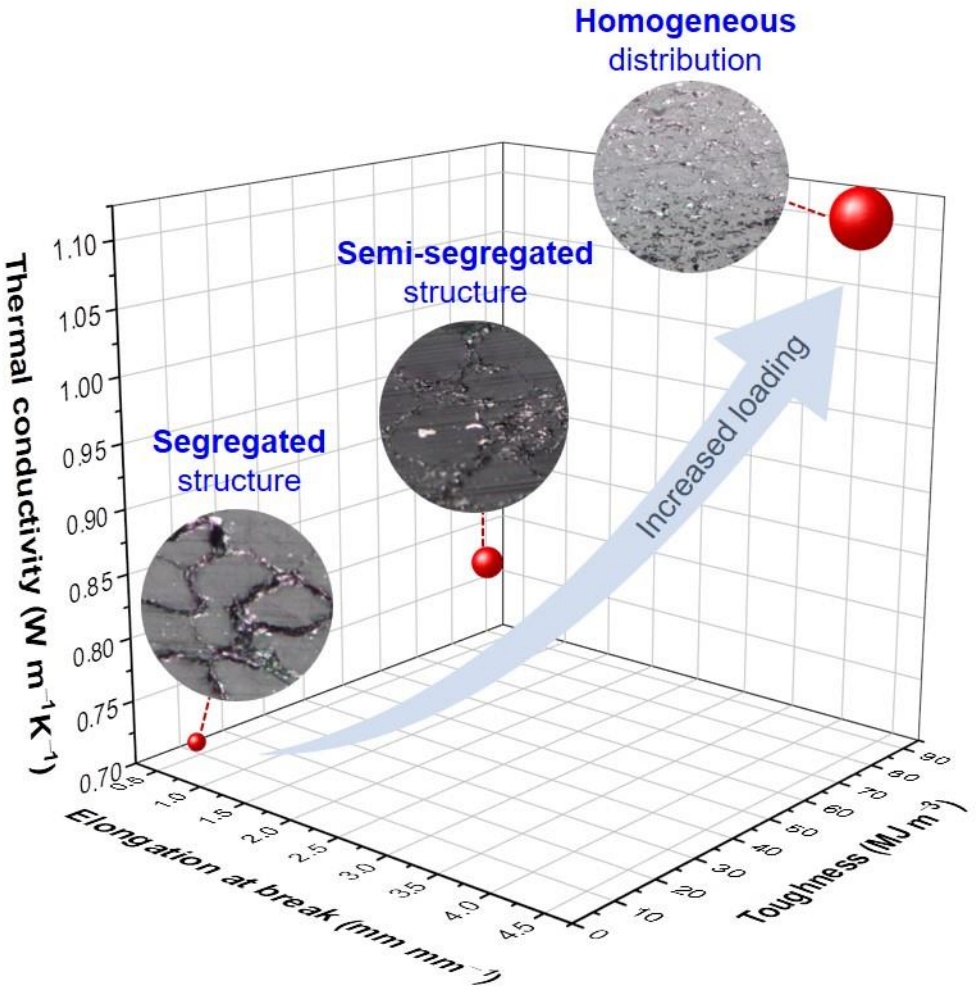

Figure 2.14. Three-dimensional plot illustrating the relationship between mechanical properties (elongation at break, toughness) and thermal conductivity for nanocomposites with different GNP distribution at loadings satisfying the antistatic criterion.

2.4. Conclusions

In this Chapter, I introduced a strategy to control the distribution of fillers in UHMWPE/GNP nanocomposites based on direct solid-state processing. The key of this strategy lies in the use of extremely fine UHMWPE particles synthesized from the nano-dispersed Ziegler-Natta type catalyst, either as the polymer matrix or in combination with commercially available UHMWPE. The small particle size of the polymer enhanced contact interfaces and suspension properties, facilitating homogeneous mixing of GNPs and polymer particles in simple, solvent-free physical blending. When used as a matrix, the subsequent compression molding resulted in nanocomposites with a homogeneous GNP distribution. When mixed with commercially available UHMWPE, pre-mixing GNPs with fine polymer particles before blending allows the preferential GNP distribution, resulting in the formation of nanocomposites with a semi-segregated structure. In this way, control of GNP distribution from homogeneous to semi-segregated structures becomes possible without the need of additional polymer for GNP dispersion, as in ternary blends. This result indicated that mechanical properties of the nanocomposites, particularly elongation at break and toughness, were primarily influenced by polymer fusion degree. Unlike UHMWPE nanocomposites with segregated structures, which suffered from mechanical deterioration due to the incomplete fusion, those with the homogeneous distribution and the semi-segregated structure maintained contact between polymer particles, preserving mechanical properties and stretchability even at high filler loadings. The conductive properties were also investigated on nanocomposites having distinct GNP distribution patterns. I found that segregated or semi-segregated structures facilitated efficient conductive paths to achieve the electrical percolation threshold at lower loadings, whereas those with the homogeneous GNP distribution required a higher loading to meet the thin film antistatic criterion. In contrast, the thermal conductivity increased in a more linear manner with loadings, indicating contributions from both fillers and the polymer matrix to the

thermal transport. At loadings satisfying the antistatic criterion, nanocomposites with homogeneous GNP distribution showed the highest elongation at break and toughness, followed by the semi-segregated and segregated structures. Thermal conductivity followed the same trend, highlighting that precise control of the filler distributions can overcome the typical trade-off between mechanical and conductive properties, which usually requires opposite ends of the filler distribution patterns. This strategy demonstrates the feasibility of designing and optimizing conductive yet stretchable UHMWPE nanocomposites using a straightforward fabrication method versatile for diverse nanofillers.

References

(1) Deplancke, T.; Lame, O.; Rousset, F.; Seguela, R.; Vigier, G.; Mechanisms of Chain Reentanglement during the Sintering of UHMWPE Nascent Powder: Effect of Molecular Weight. *Macromolecules* **2015**, *48*, 5328–5338. https://doi.org/10.1021/acs.macromol.5b00618

(2) Gote, R.P.; Mandal, D.; Patel, K.; Chaudhuri, K.; Vinod, C.P.; Lele, A.K.; Chikkali, S.H. Judicious Reduction of Supported Ti Catalyst Enables Access to Disentangled Ultrahigh Molecular Weight Polyethylene. *Macromolecules* **2018**, *51*, 4541–4552. https://doi.org/10.1021/acs.macromol.8b00590

(3) Bando, Y.; Chammingkwan, P.; Terano, M.; Taniike, T. Synthesis of Ultrahigh Molecular Weight Polyethylene Using $MgO/MgCl_2/TiCl_4$ Core–Shell Catalysts. *Macromol. Chem. Phys.* **2018**, *219*, 1800011. https://doi.org/10.1002/macp.201800011

(4) Chammingkwan, P.; Bando, Y.; Terano, M.; Taniike, T. Nano-Dispersed Ziegler-Natta Catalysts for 1 μm-Sized Ultra-High Molecular Weight Polyethylene Particles. *Front. Chem.* **2018**, *6*, 524. https://doi.org/10.3389/fchem.2018.00524

(5) Hees, T.; Schirmeister, C.G.; Pfohl, P.; Hofmann, D.; Muelhaupt, R. Self-Reinforcement via 1D Nanostructure Formation during Melt Blending of Thermoplastics and Thermoplastic Elastomers with Nanophase-Separated UHMWPE/HDPE Wax Reactor Blends. *ACS Appl. Polym. Mater.* **2021**, *3*, 3455–3464. https://doi.org/10.1021/acsapm.1c00384

(6) Gote, R.P.; van der Eem, J.; Zhao, J.; Lolage, S.; Traidia, A.; Zhang, Y.; Romano, D.; Rastogi, S. Influence of Molecular Weight and Entanglement Density on the Creep Response of the Uniaxially Drawn Tapes of *diSmall*MWPE. *Macromolecules* **2023**, *56*, 6903–6919. https://doi.org/10.1021/acs.macromol.3c01180

(7) Capaccio, G.; Ward, I.M. Effect of molecular weight on the morphology and drawing behaviour of melt crystallized linear polyethylene. *Polymer* **1975**, *16*, 239-243. https://doi.org/10.1016/0032-3861(75)90164-0

(8) Lemstra, P.J.; Van Aerle, N.A.J.M.; Bastiaansen, C.W.M. Chain-Extended Polyethylene. *Polym. J.* **1987**, *19*, 85-98. https://doi.org/10.1295/polymj.19.85

(9) Bartczak, Z. Effect of Chain Entanglements on Plastic Deformation Behavior of Linear Polyethylene. *Macromolecules* **2005**, *38*, 7702–7713. https://doi.org/10.1021/ma050815y

(10) Andersson, M.G.; Städler, R.; Hagstrand, P.-O.; Gkourmpis, T.; Andersson, M.R.; Müller, C. Influence of Molecular Weight on the Creep Resistance of Almost Molten Polyethylene Blends. *Macromol. Chem. Phys.* **2018**, *219*, 1700072. https://doi.org/10.1002/macp.201700072

(11) Rastogi, S.; Kurelec, L.; Lippits, D.; Cuijpers, J.; Wimmer, M.; Lemstra, P.J. Novel Route to Fatigue-Resistant Fully Sintered Ultrahigh Molecular Weight Polyethylene for Knee Prosthesis. *Biomacromolecules* **2005**, *6*, 942–947. https://doi.org/10.1021/bm0493638

(12) Sun, B.; Li, J.; Guo, Y.; Li, H.; Mi, H.-Y.; Dong, B.; Liu, C.; Shen, C. Superhydrophobic UHMWPE Foams with High Mechanical Robustness and Durability

Fabricated by Supercritical CO_2 Foaming. *ACS Sustainable Chem. Eng.* **2021**, *9*, 12663–12673. https://doi.org/10.1021/acssuschemeng.1c04573

(13) Wang, H.; Yan, X.; Tang, X.; Ma, Y.; Fan, X.; Li, W.; Yu, W.; Wang, J.; Yang, Y. Contribution of the Initially Entangled State and Particle Size to the Sintering Kinetics of UHMWPE. *Macromolecules* **2022**, *55*, 1310–1320. https://doi.org/10.1021/acs.macromol.1c02058

(14) Lekkala, S.; Inverardi, N.; Grindy, S.C.; Hugard, S.; Muratoglu, O.K.; Oral, E. Irradiation Behavior of Analgesic and Nonsteroidal Anti-Inflammatory Drug-Loaded UHMWPE for Joint Replacement. *Biomacromolecules* **2024**, *25*, 2312–2322. https://doi.org/10.1021/acs.biomac.3c01179

(15) Dayyoub, T.; Maksimkin, A. V.; Kaloshkin, S.; Kolesnikov, E.; Chukov, D.; Dyachkova, T.P.; Gutnik, I. The Structure and Mechanical Properties of the UHMWPE Films Modified by the Mixture of Graphene Nanoplates with Polyaniline. *Polymers* **2019**, *11*, 23. https://doi.org/10.3390/polym11010023

(16) Sharip, N.S.; Ariffin, H.; Yasim-Anuar, T.A.T.; Andou, Y.; Shirosaki, Y.; Jawaid, M.; Tahir, P.M.; Ibrahim, N.A. Melt- vs. Non-Melt Blending of Complexly Processable Ultra-High Molecular Weight Polyethylene/Cellulose Nanofiber Bionanocomposite. *Polymers* **2021**, *13*, 404. https://doi.org/10.3390/polym13030404

(17) Hikosaka, M.; Tsukijima, K.; Rastogi, S.; Keller, A. Equilibrium triple point pressure and pressure-temperature phase diagram of polyethylene*. *Polymer* **1992**, *33*, 2502-2507. https://doi.org/10.1016/0032-3861(92)91130-T

(18) Yan, X.; Zhang, Y.; Tang, X.; Ren, C.; Li, W.; Wang, J.; Yang, Y. Interplay of Particle Size and Temperature on Low-Entanglement Ultrahigh-Molecular-Weight Polyethylene Sintering in Blended Compositions: Analysis of Entanglement and Crystal Structure. *Ind. Eng. Chem. Res.* **2023**, *62*, 7950–7961. https://doi.org/10.1021/acs.iecr.3c00845

(19) Stürzel, M.; Kempe, F.; Thomann, Y.; Mark, S.; Enders, M.; Mülhaupt, R. Novel Graphene UHMWPE Nanocomposites Prepared by Polymerization Filling Using Single-Site Catalysts Supported on Functionalized Graphene Nanosheet Dispersions. *Macromolecules* **2012**, *45*, 6878–6887. https://doi.org/10.1021/ma301376q

(20) Gupta, T.K.; Choosri, M.; Varadarajan, K.M.; Kumar, S. Self-sensing and mechanical performance of CNT/GNP/UHMWPE biocompatible nanocomposites. *J. Mater. Sci.* **2018**, *53*, 7939–7952. https://doi.org/10.1007/s10853-018-2072-3

(21) Alam, F.; Choosri, M.; Gupta, T.K.; Varadarajan, K.M.; Choi, D.; Kumar, S. Electrical, mechanical and thermal properties of graphene nanoplatelets reinforced UHMWPE nanocomposites. *Mater. Sci. Eng. B* **2019**, *241*, 82–91. https://doi.org/10.1016/j.mseb.2019.02.011

(22) Al-Saleh, M.H. Electrical and electromagnetic interference shielding characteristics of GNP/UHMWPE composites. *J. Phys. D: Appl. Phys.* **2016**, *49*, 195302. https://doi.org/10.1088/0022-3727/49/19/195302

(23) Sun, X.; Pan, X.; Wu, Y.; Wang, G.; Xu, R.; Li, J.; Yan, L.; Heng, Z.; Liang, M.; Zou, H.; Zhou, S. Fabrication of Thermally Conductive and Wear-Resistant UHMWPE-Based

Composites for Nuclear Shielding Applications. *Ind. Eng. Chem. Res.* **2024**, *63*, 11030-11043. https://doi.org/10.1021/acs.iecr.4c01240

(24) Jiang, X.; Yan, D.-X.; Bao, Y.; Pang, H.; Ji, X.; Li, Z.-M. Facile, green and affordable strategy for structuring natural graphite/polymer composite with efficient electromagnetic interference shielding. *RSC Adv.* **2015**, *5*, 22587–22592. https://doi.org/10.1039/c4ra11332b

(25) Jia, L.-C.; Yan, D.-X.; Cui, C.-H.; Ji, X.; Li, Z.-M. A Unique Double Percolated Polymer Composite for Highly Efficient Electromagnetic Interference Shielding. *Macromol. Mater. Eng.* **2016**, *301*, 1232–1241. https://doi.org/10.1002/mame.201600145

(26) Pang, H.; Xu, L.; Yan, D.-X.; Li, Z.-M. Conductive polymer composites with segregated structures. *Prog. Polym. Sci.* **2014**, *39*, 1908–1933. https://doi.org/10.1016/j.progpolymsci.2014.07.007

(27) Jia, L.-C.; Yan, D.-X.; Cui, C.-H.; Jiang, X.; Ji, X.; Li, Z.-M. Electrically conductive and electromagnetic interference shielding of polyethylene composites with devisable carbon nanotube networks. *J. Mater. Chem. C* **2015**, *3*, 9369–9378. https://doi.org/10.1039/c5tc01822f

(28) Ronca, S.; Forte, G.; Tjaden, H.; Rastogi, S. Solvent-Free Solid-State-Processed Tapes of Ultrahigh-Molecular-Weight Polyethylene: Influence of Molar Mass and Molar Mass Distribution on the Tensile Properties. *Ind. Eng. Chem. Res.* **2015**, *54*, 7373–7381. https://doi.org/10.1021/acs.iecr.5b01469

(29) Gote, R.P.; Romano, D.; van der Eem, J.; Zhao, J.; Zhou, F.; Rastogi, S. Unprecedented Mechanical Properties in Linear UHMWPE Using a Heterogeneous Catalytic System. *Macromolecules* **2023**, *56*, 361–378. https://doi.org/10.1021/acs.macromol.2c02215

(30) Ruan, S.L.; Gao, P.; Yang, X.G.; Yu, T.X. Toughening high performance ultrahigh molecular weight polyethylene using multiwalled carbon nanotubes. *Polymer* **2003**, *44*, 5643–5654. https://doi.org/10.1016/S0032-3861(03)00628-1

(31) Wang, Y.; Cheng, R.; Liang, L.; Wang, Y. Study on the preparation and characterization of ultra-high molecular weight polyethylene-carbon nanotubes composite fiber. *Compos. Sci. Technol.* **2005**, *65*, 793–797. https://doi.org/10.1016/j.compscitech.2004.10.012

(32) Bin, Y.; Kitanaka, M.; Zhu, D.; Matsuo, M. Development of Highly Oriented Polyethylene Filled with Aligned Carbon Nanotubes by Gelation/Crystallization from Solutions. *Macromolecules* **2003**, *36*, 6213–6219. https://doi.org/10.1021/ma0301956

(33) Hulsey, S.; Absar, S.; Sultana, Q.N.; Sabet, S.M.; Mahfuz, H.; Khan, M. Synthesis and characterization of UHMWPE nanocomposite fibers containing carbon nanotubes coated with a PVP surfactant layer. *Polym. Compos.* **2018**, *39*, E1025–E1033. https://doi.org/10.1002/pc.24444

(34) Maksimkin, A.V.; Kaloshkin, S.D.; Kaloshkina, M.S.; Gorshenkov, M.V.; Tcherdyntsev, V.V.; Ergin, K.S.; Shchetinin, I.V. Ultra-high molecular weight polyethylene reinforced with multi-walled carbon nanotubes: Fabrication method and properties. *J. Alloys Compd.* **2012**, *536*, S538-S540. https://doi.org/10.1016/j.jallcom.2012.01.151

(35) Fang, L.; Leng, Y.; Gao, P. Processing and mechanical properties of HA/UHMWPE nanocomposites. *Biomaterials* **2006**, *27*, 3701–3707. https://doi.org/10.1016/j.biomaterials.2006.02.023

(36) Li, W.; Guan, C.; Xu, J.; Mu, J.; Gong, D.; Chen, Z.-R.; Zhou, Q. Disentangled UHMWPE/POSS nanocomposites prepared by ethylene in situ polymerization. *Polymer* **2014**, *55*, 1792–1798. https://doi.org/10.1016/j.polymer.2014.02.023

(37) Sánchez, Y.; Albano, C.; Karam, A.; Perera, R.; Casas, E. In situ Polymerization of Nanocomposites by $TpTiCl_2(Et)$ system: UHMWPE Filled with Carbon Nanotubes. *Macromol. Symp.* **2009**, *282*, 185–191. https://doi.org/10.1002/masy.200950819

(38) Ferreira, A.E.; Cerrada, M.L.; Pérez, E.; Lorenzo, V.; Cramail, H.; Lourenço, J.P.; Ribeiro, M.R. UHMWPE/SBA-15 nanocomposites synthesized by in situ polymerization. *Microporous Mesoporous Mater.* **2016**, *232*, 13–25. https://doi.org/10.1016/j.micromeso.2016.06.002

(39) Park, S.; Choi, I.S. Production of Ultrahigh-Molecular-Weight Polyethylene/Pristine MWCNT Composites by Half-Titanocene Catalysts. *Adv. Mater.* **2009**, *21*, 902–905. https://doi.org/10.1002/adma.200801674

(40) Chammingkwan, P.; Bando, Y.; Mai, L.T.T.; Wada, T.; Thakur, A.; Terano, M.; Sinthusai, L.; Taniike, T. Less Entangled Ultrahigh-Molecular-Weight Polyethylene Produced by Nano-Dispersed Ziegler-Natta Catalyst. *Ind. Eng. Chem. Res*. **2021**, *60*, 2818–2827. https://doi.org/10.1021/acs.iecr.0c05432

(41) Cheng, H.; Cao, C.; Zhang, Q.; Wang, Y.; Liu, Y.; Huang, B.; Sun, X.-L.; Guo, Y.; Xiao, L.; Chen, Q.; Qian, Q. Enhancement of Electromagnetic Interference Shielding Performance and Wear Resistance of the UHMWPE/PP Blend by Constructing a Segregated Hybrid Conductive Carbon Black-Polymer Network. *ACS Omega* **2021**, *6*, 15078–15088. https://doi.org/10.1021/acsomega.1c01240

(42) Liu, K.; Ronca, S.; Andablo-Reyes, E.; Forte, G.; Rastogi, S. Unique Rheological Response of Ultrahigh Molecular Weight Polyethylenes in the Presence of Reduced Graphene Oxide. *Macromolecules* **2015**, *48*, 131–139. https://doi.org/10.1021/ma501729y

(43) Weir, M.P.; Johnson, D.W.; Boothroyd, S.C.; Savage, R.C.; Thompson, R.L.; King, S.M.; Rogers, S.E.; Coleman, K.S.; Clarke, N. Distortion of Chain Conformation and Reduced Entanglement in Polymer-Graphene Oxide Nanocomposites. *ACS Macro Lett.* **2016**, *5*, 430–434. https://doi.org/10.1021/acsmacrolett.6b00100

(44) Li, B.; Fan, C.; Wang, H.; Ren, M.; Wu, P.; Wang, X.; Liu, X. A composite with excellent tribological performance derived from oxy-fluorinated UHMWPE particle/polyurethane. *RSC Adv.* **2014**, *4*, 9321–9325. https://doi.org/10.1039/c3ra47715k

(45) Park, H.-J.; Kim, J.; Seo, Y.; Shim, J.; Sung, M.-Y.; Kwak, S. Wear Behavior of *In situ* Polymerized Carbon Nanotube/Ultra High Molecular Weight Polyethylene Composites. *Macromol. Res.* **2013**, *21*, 965–970. https://doi.org/10.1007/s13233-013-1130-6

(46) Amini, M.; Ramazani S. A, A.; Kheradmand, A. In-Situ Polymerization of UHMWPE Using Bi-Supported Ziegler-Natta Catalyst of MoS_2 Oxide/$MgCl_2$ (Ethoxide Type)/$TiCl_4$/TiBA: Study of Thermo-Mechanical Properties of System. *Int. J. New. Chem.* **2019**, *6*, 87-108. https://doi.org/10.22034/ijnc.2019.33520

(47) Wu, J.J.; Buckley, C.P.; O'connor, J.J. Processing of Ultra-High Molecular Weight Polyethylene: Modelling the Decay of Fusion Defects. *Chem. Eng. Res. Des*. **2002**, *80*, 423–431. https://doi.org/10.1205/026387602320224003

(48) Wang, W.; Wang, H.; Chen, J. Research on Chain Diffusion and Entanglement via Controlling the Sintering Process of Nascent UHMWPE. *Macromolecules* **2024**, *57*, 2205–2217. https://doi.org/10.1021/acs.macromol.3c02361

(49) George Wypych Handout of Polymers, 3rd Edition; ChemTec Publishing, **2022**.

(50) Jiang, X.; Drzal, L.T. Improving electrical conductivity and mechanical properties of high density polyethylene through incorporation of paraffin wax coated exfoliated graphene nanoplatelets and multi-wall carbon nano-tubes. *Compos. Part A Appl. Sci. Manuf.* **2011**, *42*, 1840–1849. https://doi.org/10.1016/j.compositesa.2011.08.011

(51) Weng, W.-G.; Chen, G.-H.; Wu, D.-J.; Yan, W.-L. HDPE/expanded graphite electrically conducting composite. *Compos. Interfaces* **2004**, *11*, 131–143. https://doi.org/10.1163/156855404322971404

(52) Stankovich, S.; Dikin, D.A.; Dommett, G.H.B.; Kohlhaas, K.M.; Zimney, E.J.; Stach, E.A.; Piner, R.D.; Nguyen, S.B.T.; Ruoff, R.S. Graphene-based composite materials. *Nature* **2006**, *442*, 282–286. https://doi.org/10.1038/nature04969

(53) Li, J.; Kim, J.-K. Percolation threshold of conducting polymer composites containing 3D randomly distributed graphite nanoplatelets. *Compos. Sci. Technol.* **2007**, *67*, 2114–2120. https://doi.org/10.1016/j.compscitech.2006.11.010

(54) Yan, D.-X.; Pang, H.; Li, B.; Vajtai, R.; Xu, L.; Ren, P.-G.; Wang, J.-H.; Li, Z.-M. Structured Reduced Graphene Oxide/Polymer Composites for Ultra-Efficient Electromagnetic Interference Shielding. *Adv. Funct. Mater.* **2015**, *25*, 559–566. https://doi.org/10.1002/adfm.201403809

(55) Kargar, F.; Barani, Z.; Salgado, R.; Debnath, B.; Lewis, J.S.; Aytan, E.; Lake, R.K.; Balandin, A.A. Thermal Percolation Threshold and Thermal Properties of Composites with High Loading of Graphene and Boron Nitride Fillers. *ACS Appl. Mater. Interfaces* **2018**, *10*, 37555–37565. https://doi.org/10.1021/acsami.8b16616

(56) Xiang, J.; Drzal, L.T. Thermal Conductivity of a Monolayer of Exfoliated Graphite Nanoplatelets Prepared by Liquid-Liquid Interfacial Self-Assembly. *J. Nanomater.* **2010**, *2010*, 481753. https://doi.org/10.1155/2010/481753

(57) Ajorloo, M.; Fasihi, M.; Ohshima, M.; Taki, K. How are the thermal properties of polypropylene/graphene nanoplatelet composites affected by polymer chain configuration and size of nanofiller?. *Mater. Des.* **2019**, *181*, 108068. https://doi.org/10.1016/j.matdes.2019.108068

(58) Xu, Y.; Kraemer, D.; Song, B.; Jiang, Z.; Zhou, J.; Loomis, J.; Wang, J.; Li, M.; Ghasemi, H.; Huang, X.; Li, X.; Chen, G. Nanostructured polymer films with metal-like thermal conductivity. *Nat. Commun.* **2019**, *10*, 1771. https://doi.org/10.1038/s41467-019-09697-7

(59) Kim, C.-Y.; Dang, T.M.L.; Zhang, Y.; Yang, J.-F.; Wang, B. The alignment of AlN platelets in polymer matrix and its anisotropic thermal properties. *J. Materiomics* **2019**, *5*, 679–687. https://doi.org/10.1016/j.jmat.2019.04.011

(60) Agari, Y.; Ueda, A.; Nagai, S. Thermal conductivity of a polymer composite. *J. Appl. Polym. Sci.* **1993**, *49*, 1625–1634. https://doi.org/10.1002/app.1993.070490914

(61) Nielsen, L.E. The Thermal and Electrical Conductivity of Two-Phase Systems. *Ind. Eng. Chem. Fundamen.* **1974**, *13*, 17-20. https://doi.org/10.1021/i160049a004

(62) Thongruang, W.; Balik, C.M.; Spontak, R.J. Volume-exclusion effects in polyethylene blends filled with carbon black, graphite, or carbon fiber. *J. Polym. Sci. B Polym. Phys.* **2002**, *40*, 1013–1025. https://doi.org/10.1002/polb.10157

(63) Panin, S. V.; Kornienko, L.A.; Sondghaitam, N.; Ivanova, L.R.; Shil'ko, S.V. Abrasive Wear of Micro- and Nanocomposites Based on Ultra-High-Molecular-Weight Polyethylene (UHMWPE): Part 2. Composites Based on UHMWPE Filled by Nanoparticles and Nanofibers. *J. Frict. Wear* **2012**, *33*, 453–459. https://doi.org/10.3103/S1068366612060074.

Chapter 3

Controlling sintering behavior of UHMWPE nanocomposites for mechanical properties

ABSTRACT:

Research on ultrahigh-molecular-weight polyethylene (UHMWPE) nanocomposites has advanced toward multifunctionality, but mechanical properties remain limited by incomplete polymer fusion during sintering due to restrictions in polymer chain diffusion as well as nanoparticle agglomeration at the polymer particle interfaces. In this Chapter, the sintering and processing-dependent mechanical behavior of UHMWPE and its nanocomposites with graphene nanoplatelets (GNP) in the presence of microfine UHMWPE (Small) was investigated. Owing to their sub-micron size, the introduction of Small promoted the formation of nanocomposites with a semi-segregated structure that facilitated polymer fusion and enhanced mechanical properties. Increasing the sintering temperature further enhanced chain interdiffusion, resulting in significant strengthening in nanocomposites. Moreover, high-temperature uniaxial stretching demonstrated the potential of fabricating UHMWPE/GNP nanocomposite tapes and fibers via a solvent-free route. Despite the presence of high-aspect-ratio GNP that typically hinder fusion, a high draw ratio was achieved in the presence of Small, demonstrating its critical role in enabling both processability and mechanical reinforcement.

KEYWORDS: Ultrahigh-molecular-weight polyethylene / Nanocomposite / Graphene nanoplatelet / Conductivity / Uniaxial stretching

3.1. Introduction

Ultrahigh-molecular-weight polyethylene (UHMWPE) is a linear homopolyethylene that used as an engineering thermoplastic, owing to its exceptional high impact resistance, extreme chemical inertness, low coefficient of friction, and superior wear resistance.[1–4] Despite its outstanding properties, the processing of UHMWPE presents a considerable challenge. Conventional melt-processing methods are largely ineffective due to the absence of melt flow, which arises from an extremely high molecular weight and highly entangled chain structure.[5,6] In practical applications, UHMWPE is commonly processed directly from reactor powder using powder metallurgy techniques, which involve cold compaction followed by sintering at elevated temperature.[7] During compaction, the powder is compressed within a rigid die, leading to particle rearrangement and plastic deformation at the contact points. This is followed by sintering, where elevated temperature promote melting and coalescence of the particles. In the sintering step, integrity of the product relies on the diffusion of polymer chains into compaction voids and across particle boundaries. Due to the extremely high molecular weight and the restricted chain mobility arising from entangled network, the diffusion is significantly hindered.

As a result, microstructural regions with varying degrees of fusion develop, especially at the interparticle interfaces. These weakly fused regions can serve as stress concentrators, compromising the mechanical properties of the final product.[6,8–10] This polymer integrity issue is further amplified in UHMWPE nanocomposites, where various fillers are incorporated to enhance mechanical, thermal, electrical, electromagnetic shielding, or tribological properties.[11–16] Since melt mixing is not viable, fillers are typically mixed with UHMWPE powder prior to processing. In this approach, the fillers tend to segregate at the polymer interfaces, forming physical barriers that hinder interparticle diffusion and ultimately resulting in a significant reduction in mechanical properties even at a small amount of filler loadings.[12]

The efficiency of polymer sintering is influenced by several factors, including the initial state of polymer chain entanglement,[6,8,9,17,18] the morphology of UHMWPE powder,[17,19,20] polymer particle size,[21–24] and processing conditions.[9,17,25] Reactor powder with a fibril-like morphology[26] and reduced chain entanglement[25,27] has been shown to promote enhanced sintering. By contrast, large UHMWPE particles that create substantial interparticle voids during compaction[28,29] or particles with significant intraparticle porosity[30] often display poor consolidation because chain diffusion must occur over longer distances. To improve the integrity of pristine UHMWPE, various strategies have been investigated. These include using less-entangled UHMWPE polymers,[22,26,31] employing polymers with small particle sizes[28] or bimodal particle distributions,[21,24] applying mechanical vibration treatment to densify packing,[32] and sintering through the transient hexagonal phase,[33] among others. For UHMWPE nanocomposites, research has focused primarily on controlling filler distribution, such as using solvents to disperse both polymers and fillers,[12,34,35] in-situ polymerization with fillers serving as catalyst supports,[13] and incorporating secondary polymers that promote filler dispersion within the interstitial spaces between UHMWPE particles.[36,37] Such strategies help suppressing filler segregation to minimize weakly bonded zones, thereby restoring the mechanical integrity of UHMWPE nanocomposites.

In Chapter 2, I reported the control of filler distribution patterns using Small (Figure 3.1).[21] Owing to its extremely small particle size of less than 1 μm, the greatly increased polymer interface area enables uniform dispersion of the fillers in a simple physical mixing, resulting in a homogeneous filler distribution in the final nanocomposites instead of segregated structure reported for typical UHMWPE nanocomposites. Furthermore, when Small serves as the continuous phase in which the filler is uniformly dispersed, a semi-segregated structure is formed. This architecture allows for the preservation of mechanical properties while simultaneously achieving the percolation threshold for electrical conductivity at low filler

loadings. In this Chapter, I investigate the sintering and processing-dependent mechanical behavior of UHMWPE and its nanocomposites in the presence of Small. Specifically, I evaluate how the mechanical response of the semi-segregated structure is influenced by sintering temperature and time. Furthermore, high-temperature uniaxial stretching was performed on the nanocomposites to understand their potential to form nanocomposite tapes and fibers via a solvent-free route.

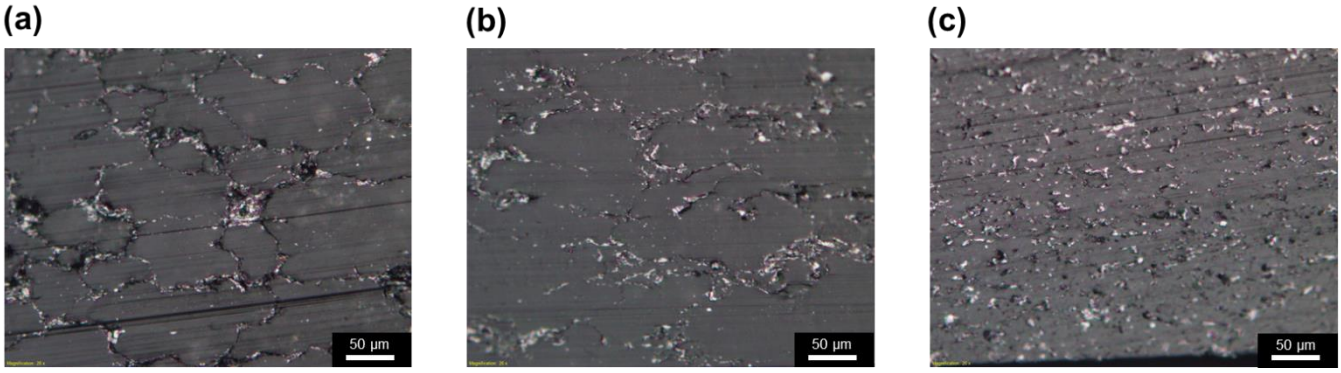

Figure 3.1. Filler distribution patterns of UHMWPE nanocomposites: a) segregated structure, b) semi-segregated structure, and c) homogeneous filler distribution.

3.2. Methods

3.2.1. Materials

Commercial ultrahigh-molecular-weight polyethylene powder (the viscosity average molecular weight (M_v) = 4.50 × 10^6 g mol^{-1}, D_{50}=68.6 µm, relative span factor (RSF) = 1.65, denoted as Large) was provided by Asahi Kasei Corp. Graphene nanoplatelets (GNP, 6–8 nm thick and 5 µm width) were purchased from Tokyo Chemical Industry Co., Ltd. Irganox 1010 was purchased from Toyotsu Chemiplas Corp. Ethanol (purity > 99.5%, Kanto chemical

Industry Co., Ltd.) was used as received. Small (M_v = 4.42 × 10^6 g mol^{-1}, D_{50}=523 nm, RSF = 0.321) was synthesized following previous researches.[22,23]

3.2.2. Preparation of nanocomposites

Nanocomposite films with a thickness of 500 μm were prepared using compression molding: the Large powder was physically mixed with Irganox 1010 (0.7 wt%) as a stabilizer and a desired loading of GNP in a dry powder form until the GNP was uniformly dispersed in the powder matrix. The blended powder was then filled into a 5 cm × 5 cm hollow aluminum sheet, sandwiched between polyimide films and iron plates, and placed in a hot press machine (AH-2003, AS ONE Corp.). The blended powder was compacted at room temperature under contact pressure for 5 min and then raised to the desired temperature. Subsequently, the powder was hot-pressed at 20 MPa at 160–230 °C for 5 min, and then quenched to room temperature. The nanocomposite films are denoted as Large/GNP*x*-*y*, where *x* and *y* represent the GNP loading in weight percent and sintering temperature, respectively. Small was introduced to Large to form a mixed matrix (denoted as Mix25) at a weight percent of 25 wt%, the composite was referred as Mix25/GNP*x*-*y*. Additionally, nanocomposites were prepared at 160 °C and 190 °C with extended sintering time of 2 h and 20 h to evaluate the effect of sintering time on the mechanical properties. The sample was labeled as Mix25/GNP*x*-*y*-*z*, where *z* represents sintering time.

3.2.3. Preparation of nanocomposites fibers by uniaxial stretching at high temperature

Nanocomposite fibers were prepared by stretching dumbbell shape specimens using a tensile tester (3365, Instron). The sample was placed in a chamber at 135 °C and held for 10 min to ensure thermal softening and stress relaxation. The specimen was then subjected to stretching at a constant rate of 20 mm min^{-1} until fracture.

3.2.4. Characterization

The particle size of UHMWPE was analyzed by light scattering (LA-950V2, HORIBA Ltd.) in ethanol suspension. The mean particle size (D_{50}) was defined as the particle diameter at 50% in the cumulative number-based particle size distribution. The film cross-section was observed by scanning electron microscope (SEM, JCM-6000Plus, JEOL Ltd.,) and optical microscope (BX51, Olympus Corp. with a digital camera (DP28 camera, Olympus Corp.)). Mechanical properties of nanocomposites were measured using a tensile tester (3365, Instron) at room temperature and a cross-head speed of 1.5 mm min^{-1}. Dumbbell shape specimens were die-cut from the film sample and the measured properties were reported as an average value from repetitive tests. The Fourier-transform infrared spectra were obtained with an FTIR spectrometer (Spectrum 100, PerkinElmer Japan G.K.) between 4000 and 400 cm^{-1} using diamond attenuated total reflection (ATR) accessory. Thermal diffusivity was measured using a laser flash method on an ai-Phase mobile 1u/2 instrument (Hitachi High-Tech Science Corp.). Thermal conductivity was calculated from the thermal diffusivity as

$$K=\alpha\rho C_{\mathrm{p}} \quad (1),$$

where K and α are the thermal conductivity and thermal diffusivity of the nanocomposite. ρ and C_{p} are the density and heat capacity of the nanocomposite. In this Chapter, ρ and C_p were not measured directly because determining C_p of the nanocomposites experimentally is challenging and requires a relatively large, homogeneous sample. Instead, I calculated ρ and C_p based on the rule of mixtures using the known values of the constituent materials (UHMWPE: $\rho = 0.94$ g cm^{-3} and $C_p = 2.0$ kJ K^{-1} kg^{-1},[38] GNP: $\rho = 2.3$ g cm^{-3} and $C_p = 1.2$ kJ K^{-1} kg^{-1}).[39] This approach has been commonly employed in nanocomposite systems and provides reasonable accuracy for comparative analysis.[40–42] Differential scanning calorimetry (DSC) measurements were performed on a DSC 822 (Mettler Toledo) under a nitrogen flow

rate of 75 mL min^{-1}. To evaluate the entanglement state of nascent UHMWPE powders, the samples were heated from 30 °C to either 160 or 230 °C at a heating rate of 4 °C min^{-1} and held for 5 min. Subsequently, the samples were cooled at a rate of 10 °C min^{-1}. The crystallization temperature during the cooling process was used as an indicator of the entanglement density of the nascent UHMWPE powders. For the evaluation of melting behavior before and after stretching, UHMWPE/GNP nanocomposite films were heated from 30 °C to 200 °C at a heating rate of 10 °C min^{-1}, held for 1 min, and then cooled to −50 °C at a rate of 10 °C min^{-1}.

3.3. Results and discussion

3.3.1. Influence of Small powder introduction on the sintering behavior of pristine polymer

The pristine UHMWPE films were prepared using either a single-component matrix (Large) or a blended matrix (Mix25). The latter was done by physically mixing Large and Small in a 75:25 weight ratio. This ratio is decided based on the ideal packing fraction of 74% for spherical particles wherein the addition of Small fills the interstitial voids between larger particles. The particle size distribution of the Large and Small is presented in Figure 3.2. The mean particle size (D_{50}) of Large and Small was 68.6 μm and 523 nm, respectively. Figure 3.3 shows SEM images of the cryo-fractured surfaces of films prepared at different temperatures. At 160 °C, the Large film exhibited a rough fracture surface with the presence of large voids (Figure 3.3a). The surface became progressively smoother at 190 °C and above, with large voids no longer observed, indicating improved fusion at elevated temperatures. In contrast, Mix25 maintained a smooth fracture surface without large voids regardless of the fabrication temperature (Figure 3.3b), demonstrating that the incorporation of smaller UHMWPE particles enhances the packing and sintering behavior of the matrix.

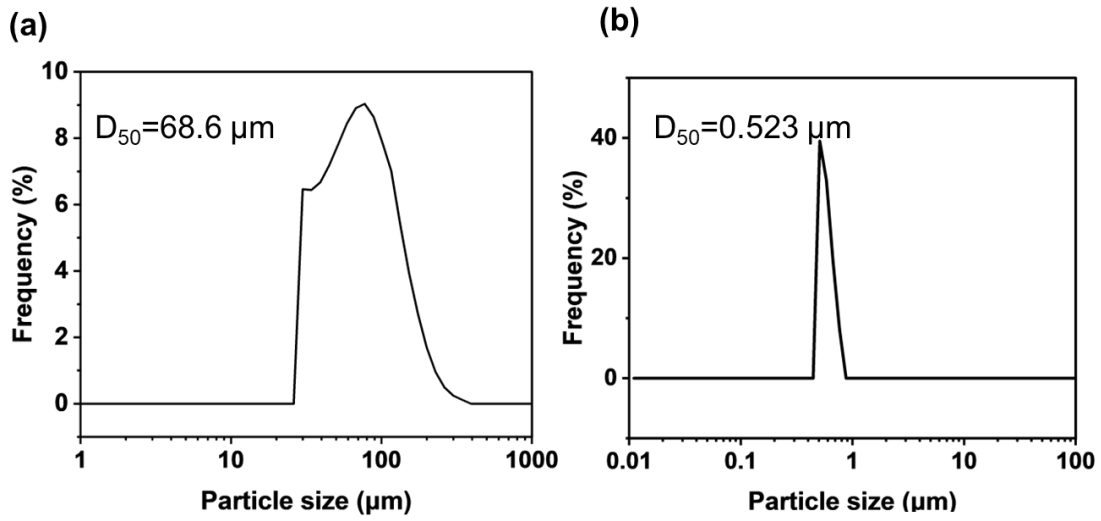

Figure 3.2. Particle size distribution of a) Large and b) Small UHMWPE.

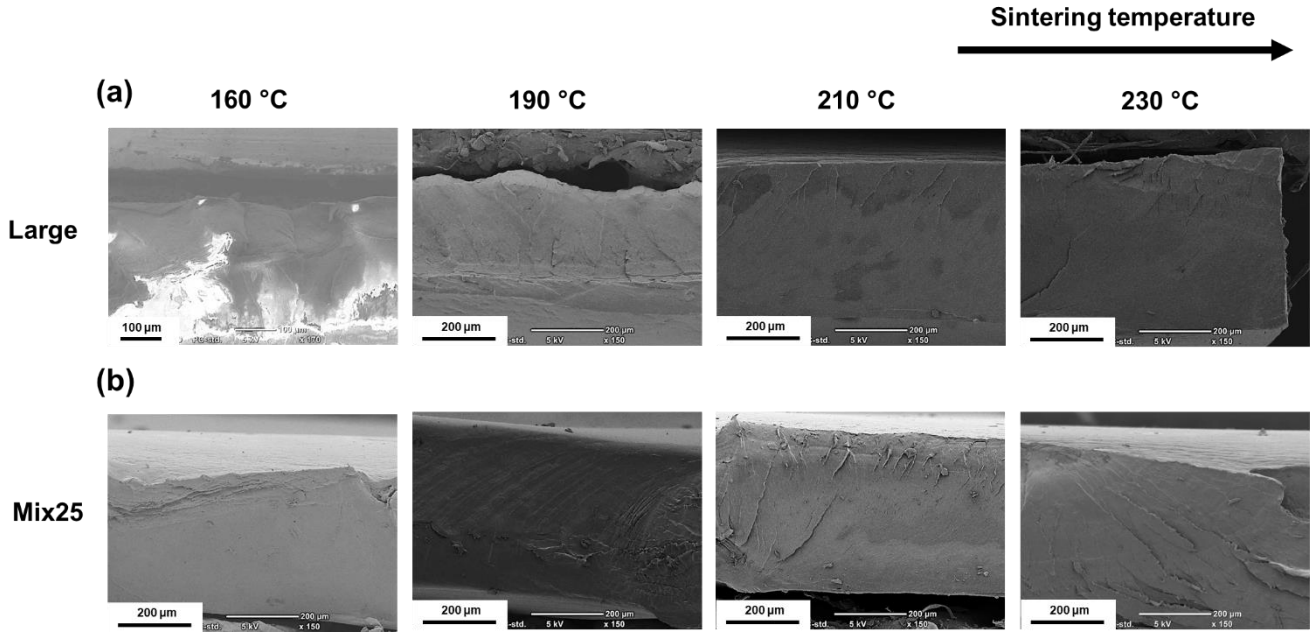

Figure 3.3. SEM images of cryo-fractured surface of pristine films: a) Large, and b) Mix25 prepared at different temperatures. The much smoother fractured surface observed in Mix25 especially at a low sintering temperature demonstrates that incorporating smaller UHMWPE particles enhances particle packing and sintering behavior in the matrix.

Mechanical properties were evaluated using a tensile tester. A dual yielding behavior was observed at sintering temperature above 190 °C (Figure 3.4).[8,43] The first yield point is associated with slippage of micro-sized crystals,[44] followed by strain hardening as polymer chains align under continued deformation to increase the resistance to further strain. The second yield point corresponds to chain slippage or yielding of more structurally robust domains, after which the material ultimately fractures. Differences in the mechanical property response to the sintering temperature were observed between the Large and Mix25 samples. Specifically, the Large sample showed improvements in stress at yield, strain at break, and toughness as the temperature increased (Figure 3.4a, Table 3.1). On the other hand, the Mix25 sample exhibited peak mechanical properties at the sintering temperature of 190 °C. At temperature above 210 °C, the elongation at break and the toughness decreased by 11–22% (Figure 3.4b, Table 3.1). To evaluate the degree of entanglement, DSC measurements were performed, and the crystallization temperature (T_c) during the cooling process was used as an indicator of the entanglement state of nascent UHMWPE powders. A lower T_c was interpreted as a higher degree of entanglement due to restricted chain mobility during crystallization. Compared with the Large and Small sintered at 160 °C, the Small exhibited a 0.9 °C higher T_c, indicating a lower degree of entanglement (Figure 3.5a,c, Table 3.2). The samples sintered at 230 °C showed lower T_c values than those sintered at 160 °C, with decrease of 5.2 °C and 8.0 °C for the Large and Small, respectively. In addition, a crystallization peak was observed around 80–85 °C in the samples sintered at 230 °C (Figure 3.5b,d, Table 3.2). These results indicate that polymer chain entanglement increases with increasing sintering temperature. Although all obtained films were transparent and showed no visible signs of degradation after compression molding, FTIR-ATR was employed to assess the possibility of thermal degradation as a cause of the observed mechanical deterioration. A trace C=O signal was

detected at 1740 cm^{-1} (Figure 3.6), however, its intensity is independent of the mechanical properties, and is rather attributed to the stabilizer than the polymer backbone. Therefore, polymer degradation can be excluded as the origin of the reduced mechanical properties. One potential cause of the reduced elongation at break for Mix25 at high temperature might be related to the molecular structure of the Small. The powder was produced using a poreless and nano-sized Ziegler–Natta catalyst to yield less-entangled polymer chains.[21] During high-temperature processing, these initially less entangled chains can undergo rapid relaxation, sometimes referred to as a "chain explosion", which encourages the formation of new entanglements.[9,28] The newly formed entanglements might act like physical crosslinks, ultimately leading to decreased elongation at break. Investigation on pristine polymer showed that the mechanical properties of UHMWPE are dependent on the processing temperature, where incorporating Small to fill intraparticle voids enables effective compaction and sintering to achieve superior mechanical properties even at low-temperature processing.

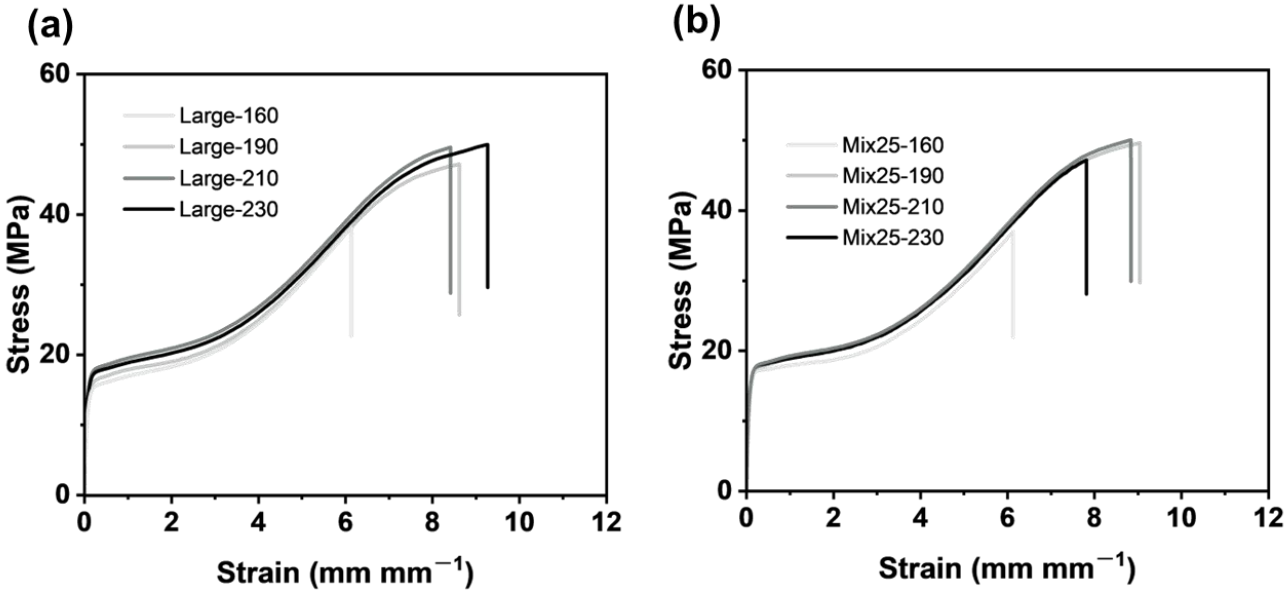

Figure 3.4. Stress-strain curves of pristine UHMWPE films prepared at different temperature: a) Large-*y*, and b) Mix25-*y*, where *y* represents the compression temperature.

Table 3.1. Mechanical Properties of UHMWPE Films.

Sample	U.T.S. (MPa)	Strain at break (mm mm^{-1})	Young's modulus (MPa)	Toughness (MJ m^{-3})	Stress at yield (MPa)
Large-160	37±1.8	6.0±0.23	310±19	140±9.8	16±0.4
Large-190	48±0.9	8.6±0.13	200±6.9	260±9.1	17±0.3
Large-210	49±0.4	8.6±0.25	210±3.1	260±10	17±0.2
Large-230	50±1.7	9.2±0.82	220±1.9	290±42	18±0.1
Mix25-160	38±0.9	6.2±0.14	220±5.0	140±4.7	18±0.2
Mix25-190	48±0.8	9.3±0.28	200±10	280±5.7	16±0.8
Mix25-210	48±0.9	8.3±0.37	210±2.3	240±19	19±0.1
Mix25-230	47±0.8	7.7±0.23	220±2.1	220±11	19±0.1

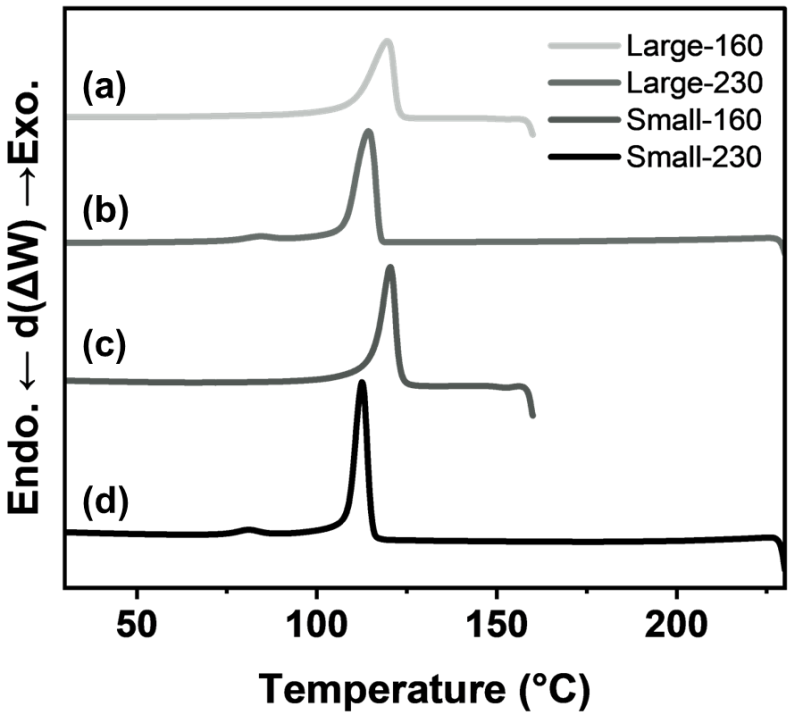

Figure 3.5. DSC cooling curves of UHMWPE nascent powders after heating to different temperatures. (a) Large heated at 160 °C, (b) Large heated at 230 °C, (c) Small heated at 160 °C, and (d) Small heated at 230 °C.

Table 3.2. T_c of UHMWPE After Heating to 160 °C and 230 °C

Sample	T_c **(°C)**
Large-160	119.6
Large-230	114.4 (84.0)[a]
Small-160	120.5
Small-230	112.5 (81.1)[a]

a) Secondary crystallization peak observed at lower temperature

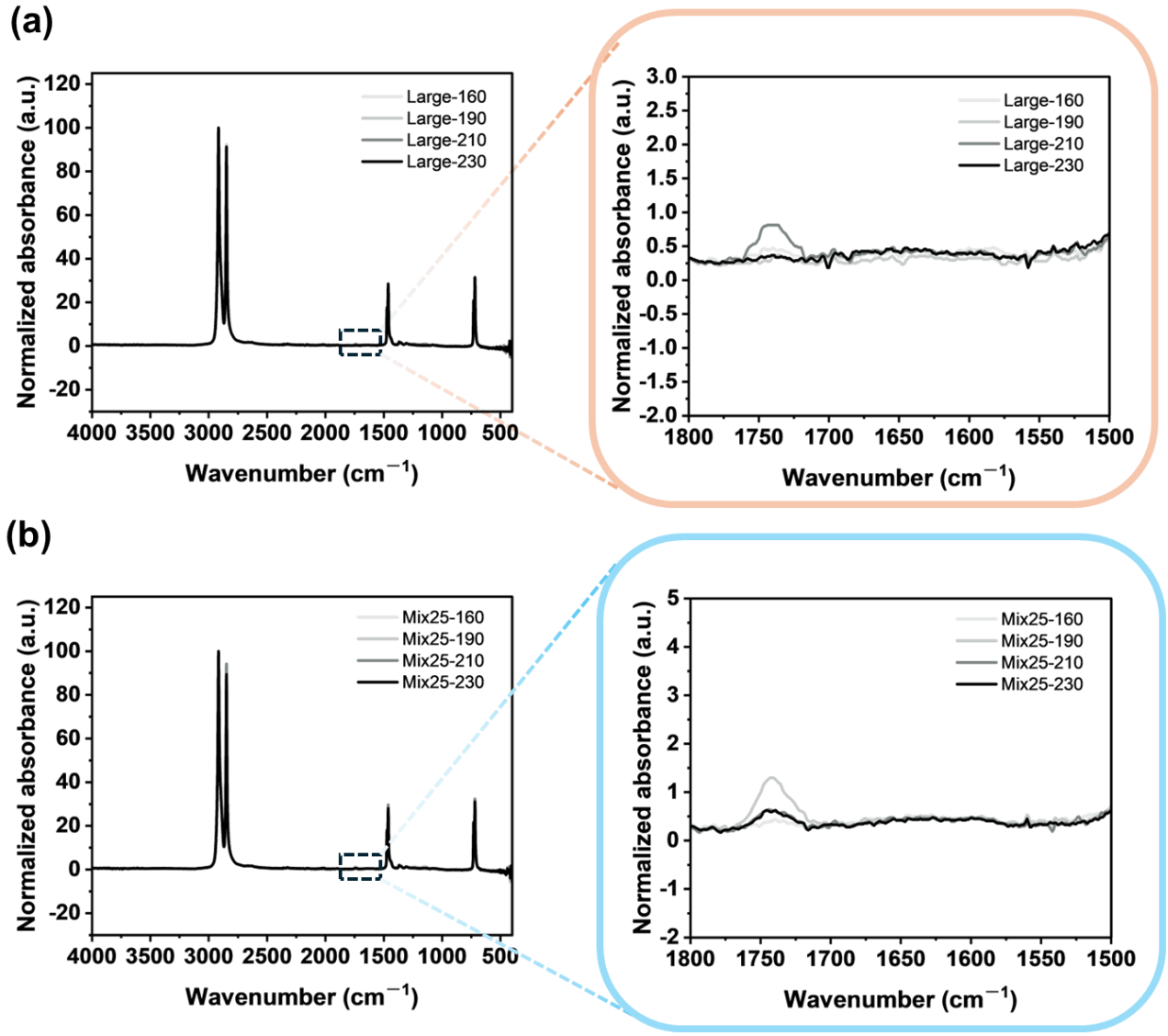

Figure 3.6. FTIR-ATR spectra of pristine UHMWPE films prepared by varying sintering temperature: a) Large and b) Mix25. The spectrum was normalized using the peak at 2916 cm^{-1}.

3.3.2. Influence of sintering temperature and sintering time on the mechanical properties of UHMWPE nanocomposites

I have previously reported the use of Small to control the distribution pattern of fillers in UHMWPE nanocomposites.[21] For instance, when Small was used as the matrix alone, it promoted a homogeneous distribution of the fillers, in contrast to the typical segregated structure observed when commercial UHMWPE was used as the matrix. Furthermore, when it was pre-mixed with the fillers prior to blending with Large, it formed a semi-segregated network, where the fillers were distributed within the continuous phase of Small. This semi-segregated structure helps retain both the conductive network, which is otherwise lost when fillers are homogeneously distributed, and the mechanical properties of the nanocomposites, which typically deteriorate due to poor polymer fusion. In this Chapter, I focus on the mechanical property response of the semi-segregated structures to processing temperature and time. The nanocomposites containing GNP of 5.0 wt% loading, Large/GNP5-*y* and Mix25/GNP5-*y*, where *y* represents the sintering temperature, were prepared following the previously reported method to form films with segregated and semi-segregated structures, respectively. Figure 3.7 shows optical microscope images of the film cross-sections. In the Large/GNP sample, GNP appears as a thick continuous line along the interfaces between polymer particles, indicating a typical segregated structure. On the other hand, with the introduction of Small powder in the Mix25/GNP sample, the GNP is more finely dispersed within the continuous domain between Large particles, forming a semi-segregated network. Figure 3.8a,b depicts the stress-strain curves of the films prepared at different temperature and the mechanical properties acquired from the stress-strain curves are summarized in Figure 3.8c,d and Table 3.3. Unlike the pristine films, the nanocomposites did not exhibit dual yielding, and the fracture occurred at lower strain, especially for Large/GNP nanocomposites. This is attributed to the introduction of weak interfacial boundaries between the polymer and the

fillers.[12] These interfaces act as stress concentrators, promoting localized failure in mechanically weak regions where filler aggregation occurs. Increasing the sintering temperature from 160 °C to 230 °C led to improvements in both elongation at break and toughness, particularly in the Mix25/GNP samples. This enhancement can be attributed to several factors associated with the semi-segregated structure. In this configuration, GNP is not strictly confined at the interparticle boundaries but is distributed within the continuous phase. At higher temperature, the increased Brownian motion of fillers facilitates their movement within the continuous phase,[45,46] enhancing filler redistribution. Furthermore, the semi-segregated structure contains fewer fillers at the interfaces of the larger matrix particles, allowing better polymer chain diffusion and fusion, which further strengthens the overall structure. This results in 8–15 times higher in toughness and 7–11 times higher in strain at break compared with Large/GNP5 (Figure 3.8c,d). In addition to mechanical properties, the thermal conductivity of the nanocomposites was evaluated. As shown in Figure 3.8e, the thermal conductivity remained relatively similar in the range of 0.8–1.0 $Wm^{-1}K^{-1}$, regardless of the matrix type (Large or Mix25) or the sintering temperature. I attribute this to the fact that both GNP and UHMWPE inherently contribute to thermal conduction, and the structural variations introduced by fusion degree exert only a minor influence on the overall thermal transport pathways.

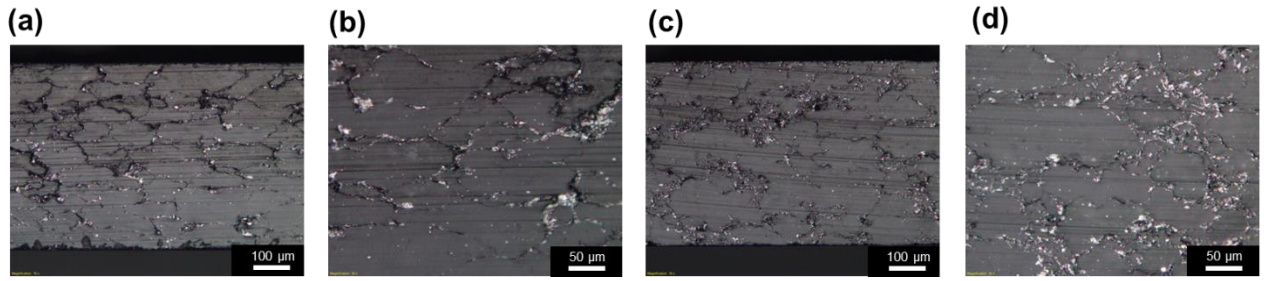

Figure 3.7. Cross-sectional optical microscope images of nanocomposites: a,b) Large/GNP5-160 and c,d) Mix25/GNP5-160. In Large/GNP, GNP forms thick, continuous lines, typical of a segregated structure, whereas in Mix25/GNP, GNP is more uniformly dispersed within the continuous polymer domains, forming a semi-segregated network.

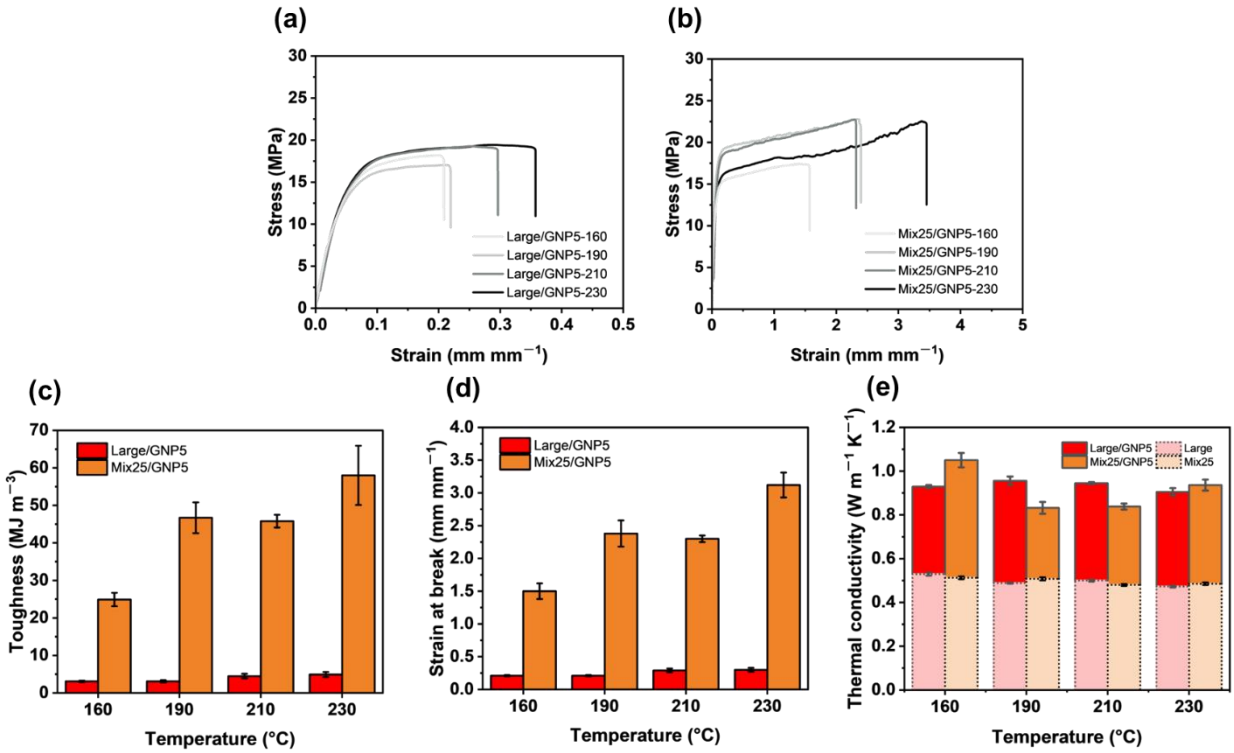

Figure 3.8. Stress-strain curves of obtained UHMWPE/GNP nanocomposites with Large and Mix25 matrices: a) Large/GNP5-*y*, b) Mix25/GNP5-*y*, where *y* represents sintering temperature. (c) Toughness, (d) strain at break, and (e) thermal conductivity of Large/GNP and Mix25/GNP at different sintering temperature.

Table 3.3. Mechanical Properties of Large/GNP5 and Mix25/GNP5 with Varying Sintering Temperature.

Sample	U.T.S. (MPa)	Strain at break (mm mm^{-1})	Young's modulus (MPa)	Toughness (MJ m^{-3})	Stress at yield (MPa)
Large/GNP5-160	18±0.2	0.21±0.01	270±4.4	3.1±0.2	17±0.3
Large/GNP5-190	17±0.2	0.21±0.01	250±1.7	3.1±0.3	16±0.1
Large/GNP5-210	18±0.5	0.29±0.03	260±8.2	4.5±0.6	17±0.4
Large/GNP5-230	19±0.4	0.30±0.03	260±8.3	4.9±0.7	18±0.1
Mix25/GNP5-160	18±0.4	1.5±0.12	230±7.3	25±1.8	17±0.6
Mix25/GNP5-190	22±0.5	2.4±0.20	260±10	47±4.1	19±0.3
Mix25/GNP5-210	22±0.5	2.3±0.05	240±23	46±1.7	19±0.3
Mix25/GNP5-230	21±2.0	3.1±0.19	220±18	58±7.9	16±1.3

The effect of sintering time was examined on the Mix25/GNP samples to understand how extended thermal exposure influences polymer fusion in the presence of fillers. As shown in Figure 3.9a,b, at 160 °C, the elongation at break increased with longer sintering time. In contrast, at 190 °C, elongation at break reached its maximum at 2 h, and further increase in sintering time did not result in significant changes in the property. In UHMWPE, which has extremely long polymer chains and a high degree of entanglement, polymer chains cannot move freely in all directions due to constraints from neighboring chains, but instead slides back and forth within a tube-like region formed by the surrounding chains according to the chain

reptation theory.[47] This motion is slow and requires time for the chain to diffuse out of its original tube into a new configuration. On the other hand, compression-molded films can be formed at much shorter time than the reptation time due to the so-called chain explosion mechanism. In this process, entropy-driven melting facilitates the rapid formation of random coils, enabling interwinding and entanglement with neighboring chains.[1,28,48,49] Unlike reptation, chain explosion is strongly dependent on temperature and heating rate, and is particularly effective in less-entangled chains.[9,49] Based on this framework, the observed behavior can be interpreted as follows: at 160 °C, the chain explosion mechanism is less effective, and entanglement develops gradually through slower reptation-driven interdiffusion of chains, leading to progressive improvements in mechanical properties. In contrast, at 190 °C, the higher temperature strongly activates chain explosion, rapidly forming heterogeneous entanglement structures. Once these structures are established, further chain mobility becomes restricted, resulting in a plateau of mechanical properties. As a result, at short sintering time (i.e., 5 min), the elongation at break is significantly higher at 190 °C than at 160 °C, indicating more efficient chain diffusion and faster structural development. However, with increasing sintering time, gradual chain interdiffusion at 160 °C allows the network structure to approach equilibrium, reducing the difference in elongation at break between the two temperatures.

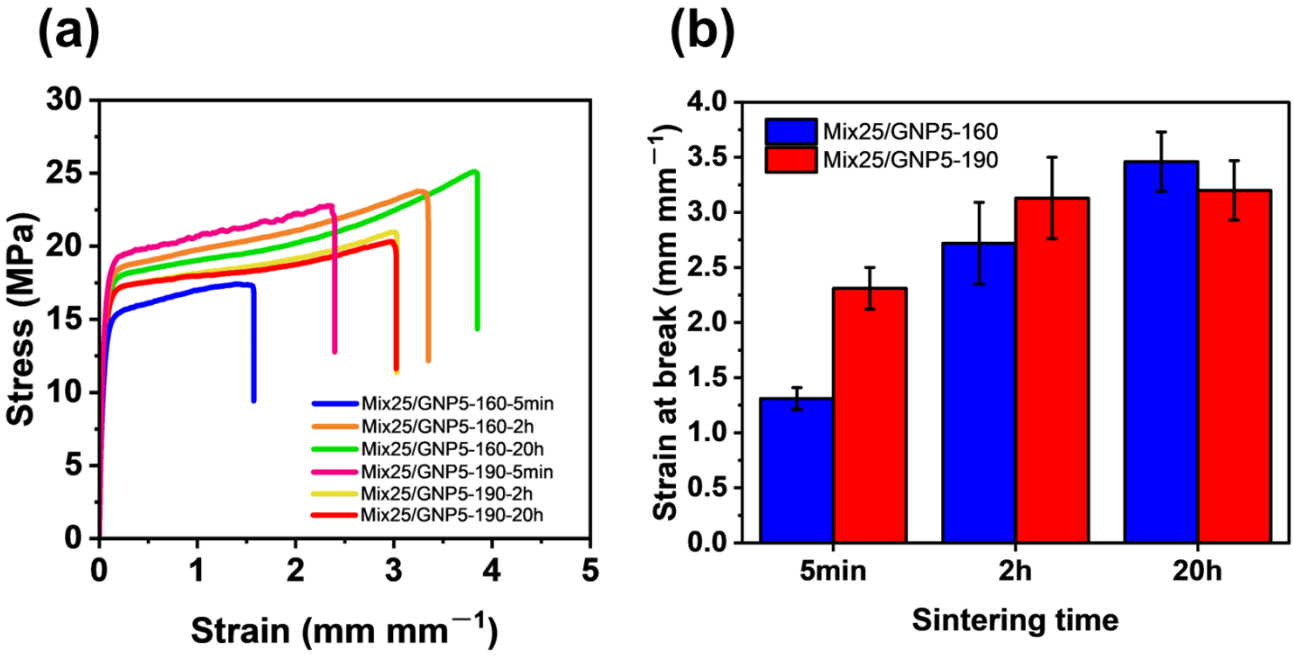

Figure 3.9. a) Mechanical properties of Mix25/GNP5 nanocomposites prepared at different temperature and time: a) stress-strain curves, and b) strain at break at different sintering time.

3.3.3. Nanocomposites fibers by uniaxial stretching at high temperature

The potential for fabricating UHMWPE/GNP nanocomposite tapes and fibers was evaluated through uniaxial stretching of the film at elevated temperature. Dumbbell-shaped specimens, die-cut from the pressed films, were first equilibrated at 135 °C for 10 min in a temperature-controlled chamber to ensure thermal softening and stress relaxation. The specimen was then subjected to stretching at a constant rate of 20 mm min^{-1} until fracture. The experimental setup and the appearance of the specimen during stretching are shown in Figure 3.10a. The stress–draw ratio curves for Large/GNP5-230 and Mix25/GNP5-230, prepared by pressing at 230 °C for 5 min, are shown in Figure 3.10b,c. The draw ratio is defined as the ratio of the final length (L) to the initial length (L_0), given by L/L_0. In Figure 3.10b, the Large/GNP5-230 sample achieved a draw ratio of 21.9 until breaking. In contrast, the Mix25/GNP5-230 sample

exhibited superior ductility and did not fracture at the maximum extension limit with the draw ratio of 27.5 (Figure 3.10c). To further enhance the draw ratio, a two-step stretching process was employed. In the first step, the specimen was stretched at 135 °C to the maximum instrumental limit. While held under tension, the sample was cooled to room temperature. The second stretching step was then carried out using a 4 cm-long segment cut from the stretched samples. Since stretching induces polymer chain orientation,[50,51] the melting temperature of the sample after the first stretching increased from 136 °C to 143 °C (Figure 3.11). Therefore, the second stretching was carried out at 145 °C, empirically optimized to approach the softening point of the sample. This temperature, slightly above the melting point of the sample, compensates for heat loss in the chamber. The total draw ratio is the product of the draw ratios from each stretching step, resulting in a total draw ratio of 38.2 after the two-step stretching process.

As far as I have been able to investigate, high draw ratios up to 70 of UHMWPE/graphene or graphene oxide nanocomposites have been reported only for nanocomposite films prepared via solution casting[52] and the xerogel method.[53] However, in a solvent-free solid-state processing route, achieving such high draw ratios in nanocomposites containing high-aspect-ratio fillers like graphene nanoplatelets has not been reported. High-aspect-ratio fillers, compared to spherical ones, tend to align horizontally along the surface of polymer particles during sintering. This alignment allows them to more effectively cover the polymer particle interfaces, which greatly hinder polymer fusion. However, in this Chapter, a high draw ratio of 38.2 was achieved even with a relatively high weight percent loading of GNP. This exceptional stretchability is attributed to the use of Small, which facilitates the formation of a semi-segregated filler structure and promotes better sintering of the polymer matrix, demonstrating potential for fabrication of nanocomposite tapes and fibers via a solvent-free route.

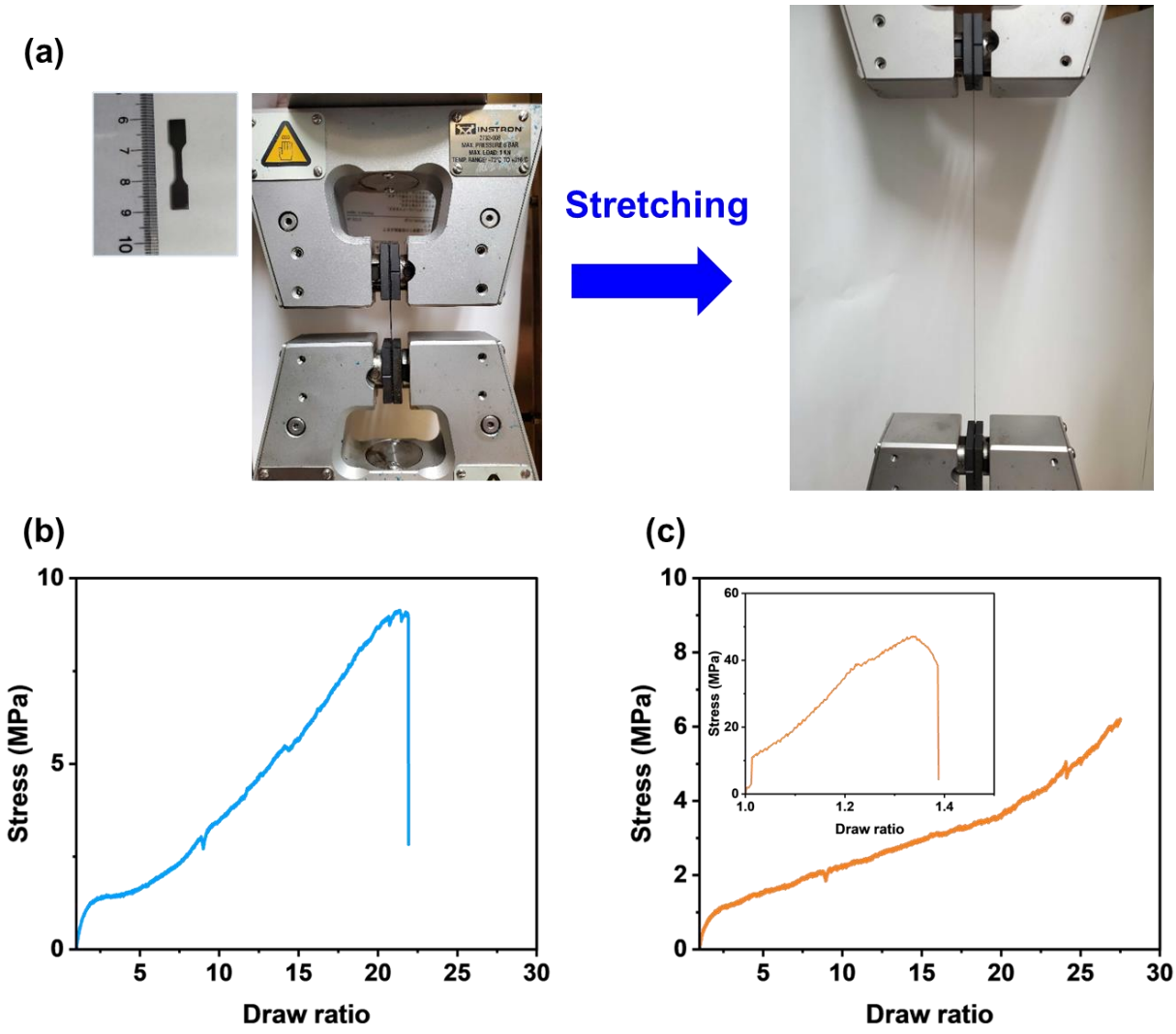

Figure 3.10. Uniaxial tensile test for UHMWPE/GNP fiber preparation: a) experimental setup and specimen appearance during the stretching process. Stress as a function of draw ratio for b) Large/GNP5-230 and c) Mix25/GNP5-230. The second stretching step of the Mix25/GNP5-230 sample is shown as an inset in Figure 3.10c. L_0= 8.0 mm.

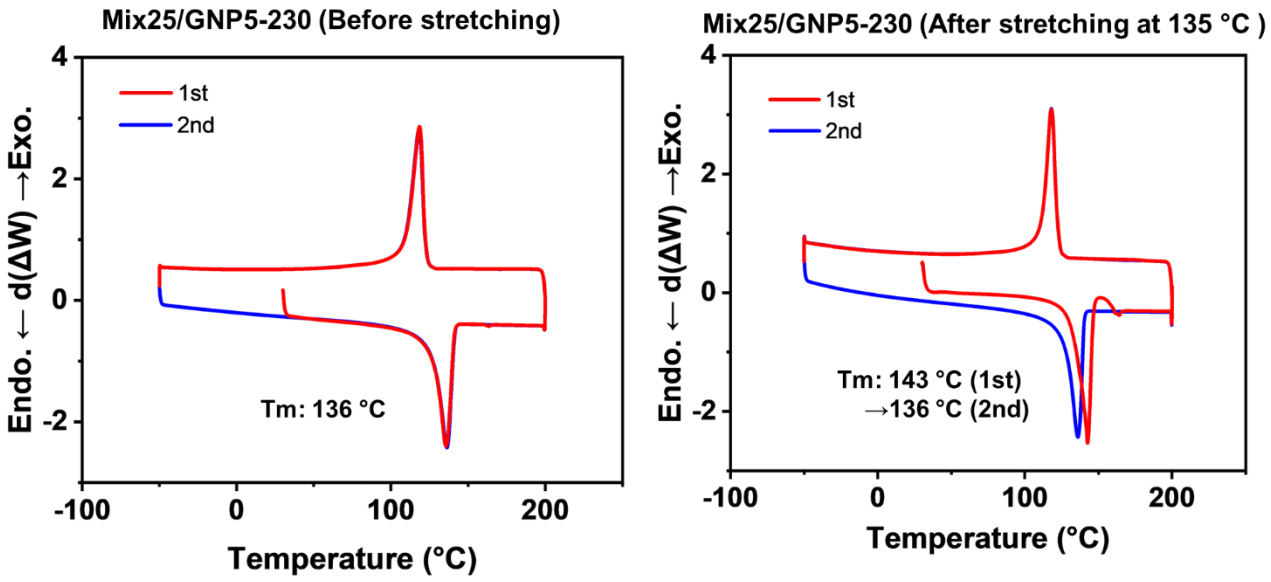

Figure 3.11. Melting profiles of Mix25/GNP5-230 before and after the first stretching at 135 °C.

3.4. Conclusions

In this Chapter, the sintering and processing-dependent mechanical behavior of UHMWPE and its nanocomposites in the presence of Small was investigated. In pristine films, increasing the sintering temperature promoted polymer particle fusion, and when sufficient sintering was achieved at the elevated temperature, the polymer exhibited dual yielding behavior. Morphological and mechanical analyses revealed that the addition of Small to fill intraparticle voids between commercial UHMWPE particles enabled effective compaction and the formation of well-fused structures, resulting in superior mechanical properties even at low processing temperature. In UHMWPE/GNP nanocomposites, the addition of Small promoted the formation of a semi-segregated structure, in which the fillers were finely dispersed within the continuous domain of Small. This configuration minimized the segregation of nanoparticles at the interfaces of larger polymer particles, leading to improved mechanical properties compared to nanocomposites prepared without Small. As the sintering temperature increased,

the mechanical properties improved further due to enhanced interdiffusion of polymer chains. At low temperature, prolonged sintering enhanced polymer fusion and consequently the mechanical properties, whereas at high temperature, the properties reached their maximum within a short period of time, likely due to a chain explosion mechanism. The potential for fabricating UHMWPE/GNP nanocomposite tapes and fibers via a solvent-free route was demonstrated through high-temperature uniaxial stretching. Despite the presence of high-aspect-ratio graphene nanoplatelets, which typically hinder polymer fusion, a high draw ratio was achieved, particularly in the sample containing Small. This enhanced stretchability was attributed to the formation of a semi-segregated filler structure and improved sintering, highlighting the effectiveness of Small in enabling both processability and mechanical performance.

References

(1) Deplancke, T.; Lame, O.; Rousset, F.; Seguela, R.; Vigier, G. Mechanisms of Chain Reentanglement during the Sintering of UHMWPE Nascent Powder: Effect of Molecular Weight. *Macromolecules* **2015**, *48*, 5328–5338. https://doi.org/10.1021/acs.macromol.5b00618.

(2) Rastogi, S.; Kurelec, L.; Lippits, D.; Cuijpers, J.; Wimmer, M.; Lemstra, P. J. Novel Route to Fatigue-Resistant Fully Sintered Ultrahigh Molecular Weight Polyethylene for Knee Prosthesis. *Biomacromolecules* **2005**, *6*, 942–947. https://doi.org/10.1021/bm0493638.

(3) Sun, B.; Li, J.; Guo, Y.; Li, H.; Mi, H. Y.; Dong, B.; Liu, C.; Shen, C. Superhydrophobic UHMWPE Foams with High Mechanical Robustness and Durability Fabricated by Supercritical CO_2 Foaming. *ACS Sustainable Chem. Eng.* **2021**, *9*, 12663–12673. https://doi.org/10.1021/acssuschemeng.1c04573.

(4) Lekkala, S.; Inverardi, N.; Grindy, S. C.; Hugard, S.; Muratoglu, O. K.; Oral, E. Irradiation Behavior of Analgesic and Nonsteroidal Anti-Inflammatory Drug-Loaded UHMWPE for Joint Replacement. *Biomacromolecules* **2024**, *25*, 2312–2322. https://doi.org/10.1021/acs.biomac.3c01179.

(5) Sharip, N. S.; Ariffin, H.; Yasim-Anuar, T. A. T.; Andou, Y.; Shirosaki, Y.; Jawaid, M.; Tahir, P. M.; Ibrahim, N. A. Melt- vs. Non-Melt Blending of Complexly Processable Ultra-High Molecular Weight Polyethylene/Cellulose Nanofiber Bionanocomposite. *Polymers* **2021**, *13*, 404. https://doi.org/10.3390/polym13030404.

(6) Wu, S.-L.; Qiao, J.; Guan, J.; Chen, H.-M.; Wang, T.; Wang, C.; Wang, Y. Nascent disentangled UHMWPE: Origin, synthesis, processing, performances and applications. *Eur. Polym. J.*, **2023**, *184*, 11799. https://doi.org/10.1016/j.eurpolymj.2022.111799.

(7) Hambir, S.; Jog, J. P. Sintering of ultra high molecular weight polyethylene. *Bull. Mater. Sci.* **2000**, *23*, 221–226. https://doi.org/10.1007/BF02719914.

(8) Deplancke, T.; Lame, O.; Rousset, F.; Aguili, I.; Seguela, R.; Vigier, G. Diffusion versus Cocrystallization of Very Long Polymer Chains at Interfaces: Experimental Study of Sintering of UHMWPE Nascent Powder. *Macromolecules* **2014**, *47*, 197–207. https://doi.org/10.1021/ma402012f.

(9) Wang, W.; Wang, H.; Chen, J. Research on Chain Diffusion and Entanglement via Controlling the Sintering Process of Nascent UHMWPE. *Macromolecules* **2024**, *57*, 2205–2217. https://doi.org/10.1021/acs.macromol.3c02361.

(10) Wu, J. J.; Buckley, C. P.; O'connor, J. J. Processing of Ultra-High Molecular Weight Polyethylene: Modelling the Decay of Fusion Defects. *Chem. Eng. Res. Des.* **2002**, *80*, 423–431. https://doi.org/10.1205/026387602320224003.

(11) Gudkov, M. V.; Brevnov, P. N.; Rabchinskii, M. K.; Baidakova, M. V.; Stolyarova, D. Y.; Antonov, G. A.; Yagovkina, M. A.; Ryvkina, N. G.; Bazhenov, S. L.; Gulin, A. A.; Shiyanova, K. A.; Peters, G. S.; Krasheninnikov, V. G.; Ryabkov, Y. D.; Goncharuk, G. P.; Gorenberg, A. Y.; Novokshonova, L. A.; Melnikov, V. P. Template-Directed Polymerization Strategy for Producing rGO/UHMWPE Composite Aerogels with Tunable Properties. *ACS Appl. Mater. Interfaces* **2023**, *15*, 5628–5643. https://doi.org/10.1021/acsami.2c19649.

(12) Alam, F.; Choosri, M.; Gupta, T. K.; Varadarajan, K. M.; Choi, D.; Kumar, S. Electrical, mechanical and thermal properties of graphene nanoplatelets reinforced UHMWPE nanocomposites. *Mater. Sci. Eng., B* **2019**, *241*, 82–91. https://doi.org/10.1016/j.mseb.2019.02.011.

(13) Zhang, H.; Liu, J.; Wang, Y.; Sun, L.; Yu, J.; Chen, L.; Sun, J.; Zhang, Q.; Li, M.; Cai, Z. Nickel-catalyzed in situ synthesis of UHMWPE/TiO_2 composites with enhanced mechanical properties and adjustable photocatalytic degradabilities. *J. Colloid Interface Sci.* **2025**, *678*, 301–312. https://doi.org/10.1016/j.jcis.2024.09.034.

(14) Shi, A.; Li, Y.; Liu, W.; Xu, J.-Z.; Yan, D.-X.; Lei, J.; Li, Z.-M. Highly thermally conductive and mechanically robust composite of linear ultrahigh molecular weight polyethylene and boron nitride via constructing nacre-like structure. *Compos. Sci. Technol.* **2019**, *184*, 107858. https://doi.org/10.1016/j.compscitech.2019.107858.

(15) Yu, W.-C.; Zhang, G.-Q.; Liu, Y.-H.; Xu, L.; Yan, D.-X.; Huang, H.-D.; Tang, J.-H.; Xu, J.-Z.; Li, Z.-M. Selective electromagnetic interference shielding performance and superior mechanical strength of conductive polymer composites with oriented segregated conductive networks. *Chem. Eng. J.* **2019**, *373*, 556–564. https://doi.org/10.1016/j.cej.2019.05.074.

(16) Stürzel, M.; Kempe, F.; Thomann, Y.; Mark, S.; Enders, M.; Mülhaupt, R. Novel Graphene UHMWPE Nanocomposites Prepared by Polymerization Filling Using Single-Site Catalysts Supported on Functionalized Graphene Nanosheet Dispersions. *Macromolecules* **2012**, *45*, 6878–6887. https://doi.org/10.1021/ma301376q.

(17) Dong, P.; Zhang, Q.; Wang, K.; Zhu, B.-H.; Su, W.; Li, J.-F.; Fu, Q. Pursuit of the correlation between yield strength and crystallinity in sintering-molded UHMWPE. *Polymer* **2021**, *215*, 123352. https://doi.org/10.1016/j.polymer.2020.123352.

(18) Yang, H.; Lolage, S.; van der Eem, J.; Rastogi, S.; Romano, D. Silica-supported catalyst for the synthesis of low entangled UHMWPE suitable for solid-state processing. *Mol. Catal.* **2024**, *552*, 113668. https://doi.org/10.1016/j.mcat.2023.113668.

(19) Liu, K.; Ronca, S.; Andablo-Reyes, E.; Forte, G.; Rastogi, S. Unique Rheological Response of Ultrahigh Molecular Weight Polyethylenes in the Presence of Reduced Graphene Oxide. *Macromolecules* **2015**, *48*, 131–139. https://doi.org/10.1021/ma501729y.

(20) Zhou, J.; Zhang, X.; Zhao, S.; Zhang, Z.; Ye, C.; Xin, Z. Influence of Modified Ziegler-Natta Catalyst on the Entanglement Behavior and Properties of Ultrahigh-Molecular-Weight Polyethylene (UHMWPE). *Ind. Eng. Chem. Res.* **2022**, *61*, 17512–17523. https://doi.org/10.1021/acs.iecr.2c03275.

(21) Amada, K.; Mai, L. T. T.; Chammingkwan, P.; Taniike, T. Conductive and Stretchable Ultra-High-Molecular-Weight Polyethylene Nanocomposites through Controlled Filler Distribution from Homogeneous to Semi-Segregated Networks. *ACS Appl. Eng. Mater*. **2025**, *3*, 547–559. https://doi.org/10.1021/acsaenm.4c00817.

(22) Chammingkwan, P.; Bando, Y.; Terano, M.; Taniike, T. Nano-Dispersed Ziegler-Natta Catalysts for 1 μm-Sized Ultra-High Molecular Weight Polyethylene Particles. *Front. Chem.* **2018**, *6*, 524. https://doi.org/10.3389/fchem.2018.00524.

(23) Chammingkwan, P.; Bando, Y.; Mai, L. T. T.; Wada, T.; Thakur, A.; Terano, M.; Sinthusai, L.; Taniike, T. Less Entangled Ultrahigh-Molecular-Weight Polyethylene Produced by Nano-Dispersed Ziegler-Natta Catalyst. *Ind. Eng. Chem. Res.* **2021**, *60*, 2818–2827. https://doi.org/10.1021/acs.iecr.0c05432.

(24) Yan, X.; Zhang, Y.; Tang, X.; Ren, C.; Li, W.; Wang, J.; Yang, Y. Interplay of Particle Size and Temperature on Low-Entanglement Ultrahigh-Molecular-Weight Polyethylene Sintering in Blended Compositions: Analysis of Entanglement and Crystal Structure. *Ind. Eng. Chem. Res.* **2023**, *62*, 7950–7961. https://doi.org/10.1021/acs.iecr.3c00845.

(25) Zhou, F.; Zhao, J.; Rastogi, S. Paradox in Sintering of Nascent Ultrahigh Molecular Weight Polymers in the Solid State. *Macromolecules* **2025**, *58*, 4602–4614. https://doi.org/10.1021/acs.macromol.5c00731.

(26) Gote, R. P.; Romano, D.; van der Eem, J.; Zhao, J.; Zhou, F.; Rastogi, S. Unprecedented Mechanical Properties in Linear UHMWPE Using a Heterogeneous Catalytic System. *Macromolecules* **2023**, *56*, 361–378. https://doi.org/10.1021/acs.macromol.2c02215.

(27) Wang, Z.; Li, B.; Liu, S.; Zeng, J.; Müller, A. J.; Zhu, C.; Xu, J. Origin of Different Crystal Orientations of Ultrahigh-Molecular-Weight Polyethylene during Uniaxial Stretching: The Effect of Entanglements and Chains Tilt. *Macromolecules* **2025**, *58*, 3841–3848. https://doi.org/10.1021/acs.macromol.5c00224.

(28) Wang, H.; Yan, X.; Tang, X.; Ma, Y.; Fan, X.; Li, W.; Yu, W.; Wang, J.; Yang, Y. Contribution of the Initially Entangled State and Particle Size to the Sintering Kinetics of UHMWPE. *Macromolecules* **2022**, *55*, 1310–1320. https://doi.org/10.1021/acs.macromol.1c02058.

(29) Sui, Y.; Li, J.; Qiu, Z.; Cui, Y.; Cong, C.; Meng, X.; Ye, H.; Zhou, Q. Effects of the sintering temperature on the superior cryogenic toughness of ultra-high molecular weight polyethylene (UHMWPE). *Chem. Eng. J.* **2022**, *444*, 136366. https://doi.org/10.1016/j.cej.2022.136366.

(30) Zhang, H.; Zhao, S.; Yu, X.; Xin, Z.; Ye, C.; Li, Z.; Xia, J. Nascent particle sizes and degrees of entanglement are responsible for the significant differences in impact strength of ultrahigh molecular weight polyethylene. *J. Polym. Sci., Part B:Polym. Phys.* **2019**, *57*, 632–641. https://doi.org/10.1002/polb.24819.

(31) Gote, R. P.; Mandal, D.; Patel, K.; Chaudhuri, K.; Vinod, C. P.; Lele, A. K.; Chikkali, S. H. Judicious Reduction of Supported Ti Catalyst Enables Access to Disentangled Ultrahigh Molecular Weight Polyethylene. *Macromolecules* **2018**, *51*, 4541–4552. https://doi.org/10.1021/acs.macromol.8b00590.

(32) Yilmaz, G.; Uslu, E. A new approach for high-quality production of UHMWPE by applying powder vibration densification before sintering. *Powder Technol.* **2023**, *427*, 118741. https://doi.org/10.1016/j.powtec.2023.118741.

(33) Rastogi, S.; Kurelec, L.; Lemstra, P. J. Chain Mobility in Polymer Systems: On the Borderline between Solid and Melt. 2. Crystal Size Influence in Phase Transition and Sintering of Ultrahigh Molecular Weight Polyethylene via the Mobile Hexagonal Phase. *Macromolecules* **1998**, *31*, 5022–5031. https://doi.org/10.1021/ma980261h

(34) Gupta, T. K.; Choosri, M.; Varadarajan, K. M.; Kumar, S. Self-sensing and mechanical performance of CNT/GNP/UHMWPE biocompatible nanocomposites. *J. Mater. Sci.* **2018**, *53*, 7939–7952. https://doi.org/10.1007/s10853-018-2072-3.

(35) Ruan, S. L.; Gao, P.; Yang, X. G.; Yu, T. X. Toughening high performance ultrahigh molecular weight polyethylene using multiwalled carbon nanotubes. *Polymer* **2003**, *44*, 5643–5654. https://doi.org/10.1016/S0032-3861(03)00628-1.

(36) Pang, H.; Yan, D.-X.; Bao, Y.; Chen, J.-B.; Chen, C.; Li, Z.-M. Super-tough conducting carbon nanotube/ultrahigh-molecular-weight polyethylene composites with segregated and double-percolated structure. *J. Mater. Chem.* **2012**, *22*, 23568–23575. https://doi.org/10.1039/C2JM34793H.

(37) Cheng, H.; Cao, C.; Zhang, Q.; Wang, Y.; Liu, Y.; Huang, B.; Sun, X.-L.; Guo, Y.; Xiao, L.; Chen, Q.; Qian, Q. Enhancement of Electromagnetic Interference Shielding Performance and Wear Resistance of the UHMWPE/PP Blend by Constructing a Segregated Hybrid Conductive Carbon Black-Polymer Network. *ACS Omega* **2021**, *6*, 15078–15088. https://doi.org/10.1021/acsomega.1c01240.

(38) George Wypych. *Handout of Polymers, 3rd Edition*, 3rd ed.; ChemTec Publishing, **2022**.

(39) Bait, O.; Si-Ameur, M. Enhanced heat and mass transfer in solar stills using nanofluids: A review. *Sol. Energy* **2018**, *170*, 694–722. https://doi.org/10.1016/j.solener.2018.06.020.

(40) Yu, X.; Steiner, P.; Zhou, Q.; Kocabas, C.; Zhang, H.; Papageorgiou, D. G.; Fenwick, O.; Yan, H.; Reece, M. J.; Bilotti, E. Simultaneous Increase in Dielectric Breakdown Strength and Thermal Conductivity of Oriented UHMWPE Containing Diamond Nanoparticles. *Macromolecules* **2023**, *56*, 8183–8191. https://doi.org/10.1021/acs.macromol.3c01003.

(41) Liu, Z.; Shen, D.; Yu, J.; Dai, W.; Li, C.; Du, S.; Jiang, N.; Li, H.; Lin, C.-T. Exceptionally high thermal and electrical conductivity of three-dimensional graphene-foam-based polymer composites. *RSC Adv.* **2016**, *6*, 22364–22369. https://doi.org/10.1039/c5ra27223h.

(42) Mani, D.; Vu, M. C.; Lim, C.-S.; Kim, J.-B.; Jeong, T.-H.; Kim, H. J.; Islam, M. A.; Lim, J.-H.; Kim, K.-M.; Kim, S.-R. Stretching induced alignment of graphene nanoplatelets in polyurethane films for superior in-plane thermal conductivity and electromagnetic interference shielding. *Carbon* **2023**, *201*, 568–576. https://doi.org/10.1016/j.carbon.2022.09.047.

(43) Galeski, A.; Bartczak, Z.; Vozniak, A.; Pawlak, A.; Walkenhorst, R. Morphology and Plastic Yielding of Ultrahigh Molecular Weight Polyethylene. *Macromolecules* **2020**, *53*, 6063–6077. https://doi.org/10.1021/acs.macromol.9b02154.

(44) Rozanski, A.; Galeski, A. Crystalline Lamellae Fragmentation during Drawing of Polypropylene. *Macromolecules* **2015**, *48*, 5310–5322. https://doi.org/10.1021/acs.macromol.5b01180.

(45) Wiwattananukul, R.; Hachiya, Y.; Endo, T.; Nobukawa, S.; Yamaguchi, M. Anomalous transfer phenomenon of carbon nanotube in the blend of polyethylene and

polycarbonate. *Composites, Part B* **2015**, *78*, 409–414. https://doi.org/10.1016/j.compositesb.2015.04.009.

(46) Nishikawa, R.; Yoon, H.; Yamaguchi, M. Rheological Evaluation of Carbon Nanotube Redistribution in Polymer Melt. *Nihon Reoroji Gakkaishi*, **2019**, *47*, 105–110. https://doi.org/10.1678/rheology.47.105.

(47) Doi, M.; Edwards, S. F. The Theory of Polymer Dynamics. Clarendon press・Oxford, **1986**.

(48) Barham, P. J.; Sadler, D. M. A neutron scattering study of the melting behaviour of polyethylene single crystals. *Polymer* **1991**, *32*, 393–395. https://doi.org/10.1016/0032-3861(91)90440-T.

(49) Litvinov, V.; Christakopoulos, F.; Lemstra, P. J. Disentangled Melt of Ultrahigh-Molecular-Weight Polyethylene: Fictitious or Real? *Macromolecules* **2024**, *57*, 3719–3730. https://doi.org/10.1021/acs.macromol.4c00271.

(50) Rastogi, S.; Yao, Y.; Ronca, S.; Bos, J.; Van Der Eem, J. Unprecedented High-Modulus High-Strength Tapes and Films of Ultrahigh Molecular Weight Polyethylene via Solvent-Free Route. *Macromolecules*. **2011**, *44*, 5558–5568. https://doi.org/10.1021/ma200667m.

(51) Ronca, S.; Forte, G.; Tjaden, H.; Yao, Y.; Rastogi, S. Tailoring molecular structure via nanoparticles for solvent-free processing of ultra-high molecular weight polyethylene composites. *Polymer* **2012**, *53*, 2897–2907. https://doi.org/10.1016/j.polymer.2012.04.051.

(52) Pan, X.; Shen, L.; Schenning, A. P. H. J.; Bastiaansen, C. W. M. Transparent, High-Thermal-Conductivity Ultradrawn Polyethylene/Graphene Nanocomposite Films. *Adv. Mater.* **2019**, *31*, 1904348. https://doi.org/10.1002/adma.201904348.

(53) Dayyoub, T.; Maksimkin, A. V.; Kaloshkin, S.; Kolesnikov, E.; Chukov, D.; Dyachkova, T. P.; Gutnik, I. The Structure and Mechanical Properties of the UHMWPE Films Modified by the Mixture of Graphene Nanoplates with Polyaniline. *Polymers* **2019**, *11*, 23. https://doi.org/10.3390/polym11010023.

Chapter 4

Microfine UHMWPE as a functional filler in polypropylene blends

ABSTRACT:

Polymer blends is a technique to enable functions such as mechanical, optical, and thermal properties that cannot be achieved with a single polymer and fascinated to improve such functions without complex polymer synthetic routes. In this Chapter, I prepared a polypropylene/ultra-high-molecular-weight polyethylene (PP/UHMWPE) blend film with microfine UHMWPE (Small, average particle size: 523 nm). The addition of Small decreased melting temperature due to partial miscibility between PP and Small, while it enhanced the degree of crystallinity. Tensile tests revealed that Young's modulus and yield stress were enhanced by 40 % and 42 %, respectively, with 1 wt% Small loading. This can be attributed to the nucleating effect of Small, which promoted heterogeneous crystallization of PP. In this Chapter, I demonstrated that Small can serve as a functional filler to improve degree of crystallinity and the stiffness of PP.

KEYWORDS: Polypropylene / Ultrahigh-molecular-weight polyethylene / filler / Nucleation agent / Polymer blends

4.1. Introduction

Polyolefin-based resins are widely used due to their excellent chemical stability, light weight, low cost, and good processability. Polypropylene (PP), in particular, is a versatile thermoplastic polymer that exhibits high mechanical strength, chemical resistance, and excellent moldability, making it suitable for applications such as packaging materials and automotive components.[1] However, PP shows brittle at low temperatures [2,3] and exhibits insufficient toughness[4] and wear resistance.[5] Various approaches have been explored to improve its mechanical performance, including blending with elastomers[2,3] or other polyolefins,[6–8] and incorporating fillers.[2,9]

Among these strategies, blending PP with other polymers such as high-density polyethylene (HDPE) or ultra-high-molecular-weight polyethylene (UHMWPE) has attracted considerable attention as an effective and relatively simple method for enhancing mechanical properties.[8,10,11] UHMWPE possesses an extremely high molecular weight, leading to a large degree of chain entanglement, which imparts exceptional toughness, ductility, abrasion resistance, and impact strength.[12–14] On the other hand, its extremely high melt viscosity makes conventional melt processing techniques such as injection or extrusion molding difficult. Consequently, the use of UHMWPE as a nascent polymer is limited, and property enhancement through blending with other polymers such as isotactic polypropylene provides a promising alternative approach.

Commercial UHMWPE is synthesized using $MgCl_2$-supported Ziegler–Natta catalysts, which are industrially advantageous for slurry and gas-phase processes owing to their high scalability, cost-effectiveness, and reduced solvent requirements.[15,16] The typical particle size of $MgCl_2$-supported catalysts ranges from 10 to 100 μm.[16,17] Because the active sites of Ziegler–Natta catalysts are spatially close to each other, polymer chains form within spatially constrained regions, which promotes molecular entanglement before crystallization,[18] and result in significantly restricted chain mobility and a drastic increase in melt viscosity as

molecular weight increases. As a result, conventional melt-processing techniques such as extrusion and injection molding are hardly applicable to UHMWPE.

In UHMWPE with large particle sizes, insufficient interparticle fusion often occurs during molding, which can lead to structural defects and stress concentration,[19,20] thereby deteriorating the mechanical performance. To overcome these challenges, various approaches have been investigated in PP/PE blends, including the addition of compatibilizers,[4,21] chemical modification,[22] copolymerization,[21,23] and crosslinking.[22] However, these methods generally involve complex processes and increased production costs.

Alternatively, from a more physical standpoint, improving the dispersibility and interfacial fusion by controlling the size and morphology of UHMWPE particles represents a promising approach for improvement of mechanical properties of PP/UHMWPE blends. Chammingkwan *et al.* synthesized UHMWPE with particle sizes below 1 μm (Small) using nanosized Ziegler–Natta catalysts, resulting in less entangled polymer chains.[15,24] The smaller and more uniform particle morphology enhanced the powder flowability and filling rate of voids, leading to improved moldability during compression and sintering processes.

In this Chapter, PP/UHMWPE with small amounts of Small were prepared to investigate their thermal and mechanical properties. In addition, to further enhance the toughness of the blends, the effect of incorporating a polyolefin-based elastomer was also examined. Through these investigations, I provide new design insights for all-polyolefin composites based on Small, focusing on the thermal and mechanical performance.

4.2. Methods

4.2.1. Materials

Isotactic polypropylene pellet (PP, mmmm= 96.0 mol%, M_n= 7.27×10^4 g mol^{-1}, M_w= 2.98×10^5 g mol^{-1}, M_w/M_n= 4.11) was purchased from Japan Polypropylene. Commercial ultrahigh-molecular-weight polyethylene (the viscosity average molecular weight (M_v) = 4.50 × 10^6 g mol^{-1}, D_{50}=68.6 μm, denoted as Large) was provided by Asahi Kasei Corp. MIPELON PM-200 (M_v= 1.8 × 10^6 g mol^{-1}, D_{50}=10 μm, denoted as Middle) was provided from Mitsui Chemical, Inc. Microfine UHMWPE (M_v = 4.42 × 10^6 g mol^{-1}, D_{50}=523 nm, denoted as Small) was synthesized following previous publications.[15,24] Irganox 1010 was purchased from Toyotsu Chemiplas Corp.

4.2.2. Film preparation of PP and PP/UHMWPE

PP, a certain amount of UHMWPE, and Irganox 1010 (1 wt%) were physically mixed and melt-mixed at 180 °C and 100 rpm for 20 min using a twin screw extruder (MC5 micro compounders, Xplore Instrument BV) and showed an extrusion force of 1400 N. The strand was cut into pellet form using scissors and then filled into a 7 cm × 7 cm hollow aluminum sheet with 200 μm thickness, sandwiched between polyimide films and iron plates, and placed in a hot press machine (AH-2003, AS ONE Corp. The plates were compacted at 230 °C under contact pressure for 5 min and then hot-pressed at 20 MPa for 5 min. Subsequently, the film was quenched at 100 °C for 5 min, and then cooled at 0 °C for 5 min. The film was labelled as PP/X (Y/Z), where X, Y, Z represent UHMWPE samples, weight percent of PP and UHMWPE, respectively.

4.2.3. Characterization

The film cross-section was observed by scanning electron microscope (SEM, JCM-6000Plus, JEOL Ltd.,). The sample was cryo-fractured by soaking liquid nitrogen and sputter-coated Au on 10 nm. Mechanical properties of nanocomposites were measured using a tensile tester (3365, Instron) at room temperature and a cross-head speed of 1.5 mm min^{-1}. Dumbbell shape specimens were die-cut from the film sample and the measured properties were reported as an average value from repetitive tests. Differential scanning calorimetry of polymer was performed on a DSC 822 (Mettler Toledo) under a nitrogen flow (75 mL min^{-1}). The sample was sealed in an aluminum pan. The temperature range was −50–200 °C at a heating and cooling rate of 10 °C min^{-1}. The temperature reached to maximum and minimum value, the temperature was held for 1 min. The melting enthalpy (ΔH_m) was calculated from heat flow curve and the crystallinity (X_c) was calculated using following equation (4.1):

$$X_c = \frac{\Delta H_m}{\Delta H_m^0} \quad (4.1),$$

Where ΔH_m^0 was the melting enthalpy which was calculated from the blend ratio of PP and PE using the melting enthalpy of their complete crystalline form (209 J/g for PP and 293 J/g for PE). Scratch properties were evaluated using Hoffman scratch tester (BYK-Gardner). Specifically, a cylindrical scratch blade with a diameter of 7 mm was set to contact the film surface at an angle of 45 °, and the testing machine was moved relative to the film.

4.3. Results and discussion

4.3.1. Cross-sectional morphology of PP/UHMWPE blends

In this Chapter, I prepared PP/UHMWPE blend film using melt-mixing by twin screw extruder at 180 °C and 100 rpm for 20 min followed by hot-pressed at 230 °C for 5 min and

then quenched at 100 °C and cooled to 0 °C. The opaque film was obtained and the cross-sectional morphology of cryo-fractured sample was observed by SEM (Figure 4.1). The interface between PP and UHMWPE was clearly observed, indicating that these polymers are immiscible. As indicated by the green arrows, PP/Small (99/1) exhibited a structure in which spherical Small UHMWPE particles with diameters of 0.5−1 μm were dispersed within the PP matrix (Figure 4.1a). In contrast, PP/Large (99/1) exhibited ellipsoidal or trapezoidal particles with sizes of approximately 50 μm (Figure 4.1b). When comparing the PP matrices, the surface of PP/Small appeared rougher than that of PP/Large. This can be attributed to Small likely acted as nucleation sites for PP crystallization,[8,25] resulting in the formation of smaller crystals. Therefore, the surface of PP/Small appeared rough due to crystal cleavage from cryo-fractured. On the other hand, Large had a smoother surface area, indicating a weaker nucleation effect.

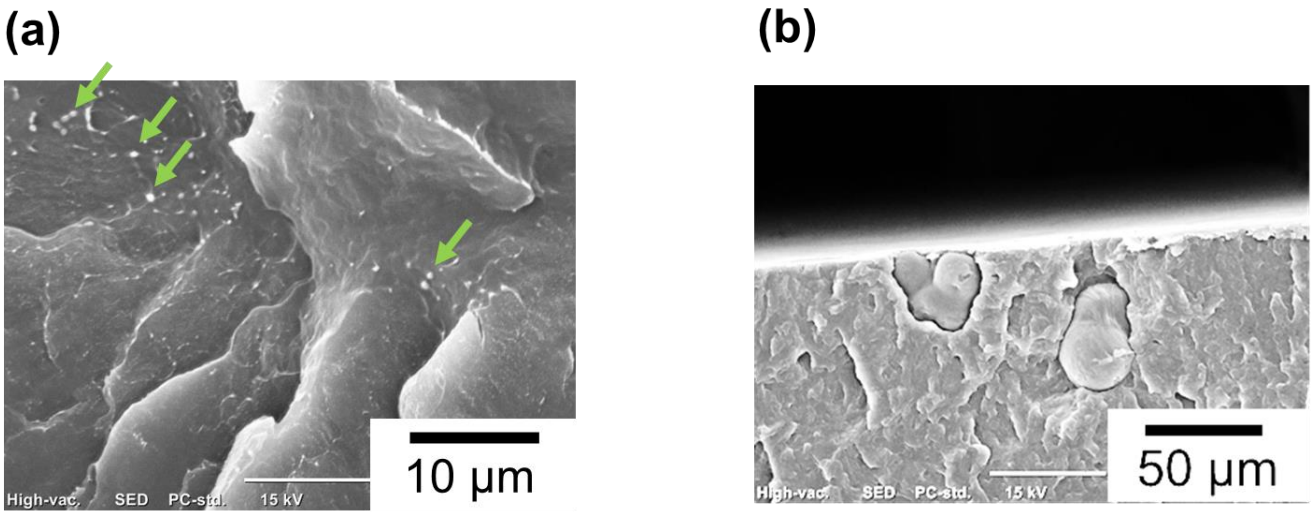

Figure 4.1. Cross-sectional SEM images of cryo-fractured surfaces. (a) PP/Small (99/1) and (b) PP/Large (99/1).

4.3.2. Thermal behavior and crystallization characteristics of PP/UHMWPE blends

To clarify the influence of UHMWPE addition on the crystallization behavior and thermal stability of PP, differential scanning calorimetry (DSC) was conducted. PP is a semi-crystalline polymer, and its crystallization temperature (T_c) and melting temperature (T_m) strongly depend on the interactions with the blend components and the nucleation behavior.[8,25] Therefore, thermal transitions during the heating and cooling processes were compared for blends containing UHMWPE with different particle sizes. The measurements were performed over a temperature range of −50 °C to 200 °C, with both heating and cooling rates set to 10 °C min^{-1}. Figure 4.2 shows the DSC curves of neat PP, Small, and PP/UHMWPE blends. Neat PP exhibited T_m of 167 °C, T_c of 112 °C, and ΔH_m of 78.4 J g^{-1} (Table 4.1). The addition of UHMWPE resulted in a decrease in T_m by 2–3 °C and an increase in T_c by 3–4 °C. The degree of crystallinity (X_c) increased by 7.7 % for PP/Small (99/1) and by 1.0 % for PP/Large (99/1) compared to neat PP (Table 4.1). These results suggest that UHMWPE partially diffused or interacted within the PP matrix, thereby affecting the crystallization behavior of PP chains. The effect was more pronounced for Small, indicating that Small promotes the crystallization of PP more effectively. Furthermore, in the DSC curve of PP/Small, a shoulder peak was observed around 158 °C during the first heating cycle, and the ΔH_m slightly increased with increasing Small content. This suggests the presence of heterogeneous nucleation induced by Small or differences in the lamellar thickness distribution.

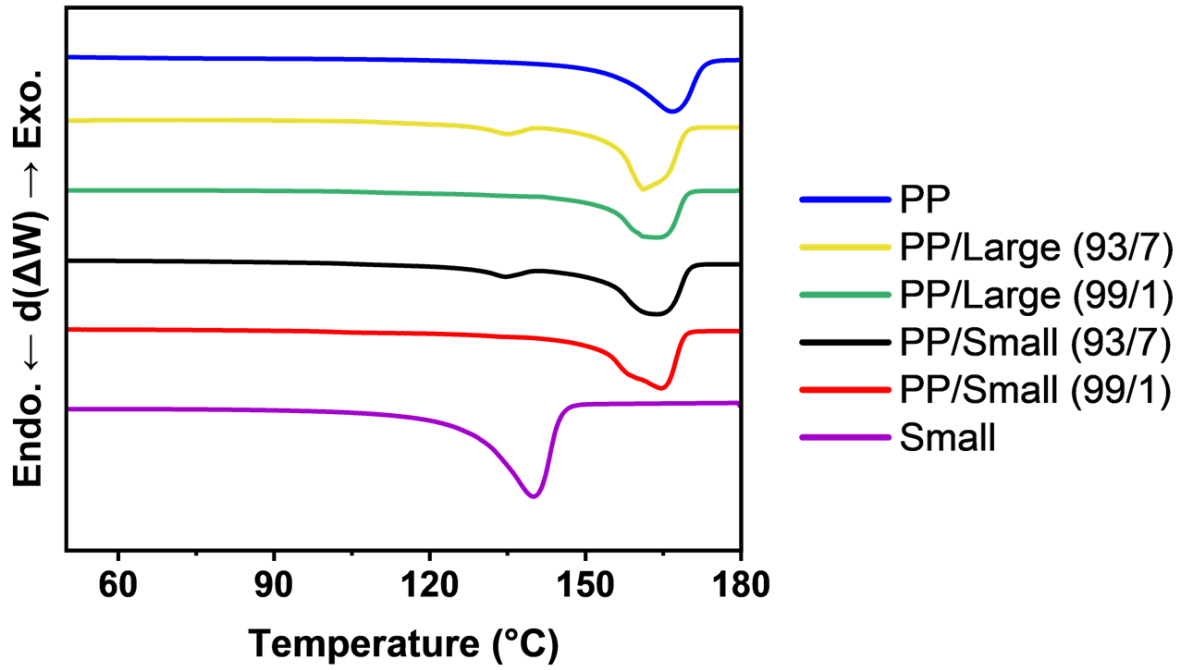

Figure 4.2. DSC curves of first heating cycle for PP, PP/UHMWPE, and Small at a heating rate of 10 °C min^{-1}.

Table 4.1. Thermal Properties of Obtained PP, PP/UHMWPE, and Small.

Sample	$T_{m,\,PP}$ (°C)	$T_{m,\,UHMWPE}$ (°C)	T_c (°C)	ΔH_m (J g^{-1})	X_c (%)
PP	166.7	-	112.1	78.4	37.5
PP/Small (99/1)	164.6	n.d.	115.9	94.9	45.2
PP/Small (93/7)	163.7	135.1	116.2	98.1	45.7
PP/Large (99/1)	163.7	n.d.	115.1	80.7	38.5
PP/Large (93/7)	161.2	134.9	115.7	84.4	39.3
Small	-	140.0	116.7	131.7	45.7

$T_{m,\ PP}$, $T_{m,\ UHMWPE}$ refer to melting temperatures of PP and UHMWPE, respectively. T_c represents the crystallization temperature, while ΔH_m and X_c denote the melting enthalpy and degree of crystallinity, respectively.

4.3.4. Effect of UHMWPE content and size on the tensile behavior of PP/UHMWPE blends

In the previous section, it was demonstrated that the addition of UHMWPE affected the crystallization behavior of PP. Changes in the crystalline structure are expected to be closely related to the mechanical properties of the blend materials.[26] Therefore, tensile tests were conducted to clarify the mechanical behavior of the PP/UHMWPE blends. Figure 4.3 shows the stress–strain curves of PP/Small. When Small content was below 3 wt%, strain-hardening behavior was observed. As Small content increased, the ultimate tensile stress, elongation at break, and toughness decreased, whereas the yield stress and Young's modulus reached their maximum values at 1 wt% Small. Specifically, the addition of 1 wt% Small increased the Young's modulus by 40% and the yield stress by 42% compared to neat PP (Figure 4.3b, Table 4.2).

The decreases in maximum stress and toughness with increasing Small content were attributed to the weak interfacial interaction between PP and UHMWPE, which caused stress concentration and served as fracture initiation sites. On the other hand, Small acted as heterogeneous nucleation sites that promoted the crystallization of PP chains. As a result, the crystallinity of PP increased with the addition of Small, leading to higher Young's modulus and yield stress than those of the neat PP matrix.[26] In PP/Small (93/7), the elongation at break and toughness decreased dramatically. This was likely due to the formation of large aggregates of Small, which weakened the interface with PP and reduced its ability to withstand deformation.

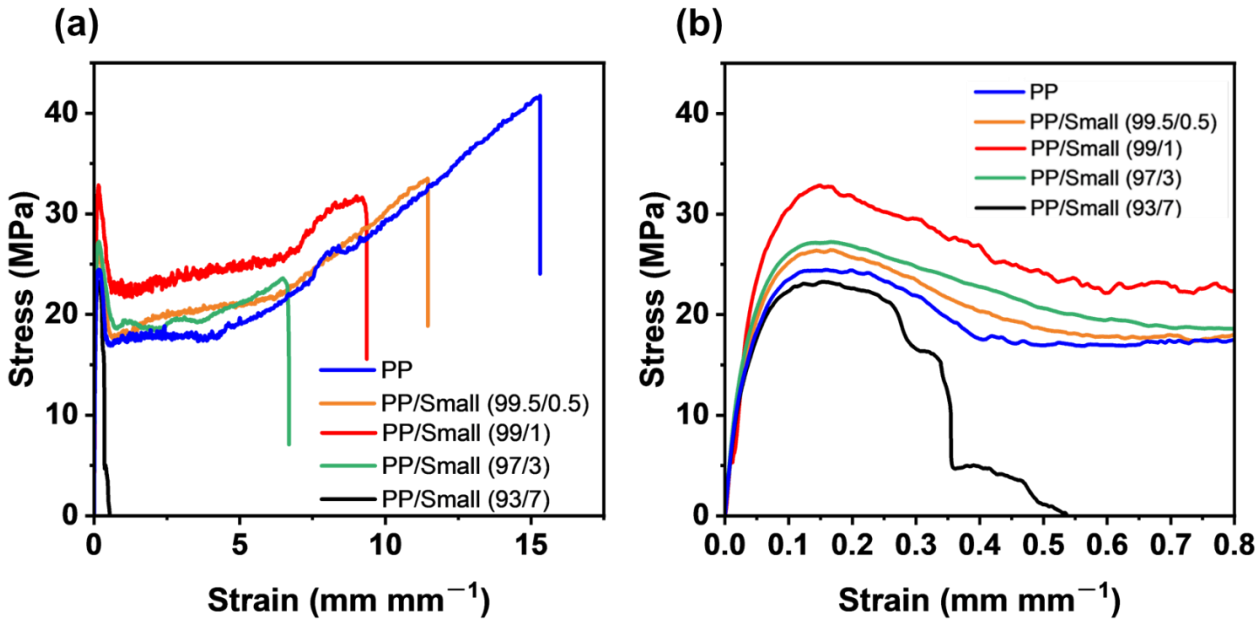

Figure 4.3. Stress-strain curves of (a) PP and PP/Small with 0.5–7.0 wt% Small loadings, and (b) an enlarged view of the strain up to 0.8 from Figure 4.3a. (Blue) PP, (orange) PP/Small (99.5/0.5), (red) PP/Small (99/1), (green) PP/Small (97/3), and (black) PP/Small (93/7).

Table 4.2. Mechanical Properties of PP and PP/Small with 0.5–7.0 wt% Small Loadings.

Sample	U.T.S. (MPa)	Strain at break (mm mm^{-1})	Young's modulus (MPa)	Toughness (MJ m^{-3})	Stress at yield (MPa)
PP	36±3.0	14±0.9	300±20	320±47	21±1.4
PP/Small (99.5/0.5)	35±1.4	12±0.5	380±5.8	280±18	27±0.3
PP/Small (99/1)	34±1.4	10±0.7	420±36	260±27	30±1.3
PP/Small (97/3)	27±1.4	7.2±0.3	390±5.6	160±7.9	27±0.4
PP/Small (93/7)	23±1.9	0.25±0	340±30	6.8±0.4	23±1.9

Based on these results, the optimal UHMWPE content was determined to be 1 wt%, and the effect of UHMWPE particle size on tensile properties was further investigated. Specifically, blends containing 1 wt% of UHMWPE with three different particle sizes (D_{50} = 523 nm for Small, 10 μm for Middle, and 68.5 μm for Large) were prepared and tested. As the UHMWPE particle size increased, the maximum stress, Young's modulus, toughness, and yield stress decreased (Figure 4.4, Table 4.3). This can be explained by the fact that Small exhibited better dispersion within the PP matrix, which helped to alleviate stress concentration and thereby enhanced toughness. Furthermore, the microfine UHMWPE particles likely functioned as effective nucleating agents, improving the crystallinity of the PP matrix and contributing to the enhancement of material stiffness.

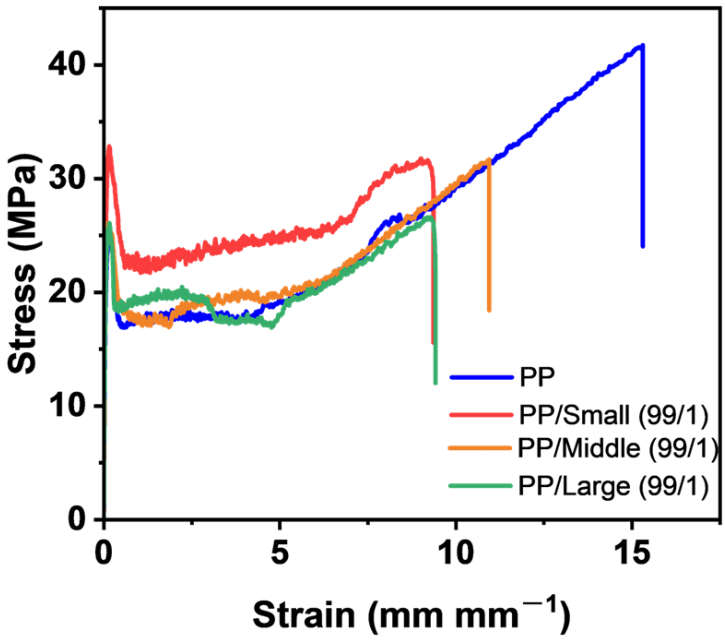

Figure 4.4. Stress-strain curves of PP and PP/UHMWPE with different UHMWPE particle sizes. (Blue) PP, (red) PP/Small (99/1), (orange) PP/Middle (99/1), and (green) PP/Large (99/1).

Table 4.3. Mechanical Properties of PP and PP/UHMWPE Blends with Varying Particle Sizes of UHMWPE.

Sample	U.T.S. (MPa)	Strain at break (mm mm^{-1})	Young's modulus (MPa)	Toughness (MJ m^{-3})	Stress at yield (MPa)
PP	36±3.0	14±0.9	300±20	320±47	21±1.4
PP/Small (99/1)	34±1.4	10±0.7	420±36	260±27	30±1.3
PP/Middle (99/1)	31±1.1	11±0.8	380±25	240±15	26±1.7
PP/Large (99/1)	28±1.4	9.2±0.6	360±9.7	200±17	26±1.1

4.3.5. Scratch properties of PP and PP/Small

Scratch properties were evaluated using a Hoffman scratch tester. Figure 4.5 showed SEM images of the surfaces of PP and PP/Small after scratching. SEM observation revealed distinct deformation mechanisms between PP and PP/Small. In PP, the scratches were continuously connected, indicating dominant plastic flow and damage delocalization along the scratching direction. In contrast, PP/Small exhibited similar scratch widths but suppressed scratch propagation, suggesting localized deformation. This behavior can be attributed to the presence of UHMWPE, which possesses a high molecular weight and chain entanglement network, providing enhanced resistance against plastic flow. Consequently, PP/Small demonstrated higher resistance to scratch propagation and improved wear resistance compared to PP.

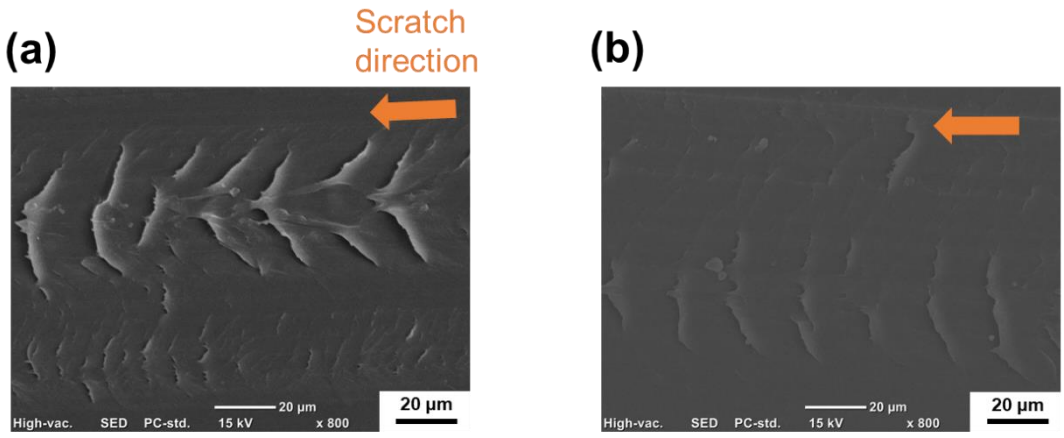

Figure 4.5. SEM images of the surfaces of (a) PP and (b) PP/Small (99/1) films after the scratch test.

4.3.6. Toughening of PP/UHMWPE blends by POE addition

When UHMWPE was added to PP, the crystallinity increased, and both the yield stress and Young's modulus improved. However, even with 1 wt% UHMWPE addition, the toughness decreased by 19 %. Therefore, to improve the toughness of PP, which is generally achieved by incorporating a polyolefin elastomer (POE), the tensile properties of PP/POE/Small blends were investigated. The blends were prepared by melt-mixing PP pellets, POE, and Small at 84 wt%, 15 wt%, and 1 wt%, respectively, using a twin screw extruder, followed by compression molding at 230 °C to obtain blend films. Figure 4.6 shows the stress–strain curves of the PP/POE/Small blends. The addition of POE led to a decrease in mechanical properties compared with PP/Small (Figure 4.6, Table 4.4), indicating that the introduction of POE reduced both the rigidity and interfacial adhesion.[27–29] Furthermore, the phase-separated structure of POE likely disrupted the dispersion state of Small and the interfacial interaction between PP and UHMWPE, thereby suppressing the reinforcing and nucleating effects of Small. In the PP/POE/Small blend, the introduction of the soft POE phase decreased the

stiffness and yield stress of the PP matrix. Consequently, the mechanical properties deteriorated compared with those of PP/Small.

To improve this system, three possible approaches are proposed: (1) the use of alternative compatibilizers (e.g., olefin block copolymer (OBC) or PP-*g*-maleic anhydride);[8,30] (2) optimization of melt-mixing conditions; and (3) surface modification of UHMWPE.[31]

The POE used in this system was a random copolymer of ethylene and 1-octene, and its random molecular arrangement likely reduced the fraction that can be compatible with both PP and UHMWPE, thereby decreasing the miscibility of the PP/UHMWPE blend.[8] Therefore, using a block copolymer such as OBC is expected to provide segments compatible with both PP and UHMWPE, acting as a molecular bridge between the two phases.

In addition, although all three components were mixed simultaneously in this Chapter, it is expected that optimizing the mixing sequence, for example by pre-mixing POE and UHMWPE to achieve a uniform dispersion of UHMWPE within the POE phase before mixing with PP, could enhance the blend morphology and mechanical performance. Surface modification of UHMWPE is also expected to improve interfacial compatibility between PP and UHMWPE, promoting better dispersion and interfacial adhesion, and thus achieving blends with superior mechanical properties.

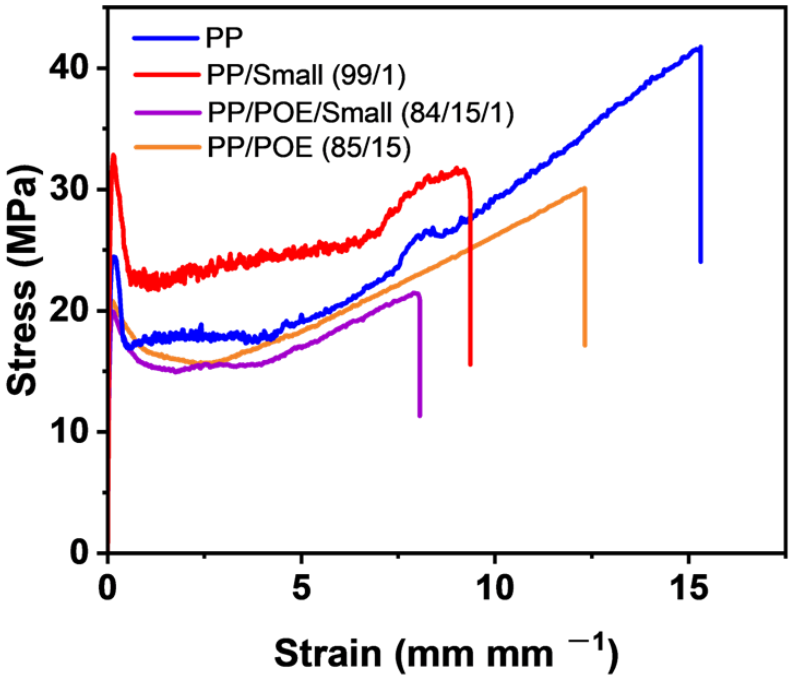

Figure 4.6. Stress-strain curves of (blue) PP, (red) PP/Small (99/1), (purple) PP/POE/Small (84/15/1), and (orange) PP/POE (85/15).

Table 4.4. Mechanical Properties of PP and PP/UHMWPE, and PP/POE Blends.

Sample	U.T.S. (MPa)	Strain at break (mm mm^{-1})	Young's modulus (MPa)	Toughness (MJ m^{-3})	Stress at yield (MPa)
PP	36±3.0	14±0.9	300±20	320±47	21±1.4
PP/Small (99/1)	34±1.4	10±0.7	420±36	260±27	30±1.3
PP/POE/Small (84/15/1)	22±0.9	7.3±1.1	300±4.2	130±22	20±0.1
PP/POE (85/15)	29±1.2	12±1.1	330±9.0	250±25	21±0.6

4.4. Conclusions

Small can be processed using twin screw extruder by blending with PP, producing PP/Small blend film. SEM observations revealed clear phase separation between PP and Small, confirming their immiscibility, while Small was agglomerated in the PP matrix to minimize their surface free energy and formed 20–40 μm agglomerates. It was demonstrated that the addition of UHMWPE slightly decreased the melting temperature and increased the crystallization temperature of PP, with the degree of crystallinity enhanced by up to 7.7 % for PP/Small (99/1). This indicates that Small acted as a nucleating agent, promoting PP crystallization more efficiently than larger UHMWPE particles. Tensile testing showed that the incorporation of 1 wt% Small improved the Young's modulus and yield stress by 40 % and 42 %, respectively, although toughness decreased by 19 % due to limited interfacial fusion between PP and UHMWPE. The optimal UHMWPE content was determined to be 1 wt%, and the mechanical performance degraded with increasing UHMWPE particle size, owing to poorer dispersion and weaker nucleation ability. In ternary blends of PP/POE/Small, the introduction of the soft POE phase led to reductions in stiffness and interfacial adhesion, suppressing the reinforcing and nucleation effects of Small. Overall, I revealed that microfine UHMWPE with submicron particle size can serve as a functional filler and nucleating agent to enhance the stiffness of PP while maintaining processability. Future improvements may be achieved through compatibilizer addition, optimized mixing sequences, or surface modification of UHMWPE to strengthen interfacial adhesion and balance rigidity with toughness.

References

(1) Maddah, H. A. Polypropylene as a Promising Plastic: A Review. *Am. J. Polym. Sci.* **2016**, *6*, 1–11. https://doi.org/10.5923/j.ajps.20160601.01.

(2) Jia, E.; Zhao, S.; Shangguan, Y.; Zheng, Q. A facile fabrication of polypropylene composites with excellent low-temperature toughness through tuning interfacial area between matrix and rubber dispersion by silica nanoparticles located at the interface. *Compos. Sci. Technol.* **2019**, *184*, 107846. https://doi.org/10.1016/j.compscitech.2019.107846.

(3) Kim, D.-K.; Lee, S. H.; Hong, S.-K.; Han, S. W.; Lee, D. H.; Yu, S. Low-Temperature-Toughened Polypropylene Blends with Highly Packed Elastomeric Domains. *ACS Appl. Polym. Mater.* **2022**, *4*, 7834–7840. https://doi.org/10.1021/acsapm.2c01221.

(4) Wolff, P.; Dickert, A.; Kretschmer, W. P.; Kempe, R. *i*PP/PE Multiblock Copolymers for Plastic Blend Recycling Synthesized by Coordinative Chain Transfer Polymerization. *Macromolecules* **2022**, *55*, 6435–6442. https://doi.org/10.1021/acs.macromol.2c00709.

(5) Mulaga, D. P.; Sharma, A. Effect of amino-functionalized MWCNTs addition on mechanical and tribological behaviour of polypropylene-based nanocomposites. *Tribol. Mater.* **2025**, *4*, 66–77. https://doi.org/10.46793/tribomat.2025.006.

(6) Chen, X.; Wang, X.; Cao, C.; Yuan, Z.; Yu, D.; Li, F.; Chen, X. Elongational Flow Field Processed Ultrahigh Molecular Weight Polyethylene/Polypropylene Blends with Distinct Interlayer Phase for Enhanced Tribological Properties. *Polymers* **2021**, *13*, 1933. https://doi.org/10.3390/polym13121933.

(7) Unger, T.; Klocke, L.; Herrington, K.; Miethlinger, J. Investigation of the rheological and mechanical behavior of Polypropylene/ultra-high molecular weight polyethylene compounds related to new online process control. *Polym. Test.* **2020**, *86*, 106442. https://doi.org/10.1016/j.polymertesting.2020.106442.

(8) Qi, L.; Wu, L.; He, R.; Cheng, H.; Liu, B.; He, X. Synergistic toughening of polypropylene with ultra-high molecular weight polyethylene and elastomer-olefin block copolymers. *RSC Adv.* **2019**, *9*, 23994–24002. https://doi.org/10.1039/c9ra01073d.

(9) Bian, J.; Wang, Z. J.; Lin, H. L.; Zhou, X.; Xiao, W. Q.; Zhao, X. W. Thermal and mechanical properties of polypropylene nanocomposites reinforced with nano-SiO_2 functionalized graphene oxide. *Composites, Part A* **2017**, *97*, 120–127. https://doi.org/10.1016/j.compositesa.2017.01.002.

(10) Hees, T.; Schirmeister, C. G.; Pfohl, P.; Hofmann, D.; Muelhaupt, R. Self-Reinforcement via 1D Nanostructure Formation during Melt Blending of Thermoplastics and Thermoplastic Elastomers with Nanophase-Separated UHMWPE/HDPE Wax Reactor Blends. *ACS Appl. Polym. Mater.* **2021**, *3*, 3455–3464. https://doi.org/10.1021/acsapm.1c00384.

(11) Xu, J.; Eagan, J. M.; Kim, S.-S.; Pan, S.; Lee, B.; Klimovica, K.; Jin, K.; Lin, T.-W.; Howard, M. J.; Ellison, C. J.; LaPointe, A. M.; Coates, G. W.; Bates, F. S. Compatibilization of Isotactic Polypropylene (*i*PP) and High-Density Polyethylene (HDPE) with *i*PP-PE Multiblock Copolymers. *Macromolecules* **2018**, *51*, 8585–8596. https://doi.org/10.1021/acs.macromol.8b01907.

(12) Sui, Y.; Li, J.; Qiu, Z.; Cui, Y.; Cong, C.; Meng, X.; Ye, H.; Zhou, Q. Effects of the sintering temperature on the superior cryogenic toughness of ultra-high molecular weight polyethylene (UHMWPE). *Chem. Eng. J.* **2022**, *444*, 136366. https://doi.org/10.1016/j.cej.2022.136366.

(13) Lee, K. H.; Sinha, T. K.; Choi, K. W.; Oh, J. S. Ultra-high-molecular-weight polyethylene reinforced polypropylene and polyamide composites toward developing low-noise automobile interior. *J. Appl. Polym. Sci.* **2020**, *137*, 48720. https://doi.org/10.1002/app.48720.

(14) Li, B.; Fan, C.; Wang, H.; Ren, M.; Wu, P.; Wang, X.; Liu, X. A composite with excellent tribological performance derived from oxy-fluorinated UHMWPE particle/polyurethane. *RSC Adv.* **2014**, *4*, 9321–9325. https://doi.org/10.1039/c3ra47715k.

(15) Chammingkwan, P.; Bando, Y.; Terano, M.; Taniike, T. Nano-Dispersed Ziegler-Natta Catalysts for 1 μm-Sized Ultra-High Molecular Weight Polyethylene Particles. *Front. Chem.* **2018**, *6*, 524. https://doi.org/10.3389/fchem.2018.00524.

(16) Klaue, A.; Kruck, M.; Friederichs, N.; Bertola, F.; Wu, H.; Morbidelli, M. Insight into the Synthesis Process of an Industrial Ziegler-Natta Catalyst. *Ind. Eng. Chem. Res.* **2019**, *58*, 886–896. https://doi.org/10.1021/acs.iecr.8b05296.

(17) Taniike, T.; Funako, T.; Terano, M. Multilateral characterization for industrial Ziegler-Natta catalysts toward elucidation of structure-performance relationship. *J. Catal.* **2014**, *311*, 33–40. https://doi.org/10.1016/j.jcat.2013.10.023.

(18) Gote, R. P.; Zhao, J.; Romano, D.; Rastogi, S. Solid-State Processing of In Situ Blended Prepolymer with Z-N Synthesized UHMWPE: Role of the Prepolymer. *Macromolecules* **2025**, *58*, 3604–3621. https://doi.org/10.1021/acs.macromol.4c03097.

(19) Alam, F.; Choosri, M.; Gupta, T. K.; Varadarajan, K. M.; Choi, D.; Kumar, S. Electrical, mechanical and thermal properties of graphene nanoplatelets reinforced UHMWPE nanocomposites. *Mater. Sci. Eng., B* **2019**, *241*, 82–91. https://doi.org/10.1016/j.mseb.2019.02.011.

(20) Amada, K.; Mai, L. T. T.; Chammingkwan, P.; Taniike, T. Conductive and Stretchable Ultra-High Molecular Weight Polyethylene Nanocomposites through Controlled Filler Distribution from Homogeneous to Semi-Segregated Networks. *ACS Appl. Eng. Mater.* **2025**, *3*, 547–559.

(21) Klimovica, K.; Pan, S.; Lin, T.-W.; Peng, X.; Ellison, C. J.; LaPointe, A. M.; Bates, F. S.; Coates, G. W. Compatibilization of *i*PP/HDPE Blends with PE-*g*-*i*PP Graft Copolymers. *ACS Macro Lett.* **2020**, *9*, 1161–1166. https://doi.org/10.1021/acsmacrolett.0c00339.

(22) Yokoyama, K.; Guan, Z. A Vitrimer Acts as a Compatibilizer for Polyethylene and Polypropylene Blends. *Angew. Chem., Int. Ed.* **2024**, *63*, e202317264. https://doi.org/10.1002/anie.202317264.

(23) Dickert, A.; Wolff, P.; Kretschmer, W. P.; Kempe, R. Synthesis of HDPE-*b*-*i*PP Diblock Copolymers via Subsequent Coordintive Chain-Transfer Polymerization and Their Use as Compatibilizers for HDPE/*i*PP Blends. *J. Poly. Sci.* **2025**, *63*, 4525–4536. https://doi.org/10.1002/pol.20250151.

(24) Chammingkwan, P.; Bando, Y.; Mai, L. T. T.; Wada, T.; Thakur, A.; Terano, M.; Sinthusai, L.; Taniike, T. Less Entangled Ultrahigh-Molecular-Weight Polyethylene Produced by Nano-Dispersed Ziegler-Natta Catalyst. *Ind. Eng. Chem. Res.* **2021**, *60*, 2818–2827. https://doi.org/10.1021/acs.iecr.0c05432.

(25) Shao, W.; Zhang, Y.; Wang, Z.; Niu, Y.; Yue, R.; Hu, W. Critical Content of Ultrahigh-Molecular-Weight Polyethylene To Induce the Highest Nucleation Rate for Isotactic Polypropylene in Blends. *Ind. Eng. Chem. Res.* **2012**, *51*, 15953–15961. https://doi.org/10.1021/ie302542x.

(26) Kimura, S.; Kida, T.; Takeshita, H.; Tokumitsu, K. Temperature Dependence of Strain-Hardening Behavior of Polyethylene Solids Evaluated by SAXS, WAXD, and Raman Spectroscopy. *Macromolecules* **2025**, *58*, 3151–3159. https://doi.org/10.1021/acs.macromol.5c00095.

(27) Mohd Yasin, S. B.; Terry, J. S.; Taylor, A. C. Fracture and mechanical properties of an impact toughened polypropylene composite: modification for automotive dashboard-airbag application. *RSC Adv.* **2023**, *13*, 27461–27475. https://doi.org/10.1039/d3ra04151d.

(28) Wang, K.; Chen, L.; Gao, Y.; Jiang, D.; Quan, Y.; Yan, S. Effect of morphology development on the low-temperature tensile properties of PP/POE blends. *J. Appl. Polym. Sci.* **2022**, *139*, 52192. https://doi.org/10.1002/app.52192.

(29) Wang, X.; Hu, S.; Guo, Y.; Li, G.; Xu, R. Toughened High-Flow Polypropylene with Polyolefin-Based Elastomers. *Polymers* **2019**, *11*, 1976. https://doi.org/10.3390/polym11121976.

(30) Shafaattalab, F.; Jalali-Arani, A. Effect of Maleic Anhydride-Grafted Polypropylene as a Compatibilizer and Dynamic Vulcanization on Morphology, Rheology, Mechanical and Thermal Properties of Polypropylene/Butadiene Rubber Blend. *J. Appl. Polym. Sci.* **2025**, *142*, e57006. https://doi.org/10.1002/app.57006.

(31) He, J.; Wang, Y.; Qian, Y.; Guo, J.; Lu, J.; Yang, W. Surface Modification of Ultra-High-Molecular-Weight Polyethylene and Applications: A Review. *Polymers* **2024**, *16*, 3431. https://doi.org/10.3390/polym16233431.

Chapter 5

General conclusion

Ultra-high-molecular-weight polyethylene (UHMWPE) possesses unique properties, including low density, high mechanical performance (e.g., toughness and impact strength), excellent tribological characteristics (e.g., wear resistance and self-lubrication), corrosion resistance, and biocompatibility. Commercial UHMWPE is typically synthesized using $MgCl_2$-supported Ziegler-Natta catalysts, which offer high catalytic activity, stereoregularity control, scalability, and cost-effectiveness. These catalysts generate macroparticles with an average particle size of 80–300 μm. In general, UHMWPE possesses highly entangled chains, resulting in extremely high melt viscosity and low melt flowability. It is difficult to process using conventional methods such as injection molding and extrusion molding. Consequently, UHMWPE is commonly processed using solid-state methods such as compression molding or ram extrusion. In these methods, particle size significantly affects the mechanical properties, with larger UHMWPE particles leading to incomplete particle fusion and decreased mechanical performance. In composite matrices, filler segregation at particle interfaces further inhibits particle fusion, dramatically reducing mechanical properties. To address these challenges, a particle engineering approach is employed that fills interparticle voids to enhance polymer fusion and control filler distribution. This is achieved by introducing microfine UHMWPE (<1 μm, termed "Small") synthesized from a nano-sized $MgO/MgCl_2/TiCl_4$ catalyst.

In Chapter 2, UHMWPE composites with graphene nanoplatelets (GNP) were prepared using Small (448 nm) and conventional Large (69.5 μm) UHMWPE particles. The particle size of UHMWPE was shown to control filler distribution: Large UHMWPE led to filler segregation at particle interfaces, yielding low mechanical performance despite achieving electrical conductivity at low filler loading. In contrast, Small allowed uniform GNP dispersion within the particles, maintaining high mechanical properties even at high filler loading, although electrical conductivity increased only at higher filler loading. A mixture of Small and Large (Mix) demonstrated a balance of high mechanical performance and electrical

conductivity even at low filler loading. These results highlight that UHMWPE particle size can be used as an effective tool to control filler distribution and mechanical and electrical properties in a simple manner.

In Chapter 3, I focused on improving mechanical performance of the Mix system by optimizing sintering conditions. The results indicated that increasing sintering temperature, rather than duration, effectively enhanced toughness by 1.7–2 times. Thermal conductivity of the composites was relatively unaffected by sintering temperature, likely due to the strong influence of polymer crystallinity, GNP defects, and the polymer-filler interface, all of which vary with sintering conditions. High-temperature uniaxial drawing of the composites achieved an extension ratio of 38.2, demonstrating that Small promoted interfacial fusion and formed a superior entanglement network. These findings suggest the potential of solid-state nanocomposite tapes and fibers.

In Chapter 4, the role of Small UHMWPE as a reinforcing component in polypropylene (PP) blends was investigated. Small acted as a nucleating agent, enhancing crystallinity and stiffness of the PP matrix. Small is demonstrated to function as an effective nucleating and reinforcing agent in polymer blends, highlighting its versatility for polymer blend applications.

In conclusion, this thesis establishes a materials-design strategy in which the particle size of UHMWPE serves as a key parameter for controlling filler distribution, thereby enabling a balance between electrical/thermal conductivity and mechanical properties. In particular, Small allowed uniform filler dispersion, maintaining high mechanical strength even at high filler loadings, and functioned as a nucleating agent in polymer blends to enhance matrix rigidity. These findings provide valuable insights into the structure–property relationships of UHMWPE-based composites and offer a new design strategy for high-performance polyolefin materials. These insights are expected to inspire future studies on particle-engineered polyolefin systems and the rational design of multifunctional nanocomposites.

List of Publications and Other Achievements

Kohei Amada

A) PUBLICATION

1. “Conductive and Stretchable Ultra-High-Molecular-Weight Polyethylene Nanocomposites through Controlled Filler Distribution from Homogeneous to Semi-Segregated Networks”, **Kohei Amada**, Le Thi Tuyet Mai, Patchanee Chammingkwan*, Toshiaki Taniike, *ACS Appl. Eng. Mater.* **2025**, *3*, 547–559. (Chapter 2)

2. "Sintering and Processing-Dependent Mechanical Behavior of UHMWPE and Its Nanocomposites in the Presence of Microfine UHMWPE”, **Kohei Amada**, Le Thi Tuyet Mai, Patchanee Chammingkwan*, Toshiaki Taniike*, *ACS Omega* **2026**, *11*, 1630–1638. (Chapter 3)

B) INTERNATIONAL CONFERENCE

1. "Optimizing Conductivity and Stretchability in Ultra-High Molecular Weight Polyethylene through Controlled Filler Distribution", **Kohei Amada**, Patchanee Chammingkwan, Toshiaki Taniike, OIST-JAIST Joint Symposium, Okinawa, Japan, November 27, poster.

2. "Syntheses of Itaconic Acid-Based Polyamides with High-Toughness and Controllable Biodegradability”, **Kohei Amada**, Huaiyu Wang, Maninder Singh, Hongrong Yin, Mohammad Asif Ali, Maiko Okajima, Kenji Takada, Tatsuo Kaneko, The 13th SPSJ International Polymer Conference, Sapporo, Japan, July 18-21, 2023, poster.

C) DOMESTIC CONFERENCE

1. "$MgO/MgCl_2/TiCl_4$ コアシェル Ziegler-Natta 触媒を用いたマイクロファイン超高分子量ポリエチレンの合成と伝導性ナノコンポジットへの応用", **天田 晃平**, Chammingkwan Patchanee, 谷池 俊明, 第 54 回石油・石油化学討論会, 広島, 2024 年 11 月 29 日, 口頭.

2. “立体規則性を制御したイタコン酸由来バイオポリアミドの合成”, **天田 晃平**, Yin Hongrong, Singh Maninder, Ali Mohammad Asif, 高田 健司, 金子 達雄, 第 72 回高分子討論会, 香川, 2023 年 9 月 28 日, ポスター.

3. “ピロリドン環配列制御によるバイオポリアミドの物性評価”, **天田 晃平**, 高田 健司, 金子 達雄, 第 31 回日本ポリイミド・芳香族系高分子会議, 東京, 2023 年 11 月 18 日, ポスター.